

# 13

## Advanced Motion Control Systems

State-of-the-art motion control systems are usually designed using PID control methods, as described in Chapter 12. This chapter presents more advanced methods for optimal and nonlinear control of marine craft. The main motivation for this is design simplicity and performance. Nonlinear control theory can often yield a more intuitive design than linear theory. Linearization destroys model properties and the results can be a more complicated design process with limited physical insight. Chapter 13 is written for the advanced user who wants to exploit a more advanced model and use this model to improve the performance of the control system. Readers of this chapter need background in optimal and nonlinear control theory.

### Preview of the Chapter

Chapter 13 starts with linear quadratic optimal control theory (Section 13.1) with the focus on regulation, trajectory-tracking control and disturbance feedforward. Optimal motion control systems are designed by considering the linearized equations of motion (Section 7.5.3) in the following form:

$$\dot{\mathbf{x}} = \mathbf{Ax} + \mathbf{Bu} + \mathbf{Ew} \quad (13.1)$$

For a marine craft, the linear model (13.1) is based on several assumptions such as zero or constant cruise speed  $u$  together with the assumptions that the velocities  $v$ ,  $w$ ,  $p$ ,  $q$  and  $r$  are small. In addition, the kinematic equation  $\dot{\boldsymbol{\eta}} = \mathbf{J}_\Theta(\boldsymbol{\eta})\mathbf{v}$  must be linearized under a set of assumptions on the Euler angles  $\phi$ ,  $\theta$  and  $\psi$ .

When linearizing the equations of motion, several model properties such as symmetry of the inertia matrix  $\mathbf{M}$ , skew-symmetry of the Coriolis and centripetal matrix  $\mathbf{C}(\mathbf{v})$  and positiveness of the damping matrix  $\mathbf{D}(\mathbf{v})$  are destroyed, and this often complicates the control design. Also physical properties that are important tools for good engineering judgement are lost. This is seen by comparing the LQ design procedure with the nonlinear techniques in Sections 13.2–13.4. It is also demonstrated how the nonlinear controllers can be related to the PID control design methods in Chapter 12 in particular, under the assumption of setpoint regulation. Often it is useful to think about the nonlinear controller as a PID control system where additional terms are added to obtain global stability results. Keeping this in mind, it is also possible to derive a nonlinear controller using advanced methods and then use engineering insight to simplify the representation of the controller. The resulting controller should be as simple as possible

but still contain the most important terms when implementing the algorithm into a computer. In fact, a so-called simplified nonlinear controller will be recognized as a PID controller with additional terms. Many nonlinear methods are popular due to their simplicity and design flexibility. The assumptions on  $u, v, w, p, q, r$  and  $\phi, \theta, \psi$  which are needed when linearizing the models are also avoided.

The nonlinear design methods in this chapter are based on the robot-like model of Fossen (1991):

$$\dot{\eta} = J_\theta(\eta)v \quad (13.2)$$

$$M\ddot{v} + C(v)v + D(v)v + g(\eta) = \tau + w \quad (13.3)$$

It is important to understand the physical properties of the model in order to know which terms in the model can be omitted when deriving a model-based nonlinear controller. This is an important question since model inaccuracies can destabilize a feedback control system. Often better results are obtained when uncertain terms are chosen to be zero in the controller.

## 13.1 Linear Quadratic Optimal Control

Optimal control deals with the problem of finding a control law for a given system such that a certain optimality criterion is achieved. This is usually a cost function that depends on the state and control variables. The optimal control law is a set of differential equations that minimize the cost functional and it can be derived using Pontryagin's maximum principle (a necessary condition) or by solving the Hamilton–Jacobi–Bellman equation (a sufficient condition). We will limit our discussion to linear systems and quadratic cost functions. This is referred to as linear quadratic (LQ) optimal control theory (Athans and Falb, 1966).

### 13.1.1 Linear Quadratic Regulator

A fundamental design problem is the regulator problem, where it is necessary to regulate the outputs  $y \in \mathbb{R}^m$  of the system to zero or a constant value while ensuring that they satisfy time-response specifications. A linear quadratic regulator (LQR) can be designed for this purpose by considering the state-space model

$$\dot{x} = Ax + Bu \quad (13.4)$$

$$y = Cx \quad (13.5)$$

where  $x \in \mathbb{R}^n$ ,  $u \in \mathbb{R}^r$  and  $y \in \mathbb{R}^m$ . In order to design a linear optimal control law the system  $(A, B, C)$  must be controllable while observability (see Definition 11.2 in Section 11.2.3) is necessary if some of the states must be estimated. Controllability for linear time-invariant systems is given by the following definition

#### **Definition 13.1 (Controllability)**

*The state and input matrix  $(A, B)$  must satisfy the controllability condition to ensure that there exists a control  $u(t)$  that can drive any arbitrary state  $x(t_0)$  to another arbitrary state  $x(t_1)$  for  $t_1 > t_0$ . The controllability condition requires that the matrix (Gelb et al., 1988)*

$$\mathcal{C} = [B \mid AB \mid \cdots \mid (A)^{n-1}B] \quad (13.6)$$

*must be of full row rank such that a right inverse exists.*

The feedback control law for the system (13.4)–(13.5) is found by minimizing the quadratic cost function

$$\begin{aligned} J &= \min_u \left\{ \frac{1}{2} \int_0^T (\mathbf{y}^\top \mathbf{Q} \mathbf{y} + \mathbf{u}^\top \mathbf{R} \mathbf{u}) dt \right. \\ &\quad \left. = \frac{1}{2} \int_0^T (\mathbf{x}^\top \mathbf{C}^\top \mathbf{Q} \mathbf{C} \mathbf{x} + \mathbf{u}^\top \mathbf{R} \mathbf{u}) dt \right\} \end{aligned} \quad (13.7)$$

where  $\mathbf{R} = \mathbf{R}^\top > 0$  and  $\mathbf{Q} = \mathbf{Q}^\top \geq 0$  are the weighting matrices. The steady-state solution to this problem is (Athans and Falb, 1966)

$$\mathbf{u} = \underbrace{-\mathbf{R}^{-1} \mathbf{B}^\top \mathbf{P}_\infty \mathbf{x}}_G \quad (13.8)$$

$$\mathbf{P}_\infty \mathbf{A} + \mathbf{A}^\top \mathbf{P}_\infty - \mathbf{P}_\infty \mathbf{B} \mathbf{R}^{-1} \mathbf{B}^\top \mathbf{P}_\infty + \mathbf{C}^\top \mathbf{Q} \mathbf{C} = \mathbf{0} \quad (13.9)$$

where  $\mathbf{P}_\infty = \lim_{t \rightarrow \infty} \mathbf{P}(t)$ . The optimal feedback control system is illustrated in Figure 13.1.

### Matlab

The steady-state LQR feedback control law is computed as (see the script `ExLQR.m`)

```

Q = diag([1]); % user editable tracking error weights (dim m x m)
R = diag([1]); % user editable input weights (dim r x r)

% System matrices
A = [0 1; -1 -2]; % user editable state matrix (dim n x n)
B = [0; 1]; % user editable input matrix (dim n x r)
C = [1 0]; % user editable output matrix (dim m x n)

% Compute the optimal feedback gain matrix G
[K, P, E] = lqr(A, B, C'*Q*C, R);
G = -K

```

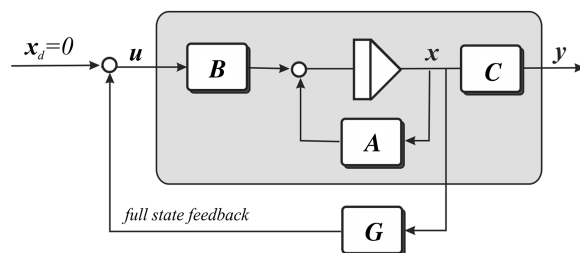


**Figure 13.1** Block diagram showing the linear quadratic regulator (LQR).

The Matlab function `lqr.m` also returns the eigenvalues of the closed-loop system

$$\dot{x} = (A + BG)x \quad (13.10)$$

denoted by the symbol  $\Xi$ .

### 13.1.2 LQR Design for Trajectory Tracking and Integral Action

The LQR can be redesigned to track a time-varying reference trajectory  $x_d \in \mathbb{R}^n$  for a large class of mechanical systems possessing certain structural properties. This section presents a simple solution to this problem while a more general solution is presented in Section 13.1.3.

#### Transformation of the LQ Tracker to a Setpoint Regulation Problem

In order to transform a trajectory-tracking problem to a setpoint regulation problem *reference feedforward* can be used. Unmeasured slowly varying or constant disturbances are compensated for by including integral action. This is usually done by augmenting an integral state  $\dot{z} = e$  to the system model. A mass–damper–spring system will be used to demonstrate the design methodology.

#### *Example 13.1 (Mass–Damper–Spring Trajectory-Tracking Problem)*

Consider the mass–damper–spring system

$$\begin{aligned}\dot{x} &= v \\ m\dot{v} + dv + kx &= \tau\end{aligned}$$

Let

$$\tau = \tau_{FF} + \tau_{LQ} \quad (13.11)$$

where the feedforward term is chosen as

$$\tau_{FF} = m\dot{v}_d + dv_d + kx_d \quad (13.12)$$

such that

$$m\ddot{e} + d\dot{e} + ke = \tau_{LQ} \quad (13.13)$$

where  $e = x - x_d$  and  $\dot{e} = v - v_d$ . The desired states are computed using a reference model:

$$\dot{x}_d = v_d \quad (13.14)$$

$$\dot{v}_d = \phi(v_d, r) \quad (13.15)$$

where  $r$  is the setpoint. The trajectory-tracking control problem has now been transformed to an LQ setpoint regulation problem given by (13.13), which can be written in state-space form as

$$\begin{aligned}\dot{x} &= \underbrace{\begin{bmatrix} 0 & 1 \\ -\frac{d}{m} & -\frac{k}{m} \end{bmatrix}}_A x + \underbrace{\begin{bmatrix} 0 \\ \frac{1}{m} \end{bmatrix}}_B u \\ e &= \underbrace{\begin{bmatrix} 1 & 0 \end{bmatrix}}_C x\end{aligned}$$

where  $x = [e, \dot{e}]^\top$  and  $u = \tau_{LQ}$ .

### Integral Action

In Example 13.1 it was shown that a feedforward term  $\tau_{\text{FF}}$  could transform the LQ trajectory-tracking problem to an LQR problem. For the system model

$$\dot{\mathbf{x}} = \mathbf{A}\mathbf{x} + \mathbf{B}\mathbf{u} \quad (13.16)$$

integral action is obtained by augmenting the integral state  $\mathbf{z} \in \mathbb{R}^m$  to the state vector. Let

$$\dot{\mathbf{z}} = \mathbf{y} = \mathbf{C}\mathbf{x} \quad (13.17)$$

where the  $\mathbf{C}$  matrix is used to extract potential integral states from the  $\mathbf{x}$  vector. This system is a standard LQR problem:

$$\dot{\mathbf{x}}_a = \mathbf{A}_a\mathbf{x}_a + \mathbf{B}_a\mathbf{u} \quad (13.18)$$

where  $\mathbf{x}_a = [\mathbf{z}^\top, \mathbf{x}^\top]^\top$  and

$$\mathbf{A}_a = \begin{bmatrix} \mathbf{0} & \mathbf{C} \\ \mathbf{0} & \mathbf{A} \end{bmatrix}, \quad \mathbf{B}_a = \begin{bmatrix} \mathbf{0} \\ \mathbf{B} \end{bmatrix} \quad (13.19)$$

The control objective is regulation of  $\mathbf{x}_a$  to zero using  $\mathbf{u}$ . This is obtained by choosing the performance index

$$J = \min_{\mathbf{u}} \left\{ \frac{1}{2} \int_0^t (\mathbf{x}_a^\top \mathbf{Q}_a \mathbf{x}_a + \mathbf{u}^\top \mathbf{R} \mathbf{u}) d\tau \right\} \quad (13.20)$$

where  $\mathbf{R} = \mathbf{R}^\top > 0$  and  $\mathbf{Q}_a = \mathbf{Q}_a^\top \geq 0$  are the weighting matrices. Hence, the solution of the LQR setpoint regulation problem is (see Section 13.1.1)

$$\begin{aligned} \mathbf{u} &= -\mathbf{R}^{-1} \mathbf{B}_a^\top \mathbf{P}_\infty \mathbf{x}_a \\ &= -\mathbf{R}^{-1} [\mathbf{0} \quad \mathbf{B}^\top] \begin{bmatrix} \mathbf{P}_{11} & \mathbf{P}_{12} \\ \mathbf{P}_{21} & \mathbf{P}_{22} \end{bmatrix} \begin{bmatrix} \mathbf{z} \\ \mathbf{x} \end{bmatrix} \\ &= -\underbrace{\mathbf{R}^{-1} \mathbf{B}^\top \mathbf{P}_{12}}_{\mathbf{K}_i} \mathbf{z} - \underbrace{\mathbf{R}^{-1} \mathbf{B}^\top \mathbf{P}_{22}}_{\mathbf{K}_p} \mathbf{x} \end{aligned} \quad (13.21)$$

where  $\mathbf{P}_{12}$  and  $\mathbf{P}_{22}$  are found by solving the *algebraic Riccati equation* (ARE)

$$\mathbf{P}_\infty \mathbf{A}_a + \mathbf{A}_a^\top \mathbf{P}_\infty - \mathbf{P}_\infty \mathbf{B}_a \mathbf{R}^{-1} \mathbf{B}_a^\top \mathbf{P}_\infty + \mathbf{Q}_a = \mathbf{0} \quad (13.22)$$

Notice that the feedback term  $\mathbf{u}$  includes feedback from the tracking errors  $\mathbf{e}$  and  $\dot{\mathbf{e}}$  as well as the integral state

$$\mathbf{z} = \int_0^t \mathbf{e}(\tau) d\tau \quad (13.23)$$

#### 13.1.3 General Solution of the LQ Trajectory-Tracking Problem

Consider the state-space model

$$\dot{\mathbf{x}} = \mathbf{A}\mathbf{x} + \mathbf{B}\mathbf{u} + \mathbf{E}\mathbf{w} \quad (13.24)$$

$$\mathbf{y} = \mathbf{C}\mathbf{x} \quad (13.25)$$

The LQ trajectory-tracking control problem is addressed under the assumption that both the state vector  $\mathbf{x}$  and disturbance vector  $\mathbf{w}$  are measured or at least obtained by state estimation. If the estimated values are used for  $\mathbf{x}$  and  $\mathbf{w}$ , stability can be proven by applying a *separation principle*. This is known as LQG control in the literature and involves the design of a *Kalman filter* for reconstruction of the unmeasured states, which again requires that the system is *observable*. For simplicity, full-state feedback is assumed in this chapter. The interested reader is recommended to consult the extensive literature on LQG control for output feedback control; see Athans and Falb (1966) and Brian *et al.* (1989), for instance.

### Reference Feedforward Assumptions

Consider a time-varying reference system:

$$\dot{\mathbf{x}}_d = \phi(\mathbf{x}_d, \mathbf{r}) \quad (13.26)$$

$$\mathbf{y}_d = \mathbf{C}\mathbf{x}_d \quad (13.27)$$

where  $\mathbf{x}_d \in \mathbb{R}^n$  is the desired state,  $\mathbf{y}_d \in \mathbb{R}^p$  ( $p \leq n$ ) is the desired output,  $\mathbf{r} \in \mathbb{R}^r$  ( $r \leq n$ ) is the setpoint and  $\phi : \mathbb{R}^n \times \mathbb{R}^r \rightarrow \mathbb{R}^p$ . If linear theory is assumed the dynamics of the desired state can be conveniently represented by

$$\phi(\mathbf{x}_d, \mathbf{r}) = \mathbf{A}_d\mathbf{x}_d + \mathbf{B}_d\mathbf{r} \quad (13.28)$$

This is a linear reference model for trajectory-tracking control; see Section 10.2.1 for how to choose  $\mathbf{A}_d$  and  $\mathbf{B}_d$ . A special case is regulation:

$$\mathbf{y}_d = \mathbf{C}\mathbf{x}_d = \text{constant} \quad (13.29)$$

### Disturbance Feedforward Assumptions

Two cases of disturbance feedforward are considered:

1. The disturbance vector  $\mathbf{w} = \text{constant}$  for all  $t > T_p$ , where  $T_p$  is the present time. An example of this is a marine craft exposed to constant (or at least slowly varying) wind forces. This is a reasonable assumption since the *average* wind speed and direction are not likely to change in minutes.
2. The disturbance  $\mathbf{w} = \mathbf{w}(t)$  varies as a function of time  $t$  for future time  $t > T_p$ . This is the case for most physical disturbances. However, a feedforward solution requires that  $\mathbf{w}$  is known (or at least estimated) for  $t \geq 0$ . In many cases this is unrealistic so the best we can do is to assume that  $\mathbf{w}(t) = \mathbf{w}(T_p) = \text{constant}$ , that is in a finite future time horizon so that it conforms to Case 1 above.

### Control Objective

The control objective is to design a linear quadratic optimal trajectory-tracking controller using a time-varying smooth reference trajectory  $\mathbf{y}_d$  given by the system (13.26)–(13.27). Assume that the desired output  $\mathbf{y}_d = \mathbf{C}\mathbf{x}_d$  is known for all time  $t \in [0, T]$ , where  $T$  is the final time. Define the error signal:

$$\begin{aligned} \mathbf{e} &:= \mathbf{y} - \mathbf{y}_d \\ &= \mathbf{C}(\mathbf{x} - \mathbf{x}_d) \end{aligned} \quad (13.30)$$

The goal is to design an optimal trajectory-tracking controller that tracks the desired output, that is regulates the error  $\mathbf{e}$  to zero while minimizing

$$J = \min_u \left\{ \frac{1}{2} \mathbf{e}^\top(T) \mathbf{Q}_f \mathbf{e}(T) + \frac{1}{2} \int_{t_0}^T (\mathbf{e}^\top \mathbf{Q} \mathbf{e} + \mathbf{u}^\top \mathbf{R} \mathbf{u}) dt \right\}$$

subject to     $\dot{\mathbf{x}} = \mathbf{A}\mathbf{x} + \mathbf{B}\mathbf{u} + \mathbf{E}\mathbf{w}, \quad \mathbf{x}(0) = \mathbf{x}_0$

(13.31)

where  $\mathbf{R} = \mathbf{R}^\top > 0$  and  $\mathbf{Q} = \mathbf{Q}^\top \geq 0$  are the tracking error and control weighting matrices, respectively. The weight matrix  $\mathbf{Q}_f = \mathbf{Q}_f^\top \geq 0$  can be included to add penalty to the final state. Notice that this is a *finite time-horizon* optimal control problem and it has to be solved by using the *differential Riccati equation* (DRE); see Athans and Falb (1966, pp. 793–801).

It is assumed that the desired output signal comes from a linear reference generator given by

$$\dot{\mathbf{x}}_d = \mathbf{A}_d \mathbf{x}_d + \mathbf{B}_d \mathbf{r} \quad (13.32)$$

$$\mathbf{y} = \mathbf{C} \mathbf{x}_d \quad (13.33)$$

where  $\mathbf{r}$  is a given reference input, which is filtered through the generator.  $\mathbf{C}$  is the same output matrix as in the plant. A special case of (13.31) is the one with no weight on the final state; that is  $\mathbf{Q}_f = \mathbf{0}$ , resulting in the quadratic performance index

$$J = \min_u \left\{ \frac{1}{2} \int_0^T (\mathbf{e}^\top \mathbf{Q} \mathbf{e} + \mathbf{u}^\top \mathbf{R} \mathbf{u}) dt \right\} \quad (13.34)$$

Substituting (13.30) into (13.34) yields the equivalent formulation

$$J = \min_u \left\{ \frac{1}{2} \int_0^T (\tilde{\mathbf{x}}^\top \tilde{\mathbf{Q}} \tilde{\mathbf{x}} + \mathbf{u}^\top \mathbf{R} \mathbf{u}) dt \right\} \quad (13.35)$$

where  $\tilde{\mathbf{x}} = \mathbf{x} - \mathbf{x}_d$  and

$$\tilde{\mathbf{Q}} = \mathbf{C}^\top \mathbf{Q} \mathbf{C} \geq 0 \quad (13.36)$$

### Linear Time-Varying Systems

It can be shown that the optimal control law is (Brian *et al.*, 1989)

$$\mathbf{u} = -\mathbf{R}^{-1} \mathbf{B}^\top [\mathbf{P}\mathbf{x} + \mathbf{h}_1 + \mathbf{h}_2] \quad (13.37)$$

where  $\mathbf{P}$ ,  $\mathbf{h}_1$  and  $\mathbf{h}_2$  originate from the *Hamiltonian* system.  $\mathbf{P}$  accounts for the feedback part,  $\mathbf{h}_1$  accounts for the feedforward part due to the time-varying nature of the reference signal  $\mathbf{y}_d$  and  $\mathbf{h}_2$  accounts for the feedforward part due to the measurable time-varying disturbance  $\mathbf{w}$ . The equations that need to be solved are

$$\dot{\mathbf{P}} = -\mathbf{P}\mathbf{A} - \mathbf{A}^\top \mathbf{P} + \mathbf{P}\mathbf{B}\mathbf{R}^{-1}\mathbf{B}^\top \mathbf{P} - \tilde{\mathbf{Q}} \quad (13.38)$$

$$\dot{\mathbf{h}}_1 = -[\mathbf{A} - \mathbf{B}\mathbf{R}^{-1}\mathbf{B}^\top \mathbf{P}]^\top \mathbf{h}_1 + \tilde{\mathbf{Q}}\mathbf{x}_d \quad (13.39)$$

$$\dot{\mathbf{h}}_2 = -[\mathbf{A} - \mathbf{B}\mathbf{R}^{-1}\mathbf{B}^\top \mathbf{P}]^\top \mathbf{h}_2 - \mathbf{P}\mathbf{E}\mathbf{w} \quad (13.40)$$

with

$$\mathbf{P}(T) = \tilde{\mathbf{Q}}_f \quad (13.41)$$

$$\mathbf{h}_1(T) = -\tilde{\mathbf{Q}}_f \mathbf{x}_d(T) \quad (13.42)$$

$$\mathbf{h}_2(T) = \mathbf{0} \quad (13.43)$$

where  $\tilde{\mathbf{Q}}_f = \mathbf{C}^\top \mathbf{Q}_f \mathbf{C}$ . Equations (13.38)–(13.40) represent three differential equations: a matrix DRE and two vector differential equations (adjoint operators), respectively. Notice that the initial conditions for these equations are not known, but rather the final conditions are known. Consequently, they have to be integrated *backward* in time a priori to find the initial conditions, and then be executed forward in time again with the closed-loop plant from  $[0, T]$ .

There are different ways of doing this. A frequently used method is to discretize the system and run the resulting difference equation backward. A simple Euler integration routine for (13.38) is given below, where  $\delta$  is set as a small *negative* sampling time. Moreover, using a first-order Taylor expansion

$$\mathbf{P}(t + \delta) \approx \mathbf{P}(t) + \delta \{-\mathbf{P}\mathbf{A} - \mathbf{A}^\top \mathbf{P} + \mathbf{P}\mathbf{B}\mathbf{R}^{-1}\mathbf{B}^\top \mathbf{P} - \tilde{\mathbf{Q}}\} \quad (13.44)$$

with  $\mathbf{P}(T) = \tilde{\mathbf{Q}}_f$  produces  $\mathbf{P}(0)$ . Another procedure is to simulate backwards in time. The system

$$\dot{\mathbf{x}} = \mathbf{f}(\mathbf{x}, t) + \mathbf{G}(\mathbf{x}, t)\mathbf{u}, \quad t \in [T, 0] \quad (13.45)$$

can be simulated backwards in time by the following change of integration variable  $t = T - \tau$  with  $dt = -d\tau$ , and

$$-\frac{d\mathbf{x}(T - \tau)}{d\tau} = \mathbf{f}(\mathbf{x}(T - \tau), T - \tau) + \mathbf{G}(\mathbf{x}(T - \tau), T - \tau)\mathbf{u}(T - \tau) \quad (13.46)$$

Let  $\mathbf{z}(\tau) = \mathbf{x}(T - \tau)$ ; then

$$\frac{d\mathbf{z}(\tau)}{d\tau} = -\mathbf{f}(\mathbf{z}(\tau), T - \tau) - \mathbf{G}(\mathbf{z}(\tau), T - \tau)\mathbf{u}(T - \tau) \quad (13.47)$$

This system can now be simulated forward in time with the initial condition  $\mathbf{z}(0) = \mathbf{x}(T)$ .

The method is demonstrated in Example 13.2, where it is assumed that both  $\mathbf{x}_d$  and  $\mathbf{w}$  are time varying but known for all future  $t$ . A special case dealing with constant values for  $\mathbf{x}_d$  and  $\mathbf{w}$  will be studied later.

### **Example 13.2 (Optimal Time-Varying LQ Trajectory-Tracking Problem)**

Consider a mass-damper-spring system:

$$m\ddot{x} + d\dot{x} + kx = u + w \quad (13.48)$$

where  $m$  is the mass,  $d$  is the damping coefficient,  $k$  is the spring stiffness coefficient,  $u$  is the input and  $w$  is the disturbance. Choosing the states as  $x_1 = x$  and  $x_2 = \dot{x}$ , the following state-space realization is obtained:

$$\begin{bmatrix} \dot{x}_1 \\ \dot{x}_2 \end{bmatrix} = \begin{bmatrix} 0 & 1 \\ -\frac{k}{m} & -\frac{d}{m} \end{bmatrix} \begin{bmatrix} x_1 \\ x_2 \end{bmatrix} + \begin{bmatrix} 0 \\ \frac{1}{m} \end{bmatrix} u + \begin{bmatrix} 0 \\ \frac{1}{m} \end{bmatrix} w \quad (13.49)$$

For simplicity, assume that  $m = k = 1$  and  $d = 2$  such that

$$\dot{\mathbf{x}} = \begin{bmatrix} 0 & 1 \\ -1 & -2 \end{bmatrix} \mathbf{x} + \begin{bmatrix} 0 \\ 1 \end{bmatrix} u + \begin{bmatrix} 0 \\ 1 \end{bmatrix} w \quad (13.50)$$

$$y = [1 \ 0] \mathbf{x} \quad (13.51)$$

where  $\mathbf{x} = [x_1, x_2]^\top$ . The disturbance signal is assumed to be known for all future time and is simply chosen as

$$w = \cos(t) \quad (13.52)$$

Similarly, the reference signal is assumed to be known for all future time and is given by the generator

$$\dot{\mathbf{x}}_d = \begin{bmatrix} 0 & 1 \\ -1 & -1 \end{bmatrix} \mathbf{x}_d + \begin{bmatrix} 0 \\ 1 \end{bmatrix} r \quad (13.53)$$

$$y_d = [1 \ 0] \mathbf{x}_d \quad (13.54)$$

where

$$r = \sin(t) \quad (13.55)$$

The Matlab MSS toolbox script `ExLQFinHor.m` demonstrates how forward and backward integration can be implemented for the mass-damper-spring system. The simulation results are shown in Figures 13.2–13.3.

### Approximate Solution for Linear Time-Invariant Systems

Unfortunately, the theory dealing with the limiting case

$$J = \min_u \left\{ \frac{1}{2} \lim_{T \rightarrow \infty} \int_0^T (\mathbf{e}^\top \mathbf{Q} \mathbf{e} + \mathbf{u}^\top \mathbf{R} \mathbf{u}) dt \right\} \quad (13.56)$$

is not available. This solution is very useful since it represents a steady-state solution of the LQ trajectory-tracking problem. Fortunately, this problem can be circumvented by assuming that  $T$  is large but still limited; that is

$$0 \ll T_1 \leq T < \infty \quad (13.57)$$

where  $T_1$  is a large constant. For  $T \rightarrow \infty$  the solution of (13.38) will tend to the constant matrix  $\mathbf{P}_\infty$  satisfying the *algebraic Riccati equation* (ARE)

$$\mathbf{P}_\infty \mathbf{A} + \mathbf{A}^\top \mathbf{P}_\infty - \mathbf{P}_\infty \mathbf{B} \mathbf{R}^{-1} \mathbf{B}^\top \mathbf{P}_\infty + \tilde{\mathbf{Q}} = \mathbf{0} \quad (13.58)$$

This solution is interpreted as the steady-state solution of (13.38) where  $\mathbf{P}(t) \approx \mathbf{P}_\infty$  for all  $t \in [0, T_1]$ . This is verified in the upper plot of Figure 13.3. Furthermore, it is assumed that

$$\mathbf{x}_d = \text{constant}, \quad \mathbf{w} = \text{constant}, \quad \forall t \in [0, T_1] \quad (13.59)$$

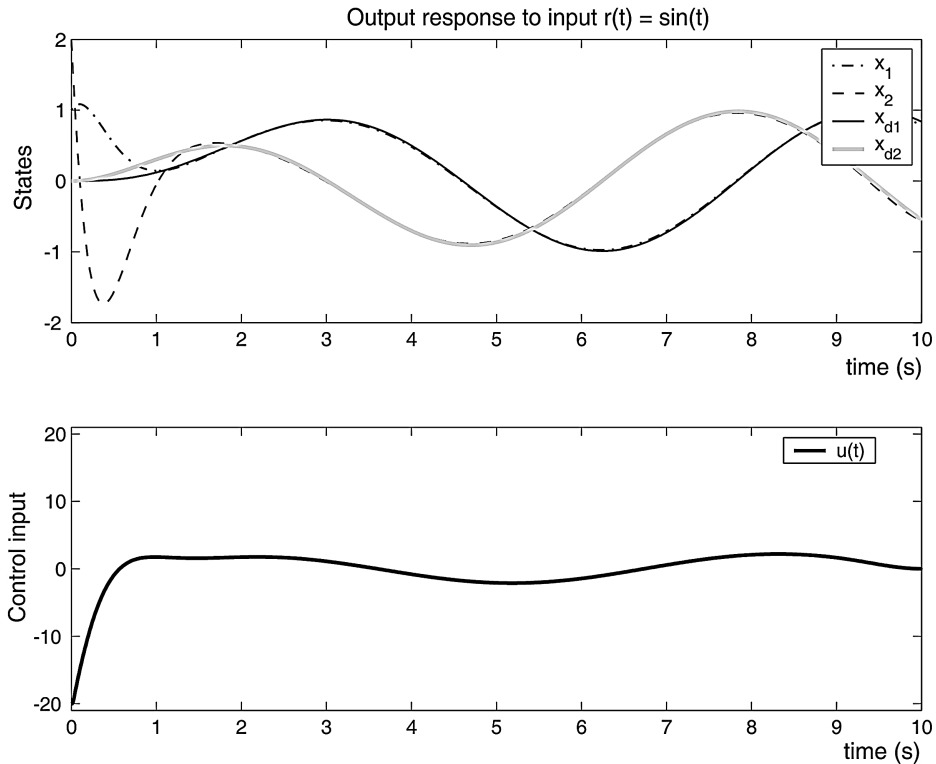


**Figure 13.2** Upper plot: states  $x_1$  and  $x_2$  and the reference trajectories  $x_{d1}$  and  $x_{d2}$  as a function of time.  
Lower plot: optimal control  $u$  as a function of time.

In practice the assumption that  $\mathbf{x}_d$  is constant can be relaxed with  $\mathbf{x}_d$  being slowly varying compared to the state dynamics. A similar argument can be used for  $\mathbf{w}$ . It is also common to drop the disturbance feedforward term since integral action in the controller can compensate for nonzero slowly varying disturbances.

Next, if the eigenvalues of the matrix

$$\mathbf{A}_c = \mathbf{A} + \mathbf{B}\mathbf{G}_1 \quad \text{where} \quad \mathbf{G}_1 = -\mathbf{R}^{-1}\mathbf{B}^\top \mathbf{P}_\infty \quad (13.60)$$

have negative real parts

$$\lambda_i(\mathbf{A}_c) < 0 \quad (i = 1, \dots, n) \quad (13.61)$$

the steady-state solution for  $\mathbf{h}_1$  and  $\mathbf{h}_2$  in (13.39) and (13.40) on  $[0, T_1]$  becomes

$$\mathbf{h}_{1\infty} = (\mathbf{A} + \mathbf{B}\mathbf{G}_1)^{-\top} \tilde{\mathbf{Q}}\mathbf{x}_d \quad (13.62)$$

$$\mathbf{h}_{2\infty} = -(\mathbf{A} + \mathbf{B}\mathbf{G}_1)^{-\top} \mathbf{P}_\infty \mathbf{E}\mathbf{w} \quad (13.63)$$

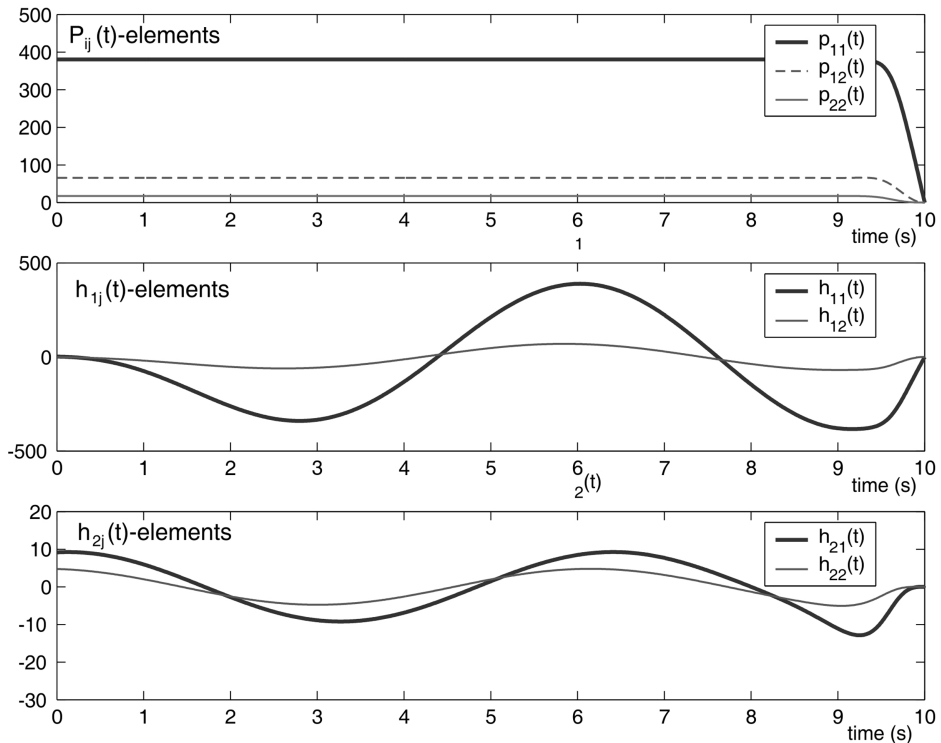


**Figure 13.3** Optimal solutions of the elements in  $\mathbf{P}$ ,  $\mathbf{h}_1$  and  $\mathbf{h}_2$  as a function of time.

Substitution of (13.58) into (13.37) yields the steady-state optimal control law (see Figure 13.4)

$$\mathbf{u} = \mathbf{G}_1 \mathbf{x} + \mathbf{G}_2 \mathbf{y}_d + \mathbf{G}_3 \mathbf{w} \quad (13.64)$$

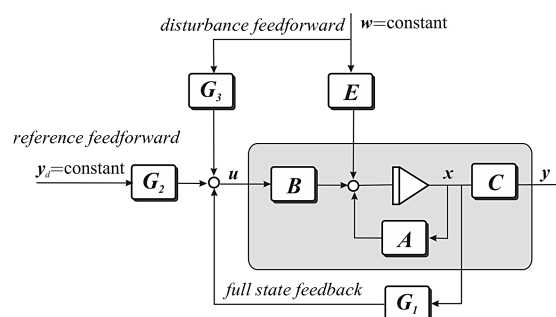


**Figure 13.4** Block diagram showing the full state feedback LQ tracker solution with disturbance feedforward.

where  $y_d = \text{constant}$  and  $w = \text{constant}$ , and

$$G_1 = -R^{-1}B^\top P_\infty \quad (13.65)$$

$$G_2 = -R^{-1}B^\top (A + BG_1)^{-\top} C^\top Q \quad (13.66)$$

$$G_3 = R^{-1}B^\top (A + BG_1)^{-\top} P_\infty E \quad (13.67)$$

### Matlab

The function `lqtracker.m` is implemented in the MSS toolbox for computation of the matrices  $G_1$ ,  $G_2$  and  $G_3$ :

```
function [G1,G2,G3] = lqtracker(A,B,C,Q,R)
[K,P,E] = lqr(A,B,C'*Q*C,R);
G1 = -inv(R)*B'*P;
Temp = inv((A+B*G1)');
G2 = -inv(R)*B'*Temp*C'*Q;
G3 = inv(R)*B'*Temp*P*E;
```

For a mass–damper–spring system the optimal trajectory tracking controller is found using `ExLQtrack.m`:

```
%Design matrices
Q = diag([1]); % tracking error weights
R = diag([1]); % input weights

% System matrices
A = [0 1; -1 -2]; % state matrix
B = [0; 1]; % input matrix
C = [1 0]; % output matrix

% Optimal gain matrices
[G1,G2,G3] = lqtracker(A,B,C,Q,R)
```

### SISO Systems

Consider the SISO state-space model

$$\dot{x} = Ax + bu + Ew \quad (13.68)$$

$$y = c^\top x \quad (13.69)$$

where  $x \in \mathbb{R}^n$ ,  $u \in \mathbb{R}$  and  $y \in \mathbb{R}$ . For SISO systems, the performance index (13.34) simplifies to

$$\begin{aligned} J &= \min_u \left\{ \frac{1}{2} \lim_{T \rightarrow \infty} \int_0^T (q e^2 + r u^2) dt \right. \\ &\quad \left. = \frac{q}{2} \lim_{T \rightarrow \infty} \int_0^T \left( e^2 + \frac{r}{q} u^2 \right) dt \right\} \end{aligned} \quad (13.70)$$

where  $q \geq 0$  and  $r > 0$  are two scalars. By choosing  $q = 1$  (without loss of generality) and defining  $\lambda := r/q > 0$ , the performance index (13.70) changes to

$$J^* = \min_u \left\{ \frac{1}{2} \lim_{T \rightarrow \infty} \int_{t_0}^T (e^2 + \lambda u^2) dt \right\} \quad (13.71)$$

Consequently, the steady-state optimal solution can be approximated as

$$u = \mathbf{g}_1^\top \mathbf{x} + g_2 y_d + \mathbf{g}_3^\top \mathbf{w} \quad (13.72)$$

where

$$\mathbf{g}_1^\top = -\frac{1}{\lambda} \mathbf{b}^\top \mathbf{P}_\infty \quad (13.73)$$

$$g_2 = -\frac{1}{\lambda} \mathbf{b}^\top (\mathbf{A} + \mathbf{b}\mathbf{g}_1^\top)^{-\top} \mathbf{c} \quad (13.74)$$

$$\mathbf{g}_3^\top = \frac{1}{\lambda} \mathbf{b}^\top (\mathbf{A} + \mathbf{b}\mathbf{g}_1^\top)^{-\top} \mathbf{P}_\infty \mathbf{E} \quad (13.75)$$

Here  $\mathbf{P}_\infty = \mathbf{P}_\infty^\top > 0$  is the solution of the ARE:

$$\mathbf{P}_\infty \mathbf{A} + \mathbf{A}^\top \mathbf{P}_\infty - \frac{1}{\lambda} \mathbf{P}_\infty \mathbf{b} \mathbf{b}^\top \mathbf{P}_\infty + \mathbf{c} \mathbf{c}^\top = \mathbf{0} \quad (13.76)$$

For a mass–damper–spring system the term  $\mathbf{g}_1^\top \mathbf{x}$  can be viewed as a PD controller while  $g_2 y_d$  and  $\mathbf{g}_3^\top \mathbf{w}$  represent reference and disturbance feedforward, respectively.

### 13.1.4 Case Study: Optimal Heading Autopilot for Ships and Underwater Vehicles

Autopilots for rudder-controlled ships and underwater vehicles can be designed by considering a linear quadratic optimization problem:

$$J = \min_\delta \left\{ \frac{\alpha}{T} \int_0^T [e^2 + \lambda_1 r^2 + \lambda_2 \delta^2] d\tau \right\} \quad (13.77)$$

where  $\alpha$  is a constant to be interpreted later,  $e = \psi_d - \psi$  is the heading error,  $\delta$  is the actual rudder angle and  $\lambda_1$  and  $\lambda_2$  are two factors weighting the cost of heading errors  $e$  and heading rate  $r$  against the control effort  $\delta$ . This criterion can also be reformulated to describe marine craft that not are turned using a single

rudder by replacing the quadratic term  $\delta^2$  with other control inputs. In the forthcoming, we will restrict our analysis to a single input.

For marine craft, operation in restricted waters usually requires accurate control, while the minimization of fuel consumption is more important in open seas. This can be obtained by changing the weights  $\lambda_1$  and  $\lambda_2$ . We will discuss three criteria for control weighting that have all been derived by considering a ship. However, the same principles apply for underwater vehicles.

### The Steering Criterion of Koyama

The first criterion was derived by Koyama (1967) who observed that the ship's swaying motion  $y$  could be approximated by a sinusoid

$$y = \sin(et) \implies \dot{y} = e \cos(et) \quad (13.78)$$

during autopilot control. The length of one arch  $L_a$  of the sinusoid is

$$L_a = \int_0^\pi \sqrt{(1 + \dot{y}^2)} d\tau = \int_0^\pi \sqrt{[1 + e^2 \cos^2(e\tau)]} d\tau \approx \pi \left(1 + \frac{e^2}{4}\right) \quad (13.79)$$

Hence, the relative elongation due to a sinusoidal course error is

$$\frac{\Delta L}{L} = \frac{L_a - L}{L} = \frac{\pi(1 + e^2/4) - \pi}{\pi} = \frac{e^2}{4} \quad (13.80)$$

This suggests that the percentage loss of speed during course control can be calculated by using the elongation in distance due to a sinusoidal course error. Consequently, Koyama (1967) proposed minimizing the speed loss term  $e^2/4$  against the increased resistance due to steering given by the quadratic term  $\delta^2$ . This motivates the following criterion:

$$J = \min_{\delta} \left\{ 100 \left( \frac{\pi}{180} \right)^2 \frac{1}{T} \int_0^T \left[ \frac{e^2}{4} + \lambda_2 \delta^2 \right] d\tau \approx \frac{0.0076}{T} \int_0^T [e^2 + \lambda_2 \delta^2] d\tau \right\} \quad (13.81)$$

In this context (13.77) can be interpreted as

$$J = \text{loss of speed (\%)} \quad (13.82)$$

$$\alpha = 0.0076 \quad (13.83)$$

Notice that  $\lambda_1 = 0$  for this method. In practice it might be desirable to penalize  $r^2$  by choosing  $\lambda_1 > 0$ . For ships, Koyama suggested a  $\lambda_2$  factor of approximately 8–10. Experiments show that such high values for  $\lambda_2$  avoid large rudder angles, and thus high turning rates. Therefore,  $\lambda_2 = 10$  will be a good choice in bad weather, where it is important to suppress high-frequency rudder motions.

### Norrbin's Steering Criterion

Another approach for computation of  $\lambda_2$  was proposed by Norrbin (1972). Consider the surge dynamics of a rudder-controlled marine craft in the form

$$(m - X_u)\dot{u} = X_{|u|u}|u|u + (1 - t)T + T_{\text{loss}} \quad (13.84)$$

where

$$T_{\text{loss}} = (m + X_{vr})vr + X_{cc\delta\delta}c^2 \delta^2 + (X_{rr} + mx_g)r^2 + X_{\text{ext}} \quad (13.85)$$

Norrbin (1972) suggested minimizing the loss term  $T_{\text{loss}}$  to obtain maximum forward speed  $u$ . Consequently, the controller should minimize the centripetal term  $vr$ , the square rudder angle  $\delta^2$  and the square heading rate  $r^2$ , while the unknown disturbance term  $X_{\text{ext}}$  is neglected in the analysis. The assumptions in doing this are as follows:

1. The sway velocity  $v$  is approximately proportional to  $r$ . From Section 7.2 it follows that

$$v(s) = \frac{K_v(T_v s + 1)}{K(T s + 1)} r(s) \approx \frac{K_v}{K} r(s) \quad (13.86)$$

if  $T_v \approx T$ . Hence, the centripetal term  $vr$  will be approximately proportional to the square of the heading rate; that is  $vr \approx (K_v/K)r^2$ .

2. The ship's yawing motion is periodic under autopilot control such that

$$r_{\max} = \omega_r e_{\max} \quad (13.87)$$

where  $\omega_r$  is the frequency of the sinusoidal yawing.

These two assumptions suggest that the loss term  $T_{\text{loss}}$  can be minimized by minimizing  $e^2$  and  $\delta^2$  which is the same result obtained in Koyama's analysis. The only difference between the criteria of Norrbin and Koyama is that the  $\lambda_2$  values arising from Norrbin's approach will be different when computed for the same ship. The performance of the controller also depends on the sea state. This suggests that a trade-off between the  $\lambda_2$  values proposed by Koyama and Norrbin could be made according to

$\underbrace{\text{(calm sea)}}_{\text{Norrbin}}$	$0.1 \leq \lambda_2 \leq 10$	$\underbrace{\text{(rough sea)}}_{\text{Koyama}}$
---	------------------------------	---

(13.88)

### Van Amerongen and Van Nauta Lemke's Steering Criterion

Experiments with the steering criteria of Koyama and Norrbin soon showed that the performance could be further improved by considering the squared yaw rate  $r^2$ , in addition to  $e^2$  and  $\delta^2$  (Van Amerongen and Van Nauta Lemke, 1978). Consequently, the following criterion was proposed:

$$J = \min_{\delta} \left\{ \frac{0.0076}{T} \int_0^T (e^2 + \lambda_1 r^2 + \lambda_2 \delta^2) d\tau \right\} \quad (13.89)$$

For a tanker and a cargo ship, Van Amerongen and Van Nauta Lemke (1978, 1980) gave the following values for the weighting factors  $\lambda_1$  and  $\lambda_2$  corresponding to the data set of Norrbin (1972):

Tanker:  $L_{pp} = 300$  m,  $\lambda_1 = 15\ 000$ ,  $\lambda_2 = 8.0$

Cargo ship:  $L_{pp} = 200$  m,  $\lambda_1 = 1\ 600$ ,  $\lambda_2 = 6.0$

The solution of the optimal steering criteria is found by considering Nomoto's first-order model in the form

$$\dot{\psi}' = r' \quad (13.90)$$

$$T'\dot{r} + (U/L)r = (U/L)^2 K' \delta \quad (13.91)$$

Straightforward application of optimal control theory to the criterion of Van Amerongen and Van Nauta Lempke (1978) yields (see Section 13.1.3)

$$\delta = -K_p(\psi - \psi_d) - K_d r \quad (13.92)$$

where the controller gains are computed using the steady-state solution (13.73) and (13.76). This gives

$$K_p = \sqrt{\frac{1}{\lambda_2}} \quad (13.93)$$

$$K_d = \frac{L}{U} \frac{\sqrt{1 + 2K_p K' T' + K'^2 (U/L)^2 (\lambda_1/\lambda_2)} - 1}{K'} \quad (13.94)$$

Consequently, the solution of the criteria of Koyama and Norrbin is obtained by setting  $\lambda_1 = 0$  and  $\lambda_2 = \lambda$ , which yields

$$K_p = \sqrt{\frac{1}{\lambda}} \quad (13.95)$$

$$K_d = \frac{L}{U} \frac{\sqrt{1 + 2K_p K' T'} - 1}{K'} \quad (13.96)$$

From these expressions it is seen that  $K_p$  depends on the weighting factor  $\lambda$ , while  $K_d$  depends on  $K_p$  as well as the model parameters  $K'$  and  $T'$ . Hence, accurate steering requires that  $K'$  and  $T'$  are known with sufficient accuracy.

An extension to Nomoto's second-order model is found by considering the state-space model (see Section 7.2)

$$\dot{\mathbf{x}} = \mathbf{A}\mathbf{x} + \mathbf{B}\mathbf{u} \quad (13.97)$$

$$\mathbf{y} = \mathbf{C}\mathbf{x} \quad (13.98)$$

where  $\mathbf{x} = [v, r, \psi]^\top$ ,  $\mathbf{u} = \delta$ ,  $\mathbf{y} = [r, \psi]^\top$  and

$$\mathbf{A} = \begin{bmatrix} a_{11} & a_{12} & 0 \\ a_{21} & a_{22} & 0 \\ 0 & 1 & 0 \end{bmatrix}, \quad \mathbf{B} = \begin{bmatrix} b_1 \\ b_2 \\ 0 \end{bmatrix}, \quad \mathbf{C} = \begin{bmatrix} 0 & 1 & 0 \\ 0 & 0 & 1 \end{bmatrix} \quad (13.99)$$

Let  $\mathbf{y} = [0, \psi_d]^\top = \text{constant}$  and

$$\begin{aligned}\mathbf{e} &= \mathbf{y} - \mathbf{y}_d \\ &= \mathbf{C}(\mathbf{x} - \mathbf{x}_d)\end{aligned}\quad (13.100)$$

The steady-state optimal solution minimizing the quadratic performance index

$$J = \min_{\mathbf{u}} \left\{ \frac{1}{2} \int_0^T (\mathbf{e}^\top \mathbf{Q} \mathbf{e} + \mathbf{u}^\top \mathbf{R} \mathbf{u}) d\tau \right\} \quad (13.101)$$

where  $\mathbf{Q} = \text{diag}\{q_{11}, q_{22}\} \geq 0$  and  $\mathbf{R} = r_{11} > 0$  are the weights (see Section 13.1.3)

$$\mathbf{u} = \mathbf{G}_1 \mathbf{x} + \mathbf{G}_2 \mathbf{y}_d \quad (13.102)$$

where

$$\mathbf{G}_1 = -\mathbf{R}^{-1} \mathbf{B}^\top \mathbf{P}_\infty \quad (13.103)$$

$$\mathbf{G}_2 = -\mathbf{R}^{-1} \mathbf{B}^\top (\mathbf{A} + \mathbf{B} \mathbf{G}_1)^{-\top} \mathbf{C}^\top \mathbf{Q} \quad (13.104)$$

and  $\mathbf{P}_\infty$  is the solution of the matrix Riccati equation:

$$\mathbf{P}_\infty \mathbf{A} + \mathbf{A}^\top \mathbf{P}_\infty - \mathbf{P}_\infty \mathbf{B} \mathbf{R}^{-1} \mathbf{B}^\top \mathbf{P}_\infty + \mathbf{C}^\top \mathbf{Q} \mathbf{C} = \mathbf{0} \quad (13.105)$$

The robustness of optimal autopilots for course-keeping control with a state estimator is analyzed in Holzhüter (1992).

### 13.1.5 Case Study: Optimal Fin and Rudder-Roll Damping Systems for Ships

The roll motion of ships and underwater vehicles can be damped by using fins alone or in combination with rudders. The main motivation for using roll stabilizing systems on merchant ships is to prevent cargo damage and to increase the effectiveness of the crew by avoiding or reducing seasickness. This is also important from a safety point of view. For naval ships critical marine operations include landing a helicopter, formation control, underway replenishment, or the effectiveness of the crew during combat.

Several *passive* and *active* (feedback control) systems have been proposed to accomplish roll reduction; see Burger and Corbet (1960), Lewis (1967) and Bhattacharyya (1978) for a more detailed discussion. Design methods for rudder-roll damping and fin stabilization systems are found in Perez (2005). Some passive solutions are:

**Bilge Keels:** Bilge keels are fins in planes approximately perpendicular to the hull or near the turn of the bilge. The longitudinal extent varies from about 25 to 50 % of the length of the ship. Bilge keels are widely used, are inexpensive but increase the hull resistance. In addition to this, they are effective mainly around the natural roll frequency of the ship. This effect significantly decreases with the speed of the ship. Bilge keels were first demonstrated in 1870.

**Hull Modifications:** The shape and size of the ship hull can be optimized for minimum rolling using hydrostatic and hydrodynamic criteria. This must, however, be done before the ship is built.

**Anti-Rolling Tanks:** The most common anti-rolling tanks in use are free-surface tanks, U-tube tanks and diversified tanks. These systems provide damping of the roll motion even at small speeds. The disadvantages are the reduction in metacenter height due to free water surface effects and that a large amount of space is required. The earliest versions were installed about the year 1874.

The most widely used systems for *active* roll damping are:

**Fin Stabilizers:** Fin stabilizers are highly useful devices for roll damping. They provide considerable damping if the speed of the ship is not too low. The disadvantage with additional fins is increased hull resistance and high costs associated with the installation, since at least two new hydraulic systems must be installed. Retractable fins are popular, since they are inside the hull when not in use (no additional drag). It should be noted that fins are not effective at low speed and that they cause underwater noise in addition to drag. Fin stabilizers were patented by *John I. Thornycroft* in 1889.

**Rudder-Roll Damping (RRD):** Roll damping by means of the rudder is relatively inexpensive compared to fin stabilizers, has approximately the same effectiveness and causes no drag or underwater noise if the system is turned off. However, RRD requires a relatively fast rudder to be effective; typically rudder rates of  $\dot{\delta}_{\max} = 5\text{--}20 \text{ deg/s}$  are needed. RRD will not be effective at low ship speeds.

**Gyroscopic Roll Stabilizers:** Gyroscopic roll stabilizers are typically used for boats and yachts under 100 feet. The ship gyroscopic stabilizer has a spinning rotor that generates a roll stabilizing moment that counteracts the wave-induced roll motions. Unlike stabilizing fins, the ship gyroscopic stabilizer can only produce a limited roll stabilizing moment and effective systems require approximately 3 to 5 % of the craft's displacement.

For a history of ship stabilization, the interested reader is advised to consult Bennett (1991), while a detailed evaluation of different ship roll stabilization systems can be found in Sellars and Martin (1992).

Rudder-roll damping (RRD) was first suggested in the late 1970s; see Cowley and Lambert (1972, 1975), Carley (1975), Lloyd (1975) and Baitis (1980). Research in the early 1980 showed that it was indeed feasible to control the heading of a ship with at least one rudder while simultaneously using the rudder for roll damping. If only one rudder is used, this is an *underactuated control* problem. In the linear case this can be solved by *frequency separation* of the steering and roll modes since heading control can be assumed to be a low-frequency trajectory-tracking control problem while roll damping can be achieved at higher frequencies.

Before designing an RRD system the applicability of the control system in terms of effectiveness should be determined (Roberts, 1993). For a large number of ships it is in fact impossible to obtain a significant roll damping effect due to limitations of the rudder servo and the relatively large inertia of the ship.

Motivated by the results in the 1970s, RRD was tested by the US Navy by Baitis *et al.* (1983, 1989), in Sweden by Källström (1987), Källström *et al.* (1988), Källström and Schultz (1990) and Källström and Theoren (1994), and in the Netherlands by Amerongen and coauthors. Van Amerongen *et al.* (1987), Van Amerongen and Van Nauta Lempe (1987) and Van der Klugt (1987) introduced LQG theory in RRD systems. A similar approach has been proposed by Katebi *et al.* (1987), while adaptive RRD is discussed in Zhou (1990).

Blanke and co-workers have developed an RRD autopilot (Blanke *et al.*, 1989) that has been implemented by the Danish Navy on 14 ships (Munk and Blanke, 1987). Sea trials show that some of the ships had less efficient RRD systems than others. In Blanke and Christensen (1993) it was shown that the cross-couplings between steering and roll were highly sensitive to parametric variations, which again resulted in robustness problems. Different loading conditions and varying rudder shapes have been identified as reasons for this (Blanke, 1996). In Stoustrup *et al.* (1995) it has been shown that a robust RRD controller can be designed by separating the roll and steering specifications and then optimizing the two controllers independently. The coupling effects between the roll and yaw modes have also been measured in model scale and compared with full-scale trial results (Blanke and Jensen, 1997), while a new approach to identification of steering-roll models has been presented by Blanke and Tiano (1997).

More recently  $H_\infty$  control has been used to deal with model uncertainties in RRD control systems. This allows the designer to specify frequency-dependent weights for frequency separation between the steering and roll modes; see Yang and Blanke (1997, 1998). Qualitative feedback theory (QFT) has also

been applied to solve the combined RRD heading control problem under model uncertainty; see Hearn and Blanke (1998). Results from sea trials are reported in Blanke *et al.* (2000).

Simulation and full-scale experimental results of RRD systems using a multivariate autoregressive model and the minimum AIC estimate procedure have been reported by Oda *et al.* (1996, 1997). Experimental results with various control strategies are also reported by Sharif *et al.* (1996). A nonlinear RRD control system using sliding-mode control for compensation of modeling errors is reported in Lauvdal and Fossen (1997).

A gain scheduling algorithm for input rate and magnitude saturations in RRD damping systems has been developed by Lauvdal and Fossen (1998). This method is motivated by the automatic gain controller (AGC) by Van der Klugt (1987) and a technique developed for stabilization of integrator chains with input rate saturation.

In this section the focus will be on linear quadratic optimal RRD. The interested reader is recommended to consult the references above and Perez (2005) for other design techniques.

### Linear Quadratic Optimal RRD Control System

Consider the 4 DOF maneuvering model (7.138) in Section 7.4:

$$\dot{\mathbf{x}} = \mathbf{Ax} + \mathbf{Bu} \quad (13.106)$$

where  $\mathbf{x} = [v, p, r, \phi, \psi]^\top$  and

$$\phi = \mathbf{c}_{\text{roll}}^\top \mathbf{x}, \quad \psi = \mathbf{c}_{\text{yaw}}^\top \mathbf{x} \quad (13.107)$$

The transfer functions corresponding to (13.106) and (13.107) are

$$\frac{\phi}{\delta}(s) = \frac{b_2 s^2 + b_1 s + b_0}{s^4 + a_3 s^3 + a_2 s^2 + a_1 s + a_0} \approx \frac{K_{\text{roll}} \omega_{\text{roll}}^2 (1 + T_5 s)}{(1 + T_4 s)(s^2 + 2\zeta\omega_{\text{roll}} s + \omega_{\text{roll}}^2)} \quad (13.108)$$

$$\frac{\psi}{\delta}(s) = \frac{c_3 s^3 + c_2 s^2 + c_1 s + c_0}{s(s^4 + a_3 s^3 + a_2 s^2 + a_1 s + a_0)} \approx \frac{K_{\text{yaw}} (1 + T_3 s)}{s(1 + T_1 s)(1 + T_2 s)} \quad (13.109)$$

The control objective is a simultaneous heading control  $\psi = \psi_d = \text{constant}$  and RRD ( $p_d = \phi_d = 0$ ) using one control input. There will be a trade-off between accurate heading control (minimizing  $\tilde{\psi} = \psi - \psi_d$ ) and control action needed to increase the natural frequency  $\omega_{\text{roll}}$  and damping ratio  $\zeta_{\text{roll}}$ . Also notice that it is impossible to regulate  $\phi$  to a nonzero value while simultaneously controlling the heading angle to a nonzero value by means of a single rudder. This can easily be seen by performing a steady-state analysis of the closed-loop system. This suggests that the output of the controller should be specified as

$$\mathbf{y} = [p, r, \phi, \psi]^\top, \quad \mathbf{y}_d = [0, 0, 0, \psi_d]^\top \quad (13.110)$$

Choosing  $\mathbf{y} = \mathbf{Cx}$  implies that

$$\mathbf{C} = \begin{bmatrix} 0 & 1 & 0 & 0 & 0 \\ 0 & 0 & 1 & 0 & 0 \\ 0 & 0 & 0 & 1 & 0 \\ 0 & 0 & 0 & 0 & 1 \end{bmatrix} \quad (13.111)$$

Application of optimal control theory implies that the control objective should be specified as an optimization problem for course keeping, roll damping and minimum fuel consumption. The trade-off between these quantities can be expressed as

$$J = \min_{\mathbf{u}} \left\{ \frac{1}{2} \int_0^T (\tilde{\mathbf{y}}^\top \mathbf{Q} \tilde{\mathbf{y}} + \mathbf{u}^\top \mathbf{R} \mathbf{u}) \, d\tau \right\} \quad (13.112)$$

where  $\tilde{\mathbf{y}} = \mathbf{y} - \mathbf{y}_d$ ,  $\tilde{\mathbf{x}} = \mathbf{x} - \mathbf{x}_d$  and  $\mathbf{x}_d = [0, 0, 0, 0, \psi_d]^\top$ . Accurate steering is weighted against roll damping by specifying the cost matrix  $\mathbf{Q} = \text{diag}\{\mathcal{Q}_p, \mathcal{Q}_r, \mathcal{Q}_\phi, \mathcal{Q}_\psi\} \geq 0$ , while  $\mathbf{R} = \text{diag}\{R_1, R_{21}, \dots, R_r\} > 0$  weights the use of the different rudder servos.

The solution to the LQ trajectory-tracking problem is (see Section 13.1.3)

$$\mathbf{u} = \mathbf{G}_1 \mathbf{x} + \mathbf{G}_2 \mathbf{y}_d \quad (13.113)$$

where

$$\mathbf{G}_1 = -\mathbf{R}^{-1} \mathbf{B}^\top \mathbf{P}_\infty \quad (13.114)$$

$$\mathbf{G}_2 = -\mathbf{R}^{-1} \mathbf{B}^\top (\mathbf{A} + \mathbf{B}\mathbf{G}_1)^{-\top} \mathbf{C}^\top \mathbf{Q} \quad (13.115)$$

with  $\mathbf{P}_\infty = \mathbf{P}_\infty^\top > 0$  given by

$$\mathbf{P}_\infty \mathbf{A} + \mathbf{A}^\top \mathbf{P}_\infty - \mathbf{P}_\infty \mathbf{B} \mathbf{R}^{-1} \mathbf{B}^\top \mathbf{P}_\infty + \mathbf{C}^\top \mathbf{Q} \mathbf{C} = \mathbf{0} \quad (13.116)$$

### Frequency Separation and Bandwidth Limitations

Since  $(\mathbf{A}, \mathbf{B})$  is controllable and full-state feedback is applied, it is possible to move all the five poles of the system. The closed-loop system becomes

$$\begin{aligned} \dot{\mathbf{x}} &= \mathbf{A}\mathbf{x} + \mathbf{B}\mathbf{u} \\ &= \underbrace{(\mathbf{A} + \mathbf{B}\mathbf{G}_1^\top)}_{\mathbf{A}_c} \mathbf{x} + \mathbf{B}\mathbf{G}_2 \underbrace{\mathbf{h}\psi_d}_{\mathbf{y}_d} \end{aligned} \quad (13.117)$$

where

$$\mathbf{h} = [0, 0, 0, 1]^\top \quad (13.118)$$

The closed-loop transfer function in yaw is

$$\psi(s) = \mathbf{c}_{\text{yaw}}^\top (s\mathbf{I} - \mathbf{A}_c)^{-1} \mathbf{B} \mathbf{G}_2 \mathbf{h} \psi_d(s) \quad (13.119)$$

which clearly satisfy

$$\lim_{t \rightarrow \infty} \psi(t) = \psi_d \quad (13.120)$$

Notice that integral action in yaw is needed in a practical implementation of the controller. Similarly, the closed-loop roll dynamics becomes

$$\phi(s) = \mathbf{c}_{\text{roll}}^\top (s\mathbf{I} - \mathbf{A}_c)^{-1} \mathbf{B} \mathbf{G}_2 \mathbf{h} \psi_d(s) \quad (13.121)$$

If one rudder is used to control both  $\phi$  and  $\psi$ , frequency separation is necessary to achieve this. Assume that the steering dynamics is slower than the frequency  $1/T_l$  and that the natural frequency in roll is higher than  $1/T_h$ . Hence, the vertical reference unit (VRU) and compass measurements can be low- and high-pass filtered according to

$$\frac{\phi}{\phi_{\text{vrui}}}(s) = h_h(s) = \frac{T_h s}{1 + T_h s} \quad (13.122)$$

$$\frac{\psi}{\psi_{\text{compass}}}(s) = h_l(s) = \frac{1}{1 + T_l s} \quad (13.123)$$

It is also necessary to filter the roll and yaw rate measurements  $p(s)$  and  $r(s)$ . These signals can also be computed by numerical differentiation of  $\phi_{\text{vrui}}(s)$  and  $\psi_{\text{vrui}}(s)$  using a state estimator.

This suggests that the bandwidth of the yaw angle control system must satisfy (frequency separation)

$$\omega_b \ll \omega_{\text{roll}} \quad (13.124)$$

This again implies that the low- and high-pass filters must satisfy

$$\underbrace{\omega_{\text{yaw}}}_{\substack{\text{cross-over} \\ \text{frequency}}} < \underbrace{\omega_b}_{\substack{\text{bandwidth} \\ \text{in yaw}}} < \underbrace{1/T_l}_{\substack{\text{low-pass filter} \\ \text{frequency}}} < \underbrace{1/T_h}_{\substack{\text{high-pass filter} \\ \text{frequency}}} < \underbrace{\omega_{\text{roll}}}_{\substack{\text{natural} \\ \text{frequency}}}$$

which clearly puts a restriction on the ships that can be stabilized. For many ships this requirement is impossible to satisfy due to limitations of the rudder servos and control forces.

### **Example 13.3 (RRD Control System Using One Rudder)**

Let  $\mathbf{G}_1 = [g_{11}, g_{12}, g_{13}, g_{14}, g_{15}]$  and  $\mathbf{G}_2 = [0, 0, 0, g_{24}]$  such that the solution (13.113) of the SISO LQ trajectory-tracking problem can be written

$$\delta = [g_{11}, g_{12}, g_{13}, g_{14}, g_{15}] \mathbf{x} + g_{24} \psi_d \quad (13.125)$$

or

$$\delta = \underbrace{-K_v v}_{\substack{\text{sway feedback}}} \underbrace{-K_p(\psi - \psi_d) - K_d r}_{\substack{\text{PD heading controller}}} \underbrace{-K_{r1} p - K_{r2} \phi}_{\substack{\text{roll damper}}} \quad (13.126)$$

where  $K_v = -g_{11}$ ,  $K_p = -g_{15} = g_{24}$ ,  $K_d = -g_{13}$ ,  $K_{r1} = -g_{12}$  and  $K_{r2} = -g_{14}$ . Frequency separation suggests that

$$\delta = h_l(s)\delta_{\text{course}} + h_h(s)\delta_{\text{roll}} \quad (13.127)$$

where

$$\delta_{\text{course}} = -K_v v - K_p(\psi - \psi_d) - K_d r \quad (13.128)$$

$$\delta_{\text{roll}} = -K_{r1} p - K_{r2} \phi \quad (13.129)$$

The controller gains can be found by using the MSS toolbox m-function (see Section 13.1.3):

$$[G1, G2] = \text{lqtracker}(A, B, C, Q, R)$$

Alternatively, the gains can be computed by using pole placement. The two subsystems (7.145) and (7.146) with heading autopilot and RRD become (neglecting the interactions between the systems)

$$\begin{bmatrix} \dot{p} \\ \dot{\phi} \end{bmatrix} = \begin{bmatrix} \underbrace{a_{22} - b_{21}K_{r1}}_{-2\zeta_{\text{roll}}\omega_{\text{roll}}} & \underbrace{(a_{24} - b_{21}K_{r2})}_{-\omega_{\text{roll}}^2} \\ 1 & 0 \end{bmatrix} \begin{bmatrix} p \\ \phi \end{bmatrix} = 0 \quad (13.130)$$

$$\begin{bmatrix} \dot{v} \\ \dot{r} \\ \dot{\psi} \end{bmatrix} = \begin{bmatrix} a_{11} - b_{11}K_v & a_{13} - b_{11}K_d & -b_{11}K_p \\ a_{31} - b_{31}K_v & a_{33} - b_{31}K_d & -b_{31}K_p \\ 0 & 1 & 0 \end{bmatrix} \begin{bmatrix} v \\ r \\ \psi - \psi_d \end{bmatrix} = 0 \quad (13.131)$$

The poles can be specified directly in Matlab using

$$[Kr1, Kr2] = \text{place}(A\_phiphi, B\_phiphi, [p\_phi1, p\_phi2])$$

$$[Kv, Kp, Kd] = \text{place}(A\_psipsi, B\_psipsi, [p\_psi1, p\_psi2, p\_psi3])$$

For roll it is seen that

$$-\omega_{\text{roll}}^2 = a_{24} - b_{21}K_{r2}, \quad -2\zeta_{\text{roll}}\omega_{\text{roll}} = a_{22} - b_{21}K_{r1} \quad (13.132)$$

or

$$K_{r1} = \frac{a_{22} + 2\zeta_{\text{roll}}\omega_{\text{roll}}}{b_{21}}, \quad K_{r2} = \frac{a_{24} + \omega_{\text{roll}}^2}{b_{21}} \quad (13.133)$$

where  $\zeta_{\text{roll}}$  and  $\omega_{\text{roll}}$  are pole-placement design parameters that can be used instead of eigenvalues. The model of Son and Nomoto (see `ExRRD2.m` in the MSS toolbox) has been used to demonstrate how an LQ optimal RRD control system can be designed. The linear state-space model for the container ship is

$$A = \begin{bmatrix} -0.0406 & -1.9614 & 0.2137 & 0.1336 & 0 \\ 0.0011 & -0.1326 & -0.1246 & -0.0331 & 0 \\ -0.0010 & 0.0147 & -0.1163 & -0.0006 & 0 \\ 0 & 1 & 0 & 0 & 0 \\ 0 & 0 & 1 & 0 & 0 \end{bmatrix}, \quad B = \begin{bmatrix} -0.0600 \\ 0.0035 \\ 0.0026 \\ 0 \\ 0 \end{bmatrix} \quad (13.134)$$

The controller gains were computed using  $[G1, G2] = \text{lqtracker}(A, B, C, Q, R)$  with the weights

$$Q = \text{diag}([10000 \ 1000 \ 10 \ 1]), \quad R = 0.5$$

resulting in

$$G1 = [0.1631 - 16.1193 - 6.7655 - 1.1644 - 0.4472], \quad G2 = [0 \ 0 \ 0 \ 0.4472]$$

Notice that  $g_{15} = -g_{24}$ . The open- and closed-loop poles are computed in Matlab by using the commands `damp(A)` and `damp(A+B*G1)`; see Table 13.1.

**Table 13.1** Eigenvalues, damping ratios and frequencies for the RRD control system

Eigenvalues		Damping		Frequencies (rad/s)	
Open loop	Closed loop	Open loop	Closed loop	Open loop	Closed loop
0	-0.061	—	1.00	—	0.016
-0.027	-0.026	1.00	1.00	0.027	0.026
-0.071 + 0.183 <i>i</i>	-0.100 + 0.165 <i>i</i>	0.36	0.52	0.197	0.193
-0.071 - 0.183 <i>i</i>	-0.100 - 0.165 <i>i</i>	0.36	0.52	0.197	0.193
-0.121	-0.131	1.00	1.00	0.121	0.131

It is seen that the natural frequency and relative damping ratio in roll are  $\omega_{\text{roll}} = 0.193 \text{ rad/s}$  and  $\zeta_{\text{roll}} = 0.36$ , respectively. This is improved to  $\omega_{\text{roll}} = 0.197 \text{ rad/s}$  and  $\zeta_{\text{roll}} = 0.52$  by roll feedback. It is difficult to increase the relative damping ratio further due to limitations of the steering machine ( $\dot{\delta}_{\text{max}} = 20 \text{ deg/s}$  and  $\delta_{\text{max}} = 20 \text{ deg}$ ). These values can, however, be changed in RRDcontainer.m.

Since the roll frequency  $\omega_{\text{roll}}$  is 0.193 rad/s and the cross-over frequency in yaw  $\omega_{\text{yaw}}$  is 0.03 rad/s, see Figure 7.7 in Example 7.7, it is approximately one decade between the frequencies  $\omega_{\text{yaw}}$  and  $\omega_{\text{roll}}$ . Therefore, frequency separation can be obtained by choosing the low-pass and high-pass filter frequencies as  $1/T_l = 0.1 \text{ rad/s}$  in yaw and  $1/T_h = 0.05 \text{ rad/s}$  in roll, respectively. It is seen that the heading controller moves the poles to -0.061, -0.026 and -0.131, resulting in satisfactory course-changing capabilities (see Figure 13.5). It is also seen that the course-keeping performance is degraded during RRD. The additional yawing motion, typically 1–2 degrees in amplitude, is the price paid for adding roll feedback to an autopilot system. Also notice that the right half-plane zero in the transfer function  $\phi/\delta_1(s)$  given by (7.147) is unchanged since feedback only moves the poles.

### Performance Criterion for RRD

The percentage roll reduction of RRD system can be computed by using the following criterion of Oda *et al.* (1992):

$$\text{Roll reduction} = \frac{\sigma_{\text{AP}} - \sigma_{\text{RRD}}}{\sigma_{\text{AP}}} \times 100 \% \quad (13.135)$$

where

$\sigma_{\text{AP}}$  = standard deviation of roll rate during course-keeping (RRD off)

$\sigma_{\text{RRD}}$  = standard deviation of roll rate during course-keeping (RRD on)

For the case study in Example 13.3,  $\sigma_{\text{AP}} = 0.0105$  and  $\sigma_{\text{RRD}} = 0.0068$ . This resulted in a roll reduction of approximately 35 % during course-keeping. For small high-speed vessels a roll reduction as high as 50–75 % can be obtained. This of course depends on the shape of the hull (hydrodynamic effects) and the capacity of the steering machine. In particular the maximum rudder rate  $\dot{\delta}_{\text{max}}$  should be in the magnitude of 15–20 % to obtain good results.

### Optimal Fin and RRD Systems

The most effective roll damping systems are those that combine stabilizing fins and rudders; see Källström (1981), Roberts and Braham (1990) and Perez (2005). Warship stabilization using integrated rudder and fins are discussed by Roberts (1992). More recently robust fin stabilizer controller design using the QFT

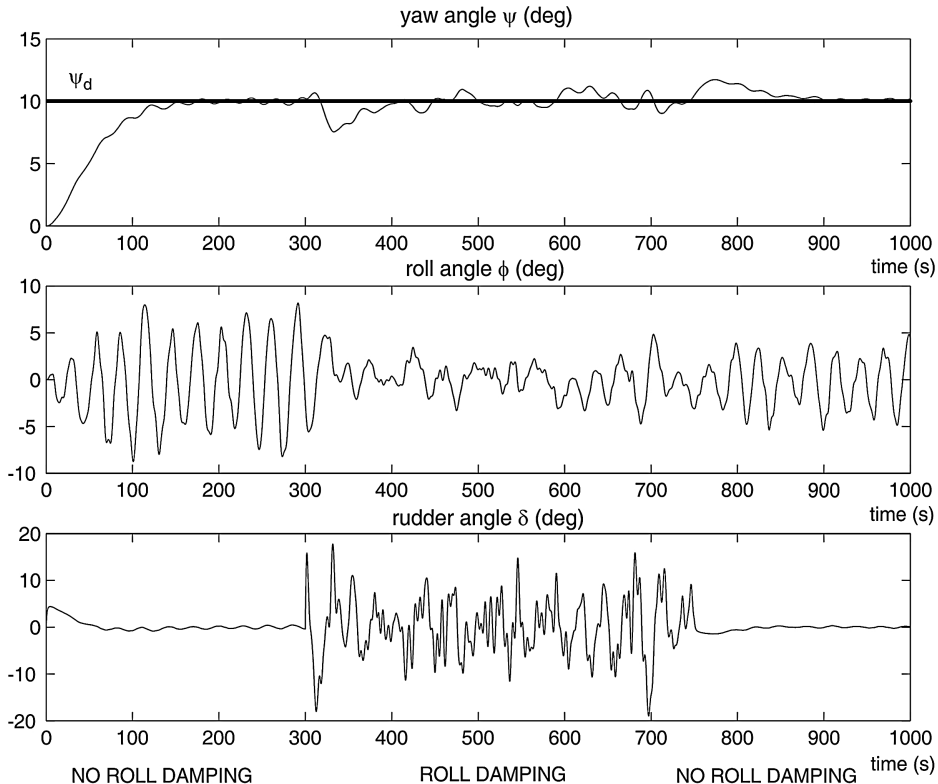


**Figure 13.5** Performance of RRD control system during course-keeping and a  $10^\circ$  course-changing maneuver. The RRD system is active between  $t = 300\text{--}700\text{ s}$ .

and  $H_\infty$  design techniques have been presented by Hearns *et al.* (2000), while the performance of classical PID, optimized PID (Hickey *et al.*, 2000) and  $H_\infty$  controllers are compared in Katebi *et al.* (2000). Sea trials with the *MV Barfleur* using PID and  $H_\infty$  controllers are presented in Hickey *et al.* (1997) and experimental results with a fin and RRD control system onboard a frigate-size Royal Naval warship are reported in Sharif *et al.* (1995, 1996).

Reduction of vertical accelerations of fast ferries using fins and a T-foil is discussed by Esteban *et al.* (2000) and Giron-Sierra *et al.* (2001), while the modeling and identification results are reported in de-la-Cruz *et al.* (1998) and Aranda *et al.* (2000).

Fin stabilizers are useful for roll reduction since they are highly effective, work on a large number of ships and are more easier to control than RRD systems, even for varying load conditions and actuator configurations. Fin stabilizers are effective at high speed, but at the price of additional drag and added noise. The most economical systems are retractable fins, where additional drag is avoided during normal operation, since fin stabilizers are not needed in moderate weather. Another advantageous feature of fin stabilizing systems is that they can be used to control  $\phi$  to a nonzero value (heel control). This is impossible with an RRD control system where the accurate control of  $\psi$  has priority.

Notice that a stand alone fin stabilization system can be constructed by simply removing the rudder inputs from the input matrix. When designing an LQ optimal fin and RRD system the following model representations can be used:

$$\mathbf{M}\dot{\mathbf{v}} + \mathbf{D}\mathbf{v} = \boldsymbol{\tau} \quad (13.136)$$

where

$$\boldsymbol{\tau} = \mathbf{T}\mathbf{f}, \quad \mathbf{f} = \mathbf{K}\mathbf{u} \quad (13.137)$$

In this representation,  $\mathbf{K}$  is the diagonal matrix of force coefficients and  $\mathbf{T}$  is the actuator configuration matrix (see Section 12.3). We can premultiply (13.136) with  $\mathbf{M}^{-1}$  to obtain

$$\dot{\mathbf{v}} = \underbrace{-\mathbf{M}^{-1}\mathbf{D}}_{\text{upper left part of } A \text{ in (7.138)}} \mathbf{v} + \underbrace{\mathbf{M}^{-1}\mathbf{T}\mathbf{K}}_{\text{upper part of } \mathbf{B} \text{ in (7.138)}} \mathbf{u} \quad (13.138)$$

In the first representation, the generalized force  $\boldsymbol{\tau}$  is used as the control input while the last representation uses  $\mathbf{u}$ , that is propeller rpm, rudder angles and fin angles. In practice it is advantageous to use (13.136) instead of (13.138), since actuator failures can be handled independently by the control allocation algorithm without redesigning the control law. Notice that the  $\mathbf{B}$  matrix in (13.138) depends on  $\mathbf{T}$  and  $\mathbf{K}$  while these matrices are not used in (13.136); see Section 12.3.

### Energy Optimal Criterion for Combined Fin and RRD

It is possible to derive LQ controllers for both models (13.136) and (13.138). This is demonstrated by considering a ship equipped with  $r_1$  rudders and  $r_2$  fins. The total number of actuators is  $r = r_1 + r_2$ , implying that  $\mathbf{u} \in \mathbb{R}^r$ . The DOFs considered are *sway*, *roll* and *yaw*; that is  $n = 3$ . Consequently,  $\mathbf{v} = [v, p, r]^\top \in \mathbb{R}^n$ . It is also assumed that the ship is fully actuated such that  $r \geq n$ . The generalized forces are

$$\begin{aligned} \boldsymbol{\tau} &= \mathbf{T}\mathbf{f} \\ &= \mathbf{T}\mathbf{K}\mathbf{u} \end{aligned} \quad (13.139)$$

It is advantageous to solve for the optimal control force  $\boldsymbol{\tau}$  and then use control allocation to compute  $\mathbf{u}$ . For most systems the inverse (see `alloc.m` in the Matlab MSS toolbox)

$$\mathbf{u} = \mathbf{K}^{-1}\mathbf{T}_w^\dagger \boldsymbol{\tau} \quad (13.140)$$

exists. An energy optimal criterion weighting  $f$ ,  $u$  or  $\tau$  against accurate tracking and roll damping is

$$\begin{aligned}
 J &= \min_f \left\{ \frac{1}{2} \int_0^T (\mathbf{e}^\top \mathbf{Q} \mathbf{e} + \mathbf{f}^\top \mathbf{R}_f \mathbf{f}) d\tau \right\} \\
 &= \min_u \left\{ \frac{1}{2} \int_0^T (\mathbf{e}^\top \mathbf{Q} \mathbf{e} + \mathbf{u}^\top \underbrace{\mathbf{K}^\top \mathbf{R}_f \mathbf{K}}_{\mathbf{R}_u} \mathbf{u}) d\tau \right\} \\
 &= \min_\tau \left\{ \frac{1}{2} \int_0^T (\mathbf{e}^\top \mathbf{Q} \mathbf{e} + \boldsymbol{\tau}^\top \underbrace{(\mathbf{T}_w^\dagger)^\top \mathbf{R}_u \mathbf{T}_w}_{\mathbf{R}_\tau} \boldsymbol{\tau}) d\tau \right\}
 \end{aligned} \tag{13.141}$$

where  $\mathbf{e} = \mathbf{y} - \mathbf{y}_d$ . The elements in  $\mathbf{Q} = \text{diag}\{Q_p, Q_r, Q_\phi, Q_\psi\} \geq 0$  are used to weight accurate steering against roll damping. The rudder and fin servos are weighted against each other by specifying the elements in  $\mathbf{R}_f = \text{diag}\{R_{\delta 1}, R_{\delta 2}, \dots, R_{\delta r_1}, R_{f1}, R_{f2}, \dots, R_{fr_2}\} > 0$ . If  $r_1 = 0$  and  $R_{\delta 1} = R_{\delta 2} = \dots = R_{\delta r_1} = 0$  only fin stabilization is obtained (no rudders).

The control weights satisfy

$$\mathbf{R}_u = \mathbf{K}^\top \mathbf{R}_f \mathbf{K}, \quad \mathbf{R}_\tau = (\mathbf{T}_w^\dagger)^\top \mathbf{R}_f \mathbf{T}_w^\dagger \tag{13.142}$$

The solution to the LQ problem (13.141) with  $\boldsymbol{\tau}$  as the control variable is (see Section 13.1.3)

$$\boldsymbol{\tau} = \mathbf{G}_1 \mathbf{x} + \mathbf{G}_2 \mathbf{y}_d \tag{13.143}$$

$$\mathbf{G}_1 = -[(\mathbf{T}_w^\dagger)^\top \mathbf{R}_f \mathbf{T}_w^\dagger]^{-1} \mathbf{B}^\top \mathbf{P}_\infty \tag{13.144}$$

$$\mathbf{G}_2 = -[(\mathbf{T}_w^\dagger)^\top \mathbf{R}_f \mathbf{T}_w^\dagger]^{-1} \mathbf{B}^\top (\mathbf{A} + \mathbf{B}\mathbf{G}_1)^{-\top} \mathbf{C}^\top \mathbf{Q} \tag{13.145}$$

where  $\mathbf{Q}$  and  $\mathbf{R}_f$  are design matrices while  $\mathbf{P}_\infty = \mathbf{P}_\infty^\top > 0$  is given by

$$\mathbf{P}_\infty \mathbf{A} + \mathbf{A}^\top \mathbf{P}_\infty - \mathbf{P}_\infty \mathbf{B} [(\mathbf{T}_w^\dagger)^\top \mathbf{R}_f \mathbf{T}_w^\dagger]^{-1} \mathbf{B}^\top \mathbf{P}_\infty + \mathbf{C}^\top \mathbf{Q} \mathbf{C} = \mathbf{0} \tag{13.146}$$

### Operability and Motion Sickness Incidence Criteria

Operability criteria for manual and intellectual work as well as motion sickness are important design criteria for the evaluation of autopilot and roll damping systems. Sea-sickness is especially important in high-speed craft and ships with high vertical accelerations.

**Human Operability Limiting Criteria in Roll:** Operability limiting criteria with regard to vertical and lateral accelerations, and roll angle for the effectiveness of the crew and the passengers are given in

**Table 13.2** Criteria for effectiveness of the crew (Faltinsen, 1990)

Standard deviation (root mean square) criteria			
Vertical acceleration ( $\dot{w}$ )	Lateral acceleration ( $\dot{v}$ )	Roll angle ( $\phi$ )	Description of work
0.20 g	0.10 g	6.0 deg	Light manual work
0.15 g	0.07 g	4.0 deg	Heavy manual work
0.10 g	0.05 g	3.0 deg	Intellectual work
0.05 g	0.04 g	2.5 deg	Transit passengers
0.02 g	0.03 g	2.0 deg	Cruise liner

Table 13.2. This gives an indication on what type of work that can be expected to be carried out for different roll angles/sea states.

**ISO 2631-3:1985 Criterion for Motion Sickness Incidence:** In addition to operability, limiting criteria passenger comfort can be evaluated with respect to motion sickness. The International Organization for Standardization (ISO) motion seasickness incidence criterion is reported in ISO 2631-1 (1997). This report replaces ISO 2631-3 (1985); see <http://www.iso.ch>. The most important factors for seasickness are vertical (heave) accelerations  $a_z$  ( $\text{m/s}^2$ ), exposure time  $t$  (hours) and encounter frequency  $\omega_e$  ( $\text{rad/s}$ ). The ISO standard criterion for MSI proposes an MSI of 10 %, which means that 10 % of the passengers become seasick during  $t$  hours. The MSI curves as a function of exposure time are shown in Figure 13.6, where

$$a_z(t, \omega_e) = \begin{cases} 0.5\sqrt{2/t} & \text{for } 0.1 \text{ Hz} < \frac{\omega_e}{2\pi} \leq 0.315 \text{ Hz} \\ 0.5\sqrt{2/t} \cdot 6.8837 \left(\frac{\omega_e}{2\pi}\right)^{1.67} & \text{for } 0.315 \text{ Hz} \leq \frac{\omega_e}{2\pi} \leq 0.63 \text{ Hz} \end{cases} \quad (13.147)$$

### Matlab

The MSI curves (13.147) as functions of the exposure time are implemented in the Matlab MSS toolbox as

```
[a_z,w_e] = ISOmsi(t)
```

Figure 13.6 is generated by using the example file

```
ExMSI
```

The main limitation of the ISO criterion is that it only predicts the exceedence of the 10 % MSI point. It is also assumed that the accelerations in the CG are representative for the entire ship and that a representative wave period can be used instead of the actual wave. In many cases it is advantageous to use the extended sickness method for more accurate predictions. This method is presented below.

**Probability Integral Method for MSI:** The O'Hanlon and McCauley (1974) probability integral method is convenient to use since it produces an MSI criterion in percentage for combinations of heave acceleration  $a_z$  ( $\text{m/s}^2$ ) and frequency of encounter  $\omega_e$  ( $\text{rad/s}$ ). The MSI index is defined as the

number of sea sick people in percentage for an exposure time of two hours; see Lloyd (1989) and Lewis (1989). The criterion is as follows:

$$\text{MSI} = 100 \left[ 0.5 \pm \text{erf} \left( \frac{\pm \log_{10}(a_z/g) \mp \mu_{\text{MSI}}}{0.4} \right) \right] \quad (\%) \quad (13.148)$$

where

$$\mu_{\text{MSI}} = -0.819 + 2.32 (\log_{10} \omega_e)^2 \quad (13.149)$$

and

$$\text{erf}(x) = \text{erf}(-x) = \frac{1}{\sqrt{2\pi}} \int_0^x \exp \left( -\frac{z^2}{2} \right) dz \quad (13.150)$$

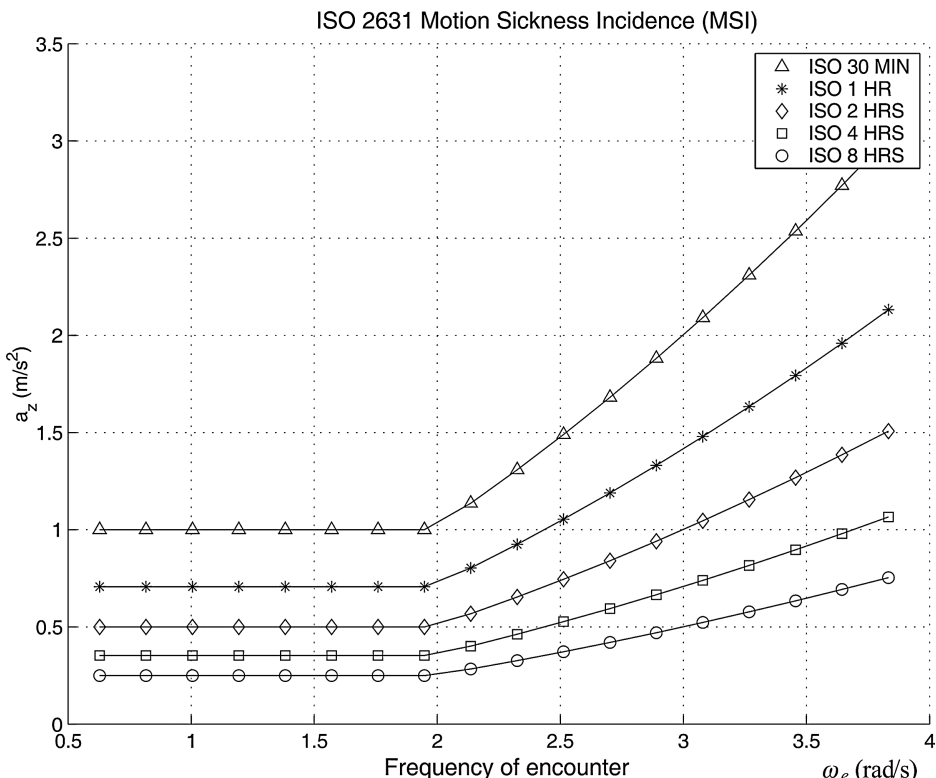


**Figure 13.6** Heave acceleration  $a_z$  ( $\text{m/s}^2$ ) as a function of frequency of encounter  $\omega_e$  ( $\text{rad/s}$ ) for different exposure times. The ISO curves represent an MSI of 10 %.

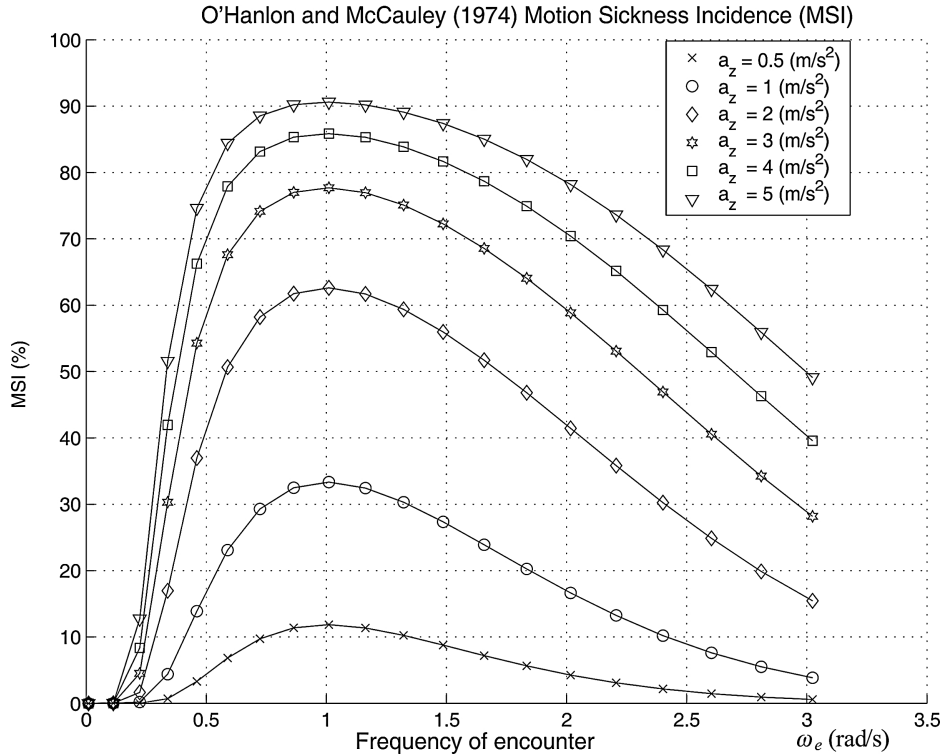


**Figure 13.7** MSI is the number of motion sick persons in percentage during a two hour exposure time as a function of encounter frequency  $\omega_e$  (rad/s) and heave acceleration  $a_z$  ( $\text{m/s}^2$ ).

### Matlab

The Matlab MSS toolbox function

```
msi = HMmsi(a_z,w_e)
```

can be used for computation of the MSI. Notice that the erf function in `HMmsi.m` is scaled differently from the Matlab function `erf.m`. The MSI curves in Figure 13.7 are plotted for different  $a_z$  and  $\omega_e$  using the example file

`ExMSI`

The major drawback of the O'Hanlon and McCauley method is that it only applies to a two hour exposure time. Another effect to take into account is that the O'Hanlon and McCauley MSI criterion is derived from tests with young men seated separately in insulated cabins. According to ISO 2631-1, the MSI number is about 1.5 higher among women and children, suggesting that the actual MSI number for passengers of average age and sex distribution should be at least 1.25 times higher.

### 13.1.6 Case Study: Optimal Dynamic Positioning System for Ships and Floating Structures

In Section 12.2.10 a nonlinear PID controller was designed for DP and the equilibrium point was rendered asymptotically stable under the assumption of full-state feedback. Output feedback in terms of a nonlinear passive observer was also discussed and UGAS of the resulting system was relying on a nonlinear separation principle (Loria *et al.*, 2000). An alternative to the nonlinear PID controller is to formulate the problem as a linear optimal control problem using vessel parallel coordinates. The LQ controller will be designed under the assumption that all states can be measured. This assumption can, however, be relaxed by combining the LQ controller with a Kalman filter for optimal state estimation; see Section 11.3.6. The resulting control law is known as the LQG optimal controller, and convergence and stability of the interconnected system can be proven using a linear separation principle (Gelb *et al.*, 1988).

**Controller Model:** Recall from Section 7.3.2 that

$$\dot{\eta}_p = v \quad (13.151)$$

$$M\dot{v} + Dv = b_p + \tau + \tau_{wind} + \tau_{wave} \quad (13.152)$$

where VP coordinates have been employed (see Section 7.5.3). The North-East positions and heading are related to  $\eta_p$  according to

$$\eta = R(\psi)\eta_p \quad (13.153)$$

In order to incorporate the limitations of the propellers, the model is augmented by actuator dynamics. The simplest way of doing this is to define three time constants in *surge*, *sway* and *yaw* such that

$$\dot{\tau} = A_{thr}(\tau - \tau_{com}) \quad (13.154)$$

where  $\tau_{com}$  is the commanded thrust and  $A_{thr} = -\text{diag}\{1/T_{surge}, 1/T_{sway}, 1/T_{yaw}\}$  is a diagonal matrix containing the time constants. The resulting state-space model becomes

$$\dot{x}_c = Ax_c + B\tau_{com} \quad (13.155)$$

where the controller states are  $x_c := [\eta_p^\top, v^\top, \tau^\top]^\top$  and

$$A = \begin{bmatrix} 0 & I & 0 \\ 0 & -M^{-1}D & M^{-1} \\ 0 & 0 & A_{thr} \end{bmatrix}, \quad B = \begin{bmatrix} 0 \\ 0 \\ -A_{thr} \end{bmatrix} \quad (13.156)$$

This model is the basis for the LQ controller.

**Observer Model:** The Kalman filter can be designed using only position and heading measurements. For this purpose the filter states are chosen as  $x_f := [\eta_p^\top, b_p^\top, v_p^\top]^\top$ . The WF model is omitted for simplicity but in an industrial system six more states should be added following the approach in

Section 11.3.6, for instance. The filter model takes the following form:

$$\dot{x}_f = Fx_f + G\tau + Ew \quad (13.157)$$

$$z = Hx_f + v \quad (13.158)$$

where

$$F = \begin{bmatrix} \mathbf{0}_{3 \times 3} & \mathbf{0}_{3 \times 3} & I_{3 \times 3} \\ \mathbf{0}_{3 \times 3} & \mathbf{0}_{3 \times 3} & \mathbf{0}_{3 \times 3} \\ \mathbf{0}_{3 \times 3} & M^{-1} & -M^{-1}D \end{bmatrix}, \quad G = \begin{bmatrix} \mathbf{0}_{3 \times 3} \\ \mathbf{0}_{3 \times 3} \\ M^{-1} \end{bmatrix}, \quad H = [I_{3 \times 3}, \mathbf{0}_{3 \times 3}, \mathbf{0}_{3 \times 3}] \quad (13.159)$$

### Controllability and Observability

It is important to be aware that the controller model must be controllable and the observer model must be observable to guarantee a stable solution for the LQG controller. These conditions can easily be verified in Matlab by considering the following example:

#### Matlab

The following example demonstrates how observability and controllability can be checked for a ship in surge, sway and yaw.

#### *Example 13.4 (Observability and Controllability of Ships)*

Consider a supply vessel with nondimensional system matrices (Fossen et al., 1996):

$$M'' = \begin{bmatrix} 1.1274 & 0 & 0 \\ 0 & 1.8902 & -0.0744 \\ 0 & -0.0744 & 0.1278 \end{bmatrix}, D'' = \begin{bmatrix} 0.0358 & 0 & 0 \\ 0 & 0.1183 & -0.0124 \\ 0 & -0.0041 & 0.0308 \end{bmatrix} \quad (13.160)$$

These values are defined in accordance to the bis system (see Section 7.2.5) such that

$$M = mT^{-2}(TM''T^{-1}), \quad D = m\sqrt{g/L} T^{-2}(TD''T^{-1}) \quad (13.161)$$

where  $T = \text{diag}\{1, 1, L\}$ . Assume that  $A_{\text{thr}} = -1/100 \times I_{3 \times 3}$ . The linear state-space model in surge, sway and yaw is computed as

$$A = \begin{bmatrix} \mathbf{0}_{3 \times 3} & I_{3 \times 3} & \mathbf{0}_{3 \times 3} \\ \mathbf{0}_{3 \times 3} & -M^{-1}D & M^{-1} \\ \mathbf{0}_{3 \times 3} & \mathbf{0}_{3 \times 3} & A_{\text{thr}} \end{bmatrix}, \quad B = \begin{bmatrix} \mathbf{0}_{3 \times 3} \\ \mathbf{0}_{3 \times 3} \\ -A_{\text{thr}} \end{bmatrix} \quad (13.162)$$

$$F = \begin{bmatrix} \mathbf{0}_{3 \times 3} & \mathbf{0}_{3 \times 3} & I_{3 \times 3} \\ \mathbf{0}_{3 \times 3} & \mathbf{0}_{3 \times 3} & \mathbf{0}_{3 \times 3} \\ \mathbf{0}_{3 \times 3} & M^{-1} & -M^{-1}D \end{bmatrix}, \quad H = [I_{3 \times 3}, \mathbf{0}_{3 \times 3}, \mathbf{0}_{3 \times 3}]$$

Notice that only the positions ( $N$ ,  $E$ ) and yaw angle  $\psi$  are defined as the outputs for the observer. Observability and controllability can be checked in Matlab using the commands (see `ExObsCtr.m`):

```
n_obs = rank(obsv(F, H))
n_ctr = rank(ctrb(A, B))
```

Since  $n_{\text{obs}} = n_{\text{ctr}} = 9$  the supply vessel is both observable and controllable.

Since the supply vessel is controllable, it is straightforward to design an optimal control law with wind feedforward and integral action. In order to do this, it is convenient to split the control input into two parts:

$$\boldsymbol{\tau}_{\text{com}} = \boldsymbol{\tau}_{\text{LQ}} - \hat{\boldsymbol{\tau}}_{\text{wind}} \quad (13.163)$$

where  $\boldsymbol{\tau}_{\text{LQ}}$  is the optimal feedback and  $\hat{\boldsymbol{\tau}}_{\text{wind}}$  is an estimate of the generalized wind forces that can be implemented using (12.214).

### Optimal Feedback Control

The LQ control objective is to obtain  $\boldsymbol{x} = \mathbf{0}$  such that  $\boldsymbol{\eta}_p = \boldsymbol{v} = \boldsymbol{\tau} = \mathbf{0}$ . This is achieved by minimizing the performance index:

$$J = \min_{\boldsymbol{\tau}_{\text{LQ}}} \left\{ \frac{1}{2} \int_0^T (\boldsymbol{x}^\top \boldsymbol{Q} \boldsymbol{x} + \boldsymbol{\tau}_{\text{LQ}}^\top \boldsymbol{R} \boldsymbol{\tau}_{\text{LQ}}) d\tau \right\} \quad (13.164)$$

where  $\boldsymbol{R} = \boldsymbol{R}^\top > 0$  and  $\boldsymbol{Q} = \boldsymbol{Q}^\top \geq 0$  are two cost matrices to be specified by the user. The  $\boldsymbol{Q}$  matrix is defined as  $\boldsymbol{Q} := \text{diag}\{\boldsymbol{Q}_1, \boldsymbol{Q}_2, \boldsymbol{Q}_3\}$  where the weights  $\boldsymbol{Q}_1$ ,  $\boldsymbol{Q}_2$  and  $\boldsymbol{Q}_3$  put penalty on position and heading  $\boldsymbol{\eta}_p$ , velocity  $\boldsymbol{v}$  and actuator dynamics  $\boldsymbol{\tau}$ , respectively. The optimal control law minimizing (13.164) is (see Section 13.1.1)

$$\boldsymbol{\tau}_{\text{LQ}} = \underbrace{-\boldsymbol{R}^{-1} \boldsymbol{B}^\top \boldsymbol{P}_\infty}_{G} \boldsymbol{x} \quad (13.165)$$

where  $\boldsymbol{P}_\infty$  is the solution of the ARE:

$$\boldsymbol{P}_\infty \boldsymbol{A} + \boldsymbol{A}^\top \boldsymbol{P}_\infty - \boldsymbol{P}_\infty \boldsymbol{B} \boldsymbol{R}^{-1} \boldsymbol{B}^\top \boldsymbol{P}_\infty + \boldsymbol{Q} = \mathbf{0} \quad (13.166)$$

### Integral Action

In order to obtain zero steady-state errors in *surge*, *sway* and *yaw*, integral action must be included in the control law. Integral action can be obtained by using state augmentation. Since we want the three outputs  $(N, E, \psi)$  to be regulated to zero, no more than three integral states can be augmented to the system. Define a new state variable:

$$z := \int_0^t y(\tau) d\tau \implies \dot{z} = y \quad (13.167)$$

Here  $y$  is a subspace of  $\boldsymbol{x}$  given by

$$\boldsymbol{y} = \boldsymbol{C} \boldsymbol{x} \quad (13.168)$$

with

$$\boldsymbol{C} = \begin{bmatrix} \boldsymbol{I}_{3 \times 3} & \mathbf{0}_{3 \times 3} & \mathbf{0}_{3 \times 3} \end{bmatrix} \quad (13.169)$$

Next consider an augmented model with state vector  $\mathbf{x}_a := [\mathbf{z}^\top, \mathbf{x}^\top]^\top$  such that

$$\dot{\mathbf{x}}_a = \mathbf{A}_a \mathbf{x}_a + \mathbf{B}_a \boldsymbol{\tau}_{\text{com}} \quad (13.170)$$

where

$$\mathbf{A}_a = \begin{bmatrix} \mathbf{0}_{3 \times 3} & \mathbf{C} \\ \mathbf{0}_{9 \times 3} & \mathbf{A} \end{bmatrix}, \quad \mathbf{B}_a = \begin{bmatrix} \mathbf{0}_{3 \times 3} \\ \mathbf{B} \end{bmatrix} \quad (13.171)$$

### Matlab

Controllability of the augmented system  $(\mathbf{A}_a, \mathbf{B}_b)$  is checked in Matlab by using the command (see ExObsCtr.m):

```
n_ctr=rank(ctrlb(Aa,Ba))
```

which gives  $n\_ctr = 12$ . Hence, the supply vessel with additional states for integral action is controllable.

The performance index for the integral controller becomes

$$J = \min_{\boldsymbol{\tau}_{\text{LQ}}} \left\{ \frac{1}{2} \int_0^T (\mathbf{x}_a^\top \mathbf{Q}_a \mathbf{x}_a + \boldsymbol{\tau}_{\text{LQ}}^\top \mathbf{R} \boldsymbol{\tau}_{\text{LQ}}) d\tau \right\} \quad (13.172)$$

where  $\mathbf{R} = \mathbf{R}^\top > 0$  and

$$\mathbf{Q}_a = \begin{bmatrix} \mathbf{Q}_I & \mathbf{0} \\ \mathbf{0} & \mathbf{Q} \end{bmatrix} \geq 0 \quad (13.173)$$

The matrix  $\mathbf{Q}_I = \mathbf{Q}_I^\top > 0$  is used to specify the integral times in *surge*, *sway* and *yaw*. The optimal PID controller is (see Section 13.1.1)

$$\boldsymbol{\tau}_{\text{LQ}} = \mathbf{G}_a \mathbf{x}_a = \mathbf{G} \mathbf{x} + \mathbf{G}_I \underbrace{\int_0^t y(\tau) d\tau}_z \quad (13.174)$$

where  $\mathbf{G}_a = [\mathbf{G}_I, \mathbf{G}]$  and

$$\mathbf{G}_a = -\mathbf{R}^{-1} \mathbf{B}_a^\top \mathbf{P}_\infty \quad (13.175)$$

$$\mathbf{P}_\infty \mathbf{A}_a + \mathbf{A}_a^\top \mathbf{P}_\infty - \mathbf{P}_\infty \mathbf{B}_a \mathbf{R}^{-1} \mathbf{B}_a^\top \mathbf{P}_\infty + \mathbf{Q}_a = \mathbf{0} \quad (13.176)$$

### LQG Control–Linear Separation Principle

In practice only some of the states are measured. A minimum requirement is that the position and heading of the craft is measured such that velocities and bias terms can be estimated by an observer. This is usually done under the assumption that the states  $\mathbf{x}$  can be replaced with the estimated states  $\hat{\mathbf{x}}$  such that the optimal integral controller (13.174) can be modified as

$$\tau_{LQ} = \mathbf{G}\hat{\mathbf{x}} + \mathbf{G}_I \mathbf{C} \int_0^t \hat{\mathbf{x}}(\tau) d\tau \quad (13.177)$$

where the state estimate  $\hat{\mathbf{x}}$  can be computed using

- Kalman filter (Section 11.3.6)
- Nonlinear passive observer (Section 11.4.1)

For the Kalman filter in cascade with the LQ controller there exists a *linear separation principle* guaranteeing that  $\hat{\mathbf{x}} \rightarrow \mathbf{x}$  and that  $\mathbf{x} \rightarrow \mathbf{0}$  (Athans and Falb, 1966). This is referred to as LQG control and it was first applied to design DP systems by Balchen *et al.* (1976, 1980a, 1980b) and Grimble *et al.* (1980a, 1980b). Optimal DP systems are used to maintain the position of offshore drilling and supply vessels (see Figure 13.8).

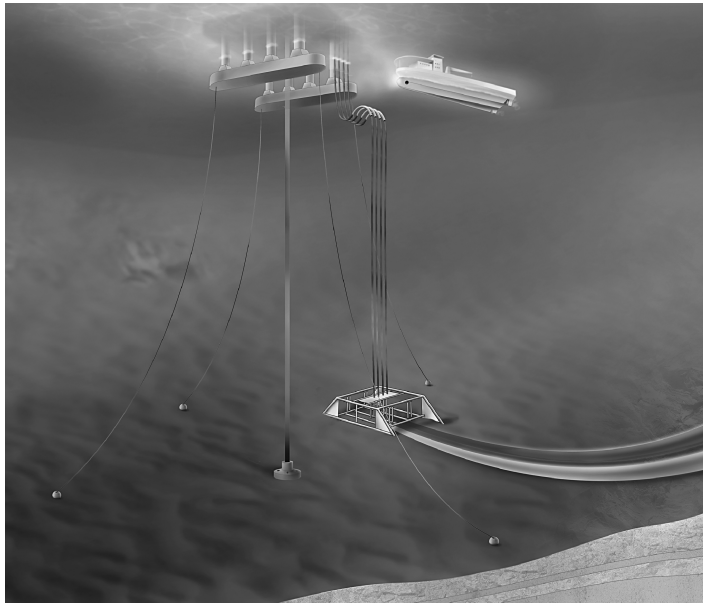


**Figure 13.8** Oil production using a dynamically positioned semi-submersible. Illustration by Bjarne Stenberg/MARINTEK.

## 13.2 State Feedback Linearization

The basic idea with feedback linearization is to transform the nonlinear system dynamics into a linear system (Freund, 1973). Feedback linearization is discussed in more detail by Isidori (1989) and Slotine and Li (1991). Conventional control techniques such as pole-placement and linear quadratic optimal control theory can then be applied to the linear system. In robotics, this technique is commonly referred to as *computed torque* control (Sciavicco and Siciliano, 1996).

Feedback linearization is easily applicable to ships and underwater vehicles since these models basically are nonlinear *mass-damper-spring* systems, which can be transformed into a linear system by using a nonlinear mapping. Transformations that can be used for applications both in BODY and NED coordinates will be presented. Trajectory-tracking control in the BODY frame is used for velocity control while NED frame applications are recognized as position and attitude control. Combined position and velocity control systems will also be discussed.

### 13.2.1 Decoupling in the BODY Frame (Velocity Control)

The control objective is to transform the marine craft dynamics into a linear system:

$$\dot{v} = a^b \quad (13.178)$$

where  $a^b$  can be interpreted as a body-fixed *commanded acceleration* vector. The body-fixed vector representation should be used to control the linear and angular velocities. Consider the nonlinear marine craft dynamics in the form

$$M\dot{v} + n(v, \eta) = \tau \quad (13.179)$$

where  $\eta$  and  $v$  are assumed to be measured and  $n$  is the nonlinear vector

$$n(v, \eta) = C(v)v + D(v)\eta + g(\eta) \quad (13.180)$$

The nonlinearities can be canceled out by simply selecting the control law as (see Figure 13.9)

$$\tau = Ma^b + n(v, \eta) \quad (13.181)$$

where the commanded acceleration vector  $a^b$  can be chosen by, for instance, pole placement or linear quadratic optimal control theory. However, note that to investigate optimality of the original system, the optimal control and cost function must be transformed back through the nonlinear mapping.

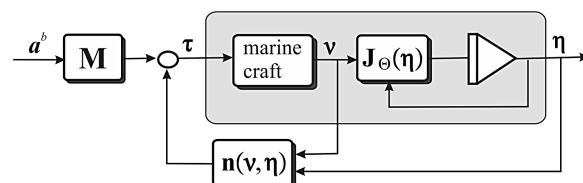


**Figure 13.9** Nonlinear decoupling in the BODY frame.

### Pole Placement

Let  $\Lambda > 0$  be a diagonal design matrix

$$\Lambda = \text{diag}\{\lambda_1, \lambda_2, \dots, \lambda_n\}$$

used to specify the desired control bandwidth,  $\mathbf{v}_d$  the desired linear and angular velocity vector and  $\tilde{\mathbf{v}} = \mathbf{v} - \mathbf{v}_d$  the velocity tracking error. Then the commanded acceleration vector can be chosen as a PI controller with acceleration feedforward:

$$\mathbf{a}^b = \dot{\mathbf{v}}_d - \mathbf{K}_p \tilde{\mathbf{v}} - \mathbf{K}_i \int_0^t \tilde{\mathbf{v}}(\tau) d\tau \quad (13.182)$$

Choosing the gains as

$$\mathbf{K}_p = 2\Lambda, \quad \mathbf{K}_i = \Lambda^2$$

yields the second-order error dynamics

$$\mathbf{M}(\ddot{\tilde{\mathbf{v}}} - \mathbf{a}^b) = \mathbf{M} \left( \ddot{\tilde{\mathbf{v}}} + 2\Lambda \tilde{\mathbf{v}} + \Lambda^2 \int_0^t \tilde{\mathbf{v}}(\tau) d\tau \right) = \mathbf{0} \quad (13.183)$$

This implies that for each DOF both poles are in  $s = -\lambda_i$  ( $i = 1, \dots, n$ ). Consequently,

$$(s + \lambda_i)^2 \int_0^t \tilde{\mathbf{v}}(\tau) d\tau = 0 \quad (i = 1, \dots, n) \quad (13.184)$$

The reference model of Section 10.2.1 can be used to generate a smooth velocity trajectory  $\mathbf{v}_d$  for trajectory-tracking control.

### 13.2.2 Decoupling in the NED Frame (Position and Attitude Control)

For position and attitude control the dynamics are decoupled in the NED reference frame. Consider

$$\ddot{\boldsymbol{\eta}} = \mathbf{a}^n \quad (13.185)$$

where  $\mathbf{a}^n$  can be interpreted as the commanded acceleration in NED. Consider the kinematic and kinetic equations in the form

$$\dot{\boldsymbol{\eta}} = \mathbf{J}_{\Theta}(\boldsymbol{\eta})\mathbf{v} \quad (13.186)$$

$$\mathbf{M}\dot{\mathbf{v}} + \mathbf{n}(\mathbf{v}, \boldsymbol{\eta}) = \boldsymbol{\tau} \quad (13.187)$$

where both  $\boldsymbol{\eta}$  and  $\mathbf{v}$  are assumed measured. Differentiation of the kinematic equation (13.186) with respect to time yields

$$\dot{\mathbf{v}} = \mathbf{J}_{\Theta}^{-1}(\boldsymbol{\eta})[\ddot{\boldsymbol{\eta}} - \dot{\mathbf{J}}_{\Theta}(\boldsymbol{\eta})\mathbf{v}] \quad (13.188)$$

The nonlinear control law

$$\tau = \mathbf{M}\mathbf{a}^b + \mathbf{n}(\mathbf{v}, \boldsymbol{\eta}) \quad (13.189)$$

applied to (13.187) yields

$$\mathbf{M}(\dot{\mathbf{v}} - \mathbf{a}^b) = \mathbf{M}\mathbf{J}_\Theta^{-1}(\boldsymbol{\eta})[\ddot{\boldsymbol{\eta}} - \dot{\mathbf{J}}_\Theta(\boldsymbol{\eta})\mathbf{v} - \mathbf{J}_\Theta(\boldsymbol{\eta})\mathbf{a}^b] = \mathbf{0} \quad (13.190)$$

Choosing

$$\mathbf{a}^n = \dot{\mathbf{J}}_\Theta(\boldsymbol{\eta})\mathbf{v} + \mathbf{J}_\Theta(\boldsymbol{\eta})\mathbf{a}^b \quad (13.191)$$

yields the linear decoupled system

$$\mathbf{M}^*(\ddot{\boldsymbol{\eta}} - \mathbf{a}^n) = \mathbf{0} \quad (13.192)$$

where  $\mathbf{M}^* = \mathbf{J}_\Theta^\top(\boldsymbol{\eta})\mathbf{M}\mathbf{J}_\Theta^{-1}(\boldsymbol{\eta}) > 0$ . From (13.191) it is seen that

$$\mathbf{a}^b = \mathbf{J}_\Theta^{-1}(\boldsymbol{\eta})[\mathbf{a}^n - \dot{\mathbf{J}}_\Theta(\boldsymbol{\eta})\mathbf{v}] \quad (13.193)$$

where the commanded acceleration  $\mathbf{a}^n$  can be chosen as a PID control law with acceleration feedforward:

$$\mathbf{a}^n = \ddot{\boldsymbol{\eta}}_d - \mathbf{K}_d \dot{\tilde{\boldsymbol{\eta}}} - \mathbf{K}_p \tilde{\boldsymbol{\eta}} - \mathbf{K}_i \int_0^t \tilde{\boldsymbol{\eta}}(\tau) d\tau \quad (13.194)$$

where  $\mathbf{K}_p$ ,  $\mathbf{K}_d$  and  $\mathbf{K}_i$  are positive definite matrices chosen such that the error dynamics

$$\ddot{\tilde{\boldsymbol{\eta}}} + \mathbf{K}_d \dot{\tilde{\boldsymbol{\eta}}} + \mathbf{K}_p \tilde{\boldsymbol{\eta}} + \mathbf{K}_i \int_0^t \tilde{\boldsymbol{\eta}}(\tau) d\tau = \mathbf{0} \quad (13.195)$$

is GES. One simple pole-placement algorithm for PID control is

$$(s + \lambda_i)^3 \int_0^t \tilde{\boldsymbol{\eta}}(\tau) d\tau = \mathbf{0} \quad (i = 1, \dots, n) \quad (13.196)$$

which yields

$$\mathbf{K}_d = 3\mathbf{\Lambda} = \text{diag}\{3\lambda_1, 3\lambda_2, \dots, 3\lambda_n\}$$

$$\mathbf{K}_p = 3\mathbf{\Lambda}^2 = \text{diag}\{3\lambda_1^2, 3\lambda_2^2, \dots, 3\lambda_n^2\}$$

$$\mathbf{K}_i = \mathbf{\Lambda}^3 = \text{diag}\{\lambda_1^3, \lambda_2^3, \dots, \lambda_n^3\}$$

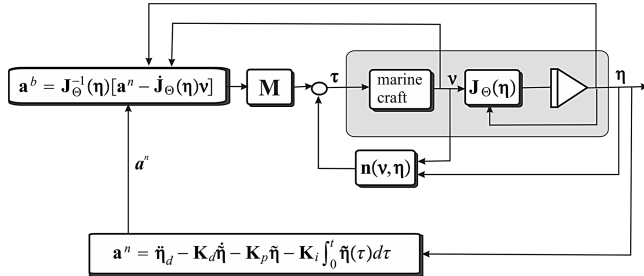


**Figure 13.10** Nonlinear decoupling in the NED frame with transformation to the BODY frame.

This is shown in Figure 13.10. When implementing the trajectory-tracking controller a third-order reference model can be used to compute smooth position and attitude trajectories  $\eta_d$  (see Section 10.2.1).

### 13.2.3 Case Study: Feedback Linearizing Speed Controller for Ships and Underwater Vehicles

Consider the following decoupled model of a ship in surge:

$$m\ddot{u} + d_1u + d_2|u|u = \tau \quad (13.197)$$

From Section 13.2.1 it follows that the commanded acceleration can be calculated as

$$a^b = \dot{u}_d - K_p(u - u_d) - K_i \int_0^t (u - u_d) d\tau \quad (13.198)$$

while the speed controller takes the following form:

$$\tau = m[\dot{u}_d - K_p(u - u_d) - K_i \int_0^t (u - u_d) d\tau] + d_1u + d_2|u|u \quad (13.199)$$

Hence, the equilibrium point of the linear system

$$\ddot{u} + K_p\ddot{u} + K_i \int_0^t \ddot{u}(\tau) d\tau = 0 \quad (13.200)$$

is GES if the gains are chosen as

$$K_p = 2\lambda \quad (13.201)$$

$$K_i = \lambda^2 \quad (13.202)$$

with  $\lambda > 0$ . In order to implement the speed controller, the following reference model can be used (see Section 10.2.1):

$$\ddot{u}_d + 2\xi\omega\dot{u}_d + \omega^2u_d = \omega^2r^b \quad (13.203)$$

where  $\xi > 0$  and  $\omega > 0$  are the reference model damping ratio and natural frequency while  $r^b$  is the setpoint specifying the desired surge speed.

### 13.2.4 Case Study: Feedback Linearizing Ship and Underwater Vehicle Autopilot

Consider the nonlinear model (Norrbom, 1963):

$$\dot{\psi} = r \quad (13.204)$$

$$m\ddot{r} + d_1\dot{r} + d_2|r|r = \tau \quad (13.205)$$

where  $\psi$  is the yaw angle. Hence, the commanded acceleration can be calculated as (Fossen and Paulsen, 1992)

$$a^n = \dot{r}_d - K_d(r - r_d) - K_p(\psi - \psi_d) - K_i \int_0^t (\psi - \psi_d) d\tau \quad (13.206)$$

where  $r_d$  is the desired yaw rate and  $\psi_d$  is the desired heading angle. For this particular example, (13.193) implies that  $a^n = a^b$ . Choosing the decoupling control law as

$$\tau = m \left[ \dot{r}_d - K_d(r - r_d) - K_p(\psi - \psi_d) - K_i \int_0^t (\psi - \psi_d) d\tau \right] + d_1r + d_2|r|r \quad (13.207)$$

finally gives the error dynamics

$$\dot{\tilde{\psi}} = \tilde{r} \quad (13.208)$$

$$\dot{\tilde{r}} + K_d\tilde{r} + K_p\tilde{\psi} = 0 \quad (13.209)$$

The reference model can be chosen as (see Section 10.2.1)

$$\dot{\psi}_d^{(3)} + (2\zeta + 1)\omega\ddot{\psi}_d + (2\zeta + 1)\omega^2\dot{\psi}_d + \omega^3\psi_d = \omega^3r^n \quad (13.210)$$

Notice that (13.207) depends on the uncertain parameters  $d_1$  and  $d_2$  while  $m$  is quite easy to estimate using hydrodynamic programs. Hence, care must be taken when implementing (13.207). For most craft, the control law (13.207) works very well even with  $d_1 = d_2 = 0$  so the need for choosing nonzero damping parameters should be seen as a trade-off between robustness and performance.

### 13.2.5 Case Study: MIMO Adaptive Feedback Linearizing Controller for Ships and Underwater Vehicles

So far only feedback linearization has been discussed under the assumption that all model parameters are *known*. This can be relaxed by using *parameter adaptation*. Consider a marine craft given by the nonlinear system

$$\dot{\eta} = J_\Theta(\eta)v \quad (13.211)$$

$$M\dot{v} + n(v, \eta) = \tau \quad (13.212)$$

Taking the control law to be

$$\tau = \hat{M}\hat{a}^b + \hat{n}(v, \eta) \quad (13.213)$$

where the *hat* denotes the adaptive parameter estimates, yields the error dynamics

$$\mathbf{M}[\dot{\mathbf{v}} - \mathbf{a}^b] = [\hat{\mathbf{M}} - \mathbf{M}]\mathbf{a}^b + [\hat{\mathbf{n}}(\mathbf{v}, \boldsymbol{\eta}) - \mathbf{n}(\mathbf{v}, \boldsymbol{\eta})] \quad (13.214)$$

If the equations of motion are linear in a parameter vector  $\boldsymbol{\theta}$ , the following parametrization can be applied:

$$[\hat{\mathbf{M}} - \mathbf{M}]\mathbf{a}^b + [\hat{\mathbf{n}}(\mathbf{v}, \boldsymbol{\eta}) - \mathbf{n}(\mathbf{v}, \boldsymbol{\eta})] = \Phi(\mathbf{a}^b, \mathbf{v}, \boldsymbol{\eta}) \tilde{\boldsymbol{\theta}} \quad (13.215)$$

Here  $\tilde{\boldsymbol{\theta}} = \hat{\boldsymbol{\theta}} - \boldsymbol{\theta}$  is the *unknown* parameter error vector and  $\Phi(\mathbf{a}^b, \mathbf{v}, \boldsymbol{\eta})$  is a *known* matrix function of measured signals usually referred to as the *regressor matrix*. Using the result  $\mathbf{a}^n = \dot{\mathbf{J}}_\Theta(\boldsymbol{\eta})\mathbf{v} + \mathbf{J}_\Theta(\boldsymbol{\eta})\mathbf{a}^b$  from (13.191) gives

$$\mathbf{M}\mathbf{J}_\Theta^{-1}(\boldsymbol{\eta})[\ddot{\mathbf{v}} - \mathbf{a}^n] = \Phi(\mathbf{a}^b, \mathbf{v}, \boldsymbol{\eta}) \tilde{\boldsymbol{\theta}} \quad (13.216)$$

Premultiplying this expression by  $\mathbf{J}_\Theta^{-T}(\boldsymbol{\eta})$  and letting  $\mathbf{M}^*(\boldsymbol{\eta}) = \mathbf{J}_\Theta^{-T}(\boldsymbol{\eta})\mathbf{M}\mathbf{J}_\Theta^{-1}(\boldsymbol{\eta})$  yields the error dynamics

$$\mathbf{M}^*(\boldsymbol{\eta})[\ddot{\mathbf{v}} - \mathbf{a}^n] = \mathbf{J}_\Theta^{-T}(\boldsymbol{\eta})\Phi(\mathbf{a}^b, \mathbf{v}, \boldsymbol{\eta}) \tilde{\boldsymbol{\theta}} \quad (13.217)$$

Furthermore, let the commanded acceleration be chosen as a PD controller with acceleration feedforward:

$$\mathbf{a}^n = \ddot{\mathbf{q}}_d - \mathbf{K}_d \dot{\tilde{\boldsymbol{\eta}}} - \mathbf{K}_p \tilde{\boldsymbol{\eta}} \quad (13.218)$$

where  $\mathbf{K}_p > 0$  and  $\mathbf{K}_d > 0$ . Hence, the error dynamics can be expressed according to

$$\mathbf{M}^*(\boldsymbol{\eta})[\ddot{\tilde{\boldsymbol{\eta}}} + \mathbf{K}_d \dot{\tilde{\boldsymbol{\eta}}} + \mathbf{K}_p \tilde{\boldsymbol{\eta}}] = \mathbf{J}_\Theta^{-T}(\boldsymbol{\eta})\Phi(\mathbf{a}^b, \mathbf{v}, \boldsymbol{\eta}) \tilde{\boldsymbol{\theta}} \quad (13.219)$$

Writing this expression in state-space form yields

$$\dot{\mathbf{x}} = \mathbf{A}\mathbf{x} + \mathbf{B}\mathbf{J}_\Theta^{-T}(\boldsymbol{\eta})\Phi(\mathbf{a}^b, \mathbf{v}, \boldsymbol{\eta}) \tilde{\boldsymbol{\theta}} \quad (13.220)$$

where  $\mathbf{x} = [\tilde{\boldsymbol{\eta}}^\top, \dot{\tilde{\boldsymbol{\eta}}}^\top]^\top$  and

$$\mathbf{A} = \begin{bmatrix} \mathbf{0} & \mathbf{I} \\ -\mathbf{K}_p & -\mathbf{K}_d \end{bmatrix}, \quad \mathbf{B} = \begin{bmatrix} \mathbf{0} \\ \mathbf{M}^*(\boldsymbol{\eta})^{-1} \end{bmatrix} \quad (13.221)$$

The convergence of  $\tilde{\boldsymbol{\eta}}$  to zero can be proven by considering

$$V(\mathbf{x}, \tilde{\boldsymbol{\theta}}, t) = \mathbf{x}^\top \mathbf{P} \mathbf{x} + \tilde{\boldsymbol{\theta}}^\top \boldsymbol{\Gamma}^{-1} \tilde{\boldsymbol{\theta}} \quad (13.222)$$

with a time-varying  $\mathbf{P} = \mathbf{P}^\top > 0$  and where  $\boldsymbol{\Gamma} = \boldsymbol{\Gamma}^\top > 0$  is a positive definite weighting matrix of appropriate dimension. Differentiating  $V$  with respect to time and substituting the error dynamics into the expression for  $\dot{V}$  yields

$$\dot{V} = \mathbf{x}^\top (\dot{\mathbf{P}} + \mathbf{P}\mathbf{A} + \mathbf{A}^\top \mathbf{P})\mathbf{x} + 2(\mathbf{x}^\top \mathbf{P}\mathbf{B}\mathbf{J}_\Theta^{-T}\Phi + \tilde{\boldsymbol{\theta}}^\top \boldsymbol{\Gamma}^{-1}) \tilde{\boldsymbol{\theta}} \quad (13.223)$$

Assume that the parameters are constant such that  $\dot{\tilde{\boldsymbol{\theta}}} = \mathbf{0}$  holds. The parameter update law is chosen as

$$\dot{\tilde{\boldsymbol{\theta}}} = -\boldsymbol{\Gamma}\Phi^\top(\mathbf{a}^b, \mathbf{v}, \boldsymbol{\eta})\mathbf{J}_\Theta^{-1}(\boldsymbol{\eta})\mathbf{y} \quad (13.224)$$

where  $\mathbf{y}$  is signal vector given by

$$\mathbf{y} = \mathbf{Cx}, \quad \mathbf{C} = \mathbf{B}^\top \mathbf{P} \quad (13.225)$$

In order to prove that  $\dot{V} \leq 0$ , let

$$\mathbf{C} = [c_0 \mathbf{I} \ c_1 \mathbf{I}] \quad (13.226)$$

where  $c_0 > 0$  and  $c_1 > 0$  are two scalars to be interpreted later. Furthermore, let

$$\mathbf{PA} + \mathbf{A}^\top \mathbf{P} = -\mathbf{Q}, \quad \mathbf{Q} = \mathbf{Q}^\top > 0 \quad (13.227)$$

where  $\mathbf{P}$  and  $\mathbf{Q}$  are defined according to Asare and Wilson (1986):

$$\mathbf{P} := \begin{bmatrix} c_0 \mathbf{M}^* \mathbf{K}_d + c_1 \mathbf{M}^* \mathbf{K}_p & c_0 \mathbf{M}^* \\ c_0 \mathbf{M}^* & c_1 \mathbf{M}^* \end{bmatrix} \quad (13.228)$$

$$\mathbf{Q} := \begin{bmatrix} 2c_0 \mathbf{M}^* \mathbf{K}_p & \mathbf{0} \\ \mathbf{0} & 2(c_1 \mathbf{M}^* \mathbf{K}_d - c_0 \mathbf{M}^*) \end{bmatrix} \quad (13.229)$$

Assume that there exists a constant  $\beta > 0$  such that

$$\mathbf{x}^\top \dot{\mathbf{P}} \mathbf{x} = \mathbf{x}^\top \begin{bmatrix} c_0 \dot{\mathbf{M}}^* \mathbf{K}_d + c_1 \dot{\mathbf{M}}^* \mathbf{K}_p & c_0 \dot{\mathbf{M}}^* \\ c_0 \dot{\mathbf{M}}^* & c_1 \dot{\mathbf{M}}^* \end{bmatrix} \mathbf{x} \leq \beta \mathbf{x}^\top \begin{bmatrix} \mathbf{M}^* & \mathbf{0} \\ \mathbf{0} & \mathbf{M}^* \end{bmatrix} \mathbf{x} \quad (13.230)$$

Hence,  $\mathbf{P} = \mathbf{P}^\top > 0$ ,  $c_0 > 0$ ,  $c_1 > 0$  and  $\mathbf{x}^\top \mathbf{Q} \mathbf{x} > \mathbf{x}^\top \dot{\mathbf{P}} \mathbf{x}$  implies that

$$\dot{V} = \mathbf{x}^\top (\dot{\mathbf{P}} - \mathbf{Q}) \mathbf{x} \leq 0 \quad (13.231)$$

if the following requirements are satisfied:

- (i)  $(c_0 \mathbf{K}_d + c_1 \mathbf{K}_p)c_1 > c_0^2 \mathbf{I}$
- (ii)  $2c_0 \mathbf{K}_p > \beta \mathbf{I}$
- (iii)  $2(c_1 \mathbf{K}_d - c_0 \mathbf{I}) > \beta \mathbf{I}$

Here  $\beta$  is usually taken to be a small positive constant while  $\mathbf{K}_p > 0$  and  $\mathbf{K}_d > 0$  can be chosen as diagonal matrices. Consequently, convergence of  $\tilde{\eta}$  and  $\dot{\tilde{\eta}}$  to zero is guaranteed by applying *Barbălat's lemma* (Barbălat, 1959); see Appendix A.2. It is also seen that the parameter vector  $\tilde{\theta}$  will be bounded but not necessarily convergent.

Adaptive feedback linearization has been applied to the ship autopilot control problem by Fossen and Paulsen (1992). The assumption that  $\mathbf{x}^\top \dot{\mathbf{P}} \mathbf{x}$  is bounded by a positive constant  $\beta$  can be relaxed by using adaptive slide-mode control where the skew-symmetric property  $\mathbf{x}^\top [\dot{\mathbf{M}} - 2\mathbf{C}(\mathbf{v})] \mathbf{x} = \mathbf{0}$  is exploited (see Slotine and Benedetto, 1990, Fossen, 1993).

### 13.3 Integrator Backstepping

Backstepping is a design methodology for construction of a feedback control law through a *recursive* construction of a control Lyapunov function. Nonlinear backstepping designs are strongly related to feedback linearization. However, while feedback linearization methods cancel all nonlinearities in the system it will be shown that when applying the backstepping design methodology more design flexibility is obtained. In particular, the designer is given the possibility to exploit “good” nonlinearities while “bad” nonlinearities can be dominated by adding nonlinear damping, for instance. Hence, additional robustness

is obtained, which is important in industrial control systems since cancelation of all nonlinearities requires precise models that are difficult to obtain in practice.

### 13.3.1 A Brief History of Backstepping

The idea of integrator backstepping seems to have appeared simultaneously, often implicit, in the works of Koditschek (1987), Sonntag and Sussmann (1988), Tsinias (1989) and Byrnes and Isidori (1989). Stabilization through an integrator (Kokotovic and Sussmann, 1989) can be viewed as a special case of stabilization through an SPR transfer function, which is a frequently used technique in the early adaptive designs (see Parks, 1966, Landau, 1979, Narendra and Annaswamy, 1989). Extensions to nonlinear cascades by using passivity arguments have been done by Ortega (1991) and Byrnes *et al.* (1991). Integrator backstepping appeared as a recursive design technique in Saberi *et al.* (1990) and was further developed by Kanellakopoulos *et al.* (1992). The relationship between backstepping and passivity has been established by Lozano *et al.* (1992). For the interested reader, a tutorial overview of backstepping is given in Kokotovic (1991).

Adaptive and nonlinear backstepping designs are described in detail by Krstic *et al.* (1995). This includes methods for parameter adaptation, tuning functions and modular designs for both full-state feedback and output feedback (observer backstepping). Sepulchre *et al.* (1997) make extensions to forwarding, passivity and cascaded designs. Also discussions on stability margins and optimality are included. The concept of vectorial backstepping was first introduced by Fossen and Berge (1997). Vectorial backstepping exploits the structural properties of nonlinear MIMO systems and this simplifies design and analysis significantly.

Krstic and Deng (1998) present stochastic systems with a focus on stochastic stability and regulation.

The focus of this section is practical designs with implementation considerations for mechanical systems. This is done by exploiting the nonlinear system properties of mechanical systems such as dissipativity (good damping), symmetry of the inertia matrix and the skew-symmetric property of the Coriolis and centripetal matrix. In addition, emphasis is placed on control design with integral action. Two techniques for integral action in nonlinear systems using backstepping designs are discussed (see Loria *et al.*, 1999, Fossen *et al.*, 2001).

### 13.3.2 The Main Idea of Integrator Backstepping

Integrator backstepping is a *recursive* design technique using *control Lyapunov functions (CLF)*. The CLF concept is a generalization of Lyapunov design results by, for instance, Jacobson (1977) and Jurdjevic and Quinn (1978).

#### **Definition 13.2 (Control Lyapunov Function)**

A smooth positive definite and radially unbounded function  $V : \mathbb{R}^n \rightarrow \mathbb{R}_+$  is called a *control Lyapunov function* for (see Arstein, 1983, Sontag, 1983)

$$\dot{x} = f(x, u) \quad (13.232)$$

where  $x \in \mathbb{R}^n$  and  $u \in \mathbb{R}^r$  if

$$\inf_{u \in \mathbb{R}^r} \left\{ \frac{\partial V}{\partial x}(x) f(x, u) \right\} < 0, \quad \forall x \neq 0 \quad (13.233)$$

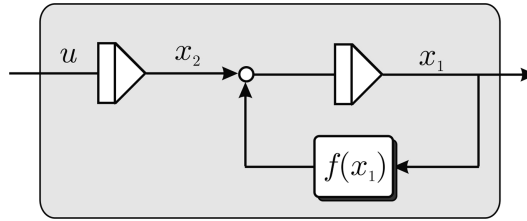


**Figure 13.11** Second-order nonlinear system with one single nonlinearity  $f(x_1)$  and a pure integrator at the input.

The main idea of integrator backstepping can be demonstrated by considering a simple nonlinear scalar system:

$$\dot{x}_1 = f(x_1) + x_2 \quad (13.234)$$

$$\dot{x}_2 = u \quad (13.235)$$

$$y = x_1 \quad (13.236)$$

where  $x_1 \in \mathbb{R}$ ,  $x_2 \in \mathbb{R}$ ,  $y \in \mathbb{R}$  and  $u \in \mathbb{R}$ . The second equation represents a pure integrator (see Figure 13.11).

Let the design objective be regulation of  $y \rightarrow 0$  as  $t \rightarrow \infty$ . The only equilibrium point with  $y = 0$  is  $(x_1, x_2) = (0, -f(0))$  corresponding to  $\dot{x}_1 = f(0) + x_2 = 0$ . The design objective is to render the equilibrium point GAS or GES. Since the nonlinear system (13.234)–(13.235) consists of two states  $x_1$  and  $x_2$ , this will be a recursive design in two steps. Equations (13.234)–(13.235) are therefore treated as two cascaded systems, each with a single input and output. The recursive design starts with the system  $x_1$  and continues with  $x_2$ . A change of coordinates

$$z = \phi(x) \quad (13.237)$$

is introduced during the recursive design process where  $z$  is a new state vector and  $\phi(x) : \mathbb{R}^n \rightarrow \mathbb{R}^n$  is a transformation to be interpreted later. The backstepping transformation is a *global diffeomorphism*, that is a mapping with smooth functions  $\phi(x)$  and  $\phi^{-1}(x)$ . Hence, the existence of an inverse transformation

$$x = \phi^{-1}(z) \quad (13.238)$$

is guaranteed.

**Step 1:** For the first system (13.234) the state  $x_2$  is chosen as a *virtual control* input while it is recalled that our design objective is to regulate the output  $y = x_1$  to zero. Hence, the first backstepping variable is chosen as

$$z_1 = x_1 \quad (13.239)$$

The virtual control is defined as

$$x_2 := \alpha_1 + z_2 \quad (13.240)$$

where

$\alpha_1$  = stabilizing function  
 $z_2$  = new state variable

Hence, the  $z_1$  system can be written

$$\dot{z}_1 = f(z_1) + \alpha_1 + z_2 \quad (13.241)$$

The new state variable  $z_2$  will not be used in the first step, but its presence is important since  $z_2$  is needed to couple the  $z_1$  system to the next system, that is the  $z_2$  system to be considered in the next step. Moreover, integrator backstepping implies that the coordinates during the recursive design are changed from  $x = [x_1, x_2]^\top$  to  $z = [z_1, z_2]^\top$ .

A CLF for the  $z_1$  system is

$$V_1 = \frac{1}{2}z_1^2 \quad (13.242)$$

$$\begin{aligned} \dot{V}_1 &= z_1 \dot{z}_1 \\ &= z_1(f(z_1) + \alpha_1) + z_1 z_2 \end{aligned} \quad (13.243)$$

We now turn our attention to the design of the stabilizing function  $\alpha_1$  which will provide the necessary feedback for the  $z_1$  system. For instance, choosing the stabilizing function as a feedback linearizing controller

$$\alpha_1 = -f(z_1) - k_1 z_1 \quad (13.244)$$

where  $k_1 > 0$  is the feedback gain, yields

$$\dot{V}_1 = -k_1 z_1^2 + z_1 z_2 \quad (13.245)$$

and

$$\dot{z}_1 = -k_1 z_1 + z_2 \quad (13.246)$$

A block diagram showing the stabilizing function and the new state variable is shown in Figure 13.12. Hence, if  $z_2 = 0$  then the  $z_1$  system is stabilized. We now turn our attention to the  $z_2$  system.

**Step 2:** The  $z_2$  dynamics is computed by time differentiation of (13.240):

$$\begin{aligned} \dot{z}_2 &= \dot{x}_2 - \dot{\alpha}_1 \\ &= u - \dot{\alpha}_1 \end{aligned} \quad (13.247)$$

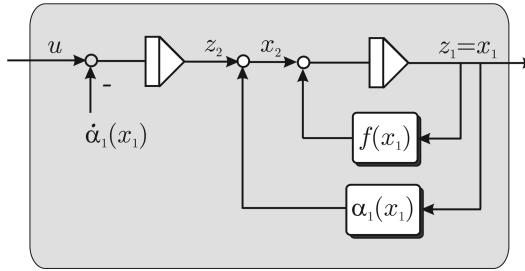


**Figure 13.12** Stabilization of the  $x_1$  system by means of the stabilizing function  $\alpha_1 = \alpha_1(x_1)$ . Note that  $-\dot{\alpha}_1(x_1)$  when integrated cancels out the feedback term  $\alpha_1(x_1)$ .

A CLF for the  $z_2$  system is

$$V_2 = V_1 + \frac{1}{2}z_2^2 \quad (13.248)$$

$$\begin{aligned} \dot{V}_2 &= \dot{V}_1 + \dot{z}_2 z_2 \\ &= (-k_1 z_1^2 + z_1 z_2) + \dot{z}_2 z_2 \\ &= -k_1 z_1^2 + z_2(z_1 + \dot{z}_2) \\ &= -k_1 z_1^2 + z_2(u - \dot{\alpha}_1 + z_1) \end{aligned} \quad (13.249)$$

Since our system has relative degree two, the control input  $u$  appears in the second step (see Figure 13.13). Hence, choosing the control law as

$$u = \dot{\alpha}_1 - z_1 - k_2 z_2 \quad (13.250)$$

with  $k_2 > 0$  yields

$$\dot{V}_2 = -k_1 z_1^2 - k_2 z_2^2 < 0, \quad \forall z_1 \neq 0, z_2 \neq 0 \quad (13.251)$$

### Implementation Aspects

When implementing the control law (13.250) it is important to avoid expressions involving the time derivatives of the states. For this simple system only  $\dot{\alpha}_1$  must be evaluated. This can be done by

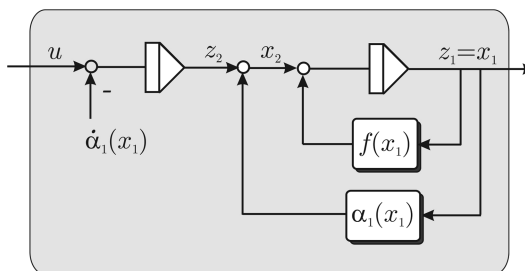


**Figure 13.13** Stabilization of the  $x_2$  system by means of the control input  $u = u(\dot{\alpha}_1, z_1, z_2)$ .

time differentiation of  $\alpha_1(x_1)$  along the trajectory of  $x_1$ . Hence,  $\dot{\alpha}_1$  can be computed without using the state derivatives:

$$\begin{aligned}\dot{\alpha}_1 &= -\frac{\partial f(x_1)}{\partial x_1} \dot{x}_1 - k_1 \dot{x}_1 \\ &= -\left(\frac{\partial f(x_1)}{\partial x_1} + k_1\right) (f(x_1) + x_2)\end{aligned}\quad (13.252)$$

The final expression for the control law is then

$$u = -\left(\frac{\partial f(x_1)}{\partial x_1} + k_1\right) (f(x_1) + x_2) - x_1 - k_2(x_2 + f(x_1) + k_1 x_1) \quad (13.253)$$

If  $f(x_1) = -x_1$  (linear theory), it is seen that

$$\begin{aligned}u &= -(-1 + k_1)(-x_1 + x_2) - x_1 - k_2(x_2 - x_1 + k_1 x_1) \\ &= -\underbrace{(2 + k_1 k_2 - k_1 - k_2)}_{K_p} x_1 - \underbrace{(k_1 + k_2 - 1)}_{K_d} x_2\end{aligned}\quad (13.254)$$

which is a standard PD control law. In general, the expression for  $u$  is a nonlinear feedback control law depending on the nonlinear function  $f(x_1)$ .

### Backstepping Coordinate Transformation

The backstepping coordinate transformation  $z = \phi(x)$  takes the form

$$\begin{bmatrix} z_1 \\ z_2 \end{bmatrix} = \begin{bmatrix} x_1 \\ x_2 + f(x_1) + k_1 x_1 \end{bmatrix} \quad (13.255)$$

while the inverse transformation  $x = \phi^{-1}(z)$  is

$$\begin{bmatrix} x_1 \\ x_2 \end{bmatrix} = \begin{bmatrix} z_1 \\ z_2 - f(z_1) - k_1 z_1 \end{bmatrix} \quad (13.256)$$

### The Final Check

If you have performed the backstepping design procedure correctly the dynamics of the closed-loop system in  $(z_1, z_2)$  coordinates can always be written as the sum of a diagonal and skew-symmetric matrix times the state vector. This can be seen by writing the resulting dynamics in the form

$$\begin{bmatrix} \dot{z}_1 \\ \dot{z}_2 \end{bmatrix} = -\underbrace{\begin{bmatrix} k_1 & 0 \\ 0 & k_2 \end{bmatrix}}_{\text{diagonal matrix}} \begin{bmatrix} z_1 \\ z_2 \end{bmatrix} + \underbrace{\begin{bmatrix} 0 & 1 \\ -1 & 0 \end{bmatrix}}_{\text{skew-symmetrical matrix}} \begin{bmatrix} z_1 \\ z_2 \end{bmatrix} \quad (13.257)$$

or equivalently

$$\dot{z} = -Kz + Sz \quad (13.258)$$

where  $\mathbf{z} = [z_1, z_2]^\top$ ,  $\mathbf{K} = \text{diag}\{k_1, k_2\} > 0$  and

$$\mathbf{S} = -\mathbf{S}^\top = \begin{bmatrix} 0 & 1 \\ -1 & 0 \end{bmatrix} \quad (13.259)$$

where  $\mathbf{S}$  satisfies  $\mathbf{z}^\top \mathbf{S} \mathbf{z} = 0, \forall \mathbf{z}$ . In some cases the diagonal matrix will be a function of the state; that is  $\mathbf{K}(\mathbf{z}) > 0$ . This is the case when nonlinear damping is added or when some of the nonlinearities not are canceled by the controller.

### Investigation of Stability

It is also seen that

$$V_2 = \frac{1}{2} \mathbf{z}^\top \mathbf{z} \quad (13.260)$$

$$\begin{aligned} \dot{V}_2 &= \mathbf{z}^\top (-\mathbf{K} \mathbf{z} + \mathbf{S} \mathbf{z}) \\ &= -\mathbf{z}^\top \mathbf{K} \mathbf{z} \end{aligned} \quad (13.261)$$

Hence, Lyapunov's direct method for autonomous systems ensures that the equilibrium point  $(x_1, x_2) = (0, -f(0))$  is GAS. In fact, this system will also be GES since it can be shown that the state vector  $\mathbf{x}$  decays exponentially to zero by using Theorem A.3; that is

$$\|\mathbf{z}(t)\|_2 \leq e^{-\beta(t-t_0)} \|\mathbf{z}(t_0)\|_2 \quad (13.262)$$

where  $\beta = \lambda_{\min}(\mathbf{K}) > 0$  is the convergence rate.

A generalization to SISO mass–damper–spring systems is done in Section 13.3.3 while extensions to MIMO control are made in Section 13.3.6.

### Backstepping versus Feedback Linearization

The backstepping control law of the previous section is in fact equal to a feedback linearizing controller since the nonlinear function  $f(x_1)$  is perfectly compensated for by choosing the stabilizing function as

$$\alpha_1 = -f(x_1) - k_1 z_1 \quad (13.263)$$

The disadvantage with this approach is that a perfect model is required. This is impossible in practice. Consequently, an approach of canceling all the nonlinearities may be sensitive for modeling errors.

One of the nice features of backstepping is that the stabilizing functions can be modified to exploit so-called “good” nonlinearities. For instance, assume that

$$f(x_1) = -a_0 x_1 - a_1 x_1^2 - a_2 |x_1| x_1 \quad (13.264)$$

where  $a_0, a_1$  and  $a_2$  are assumed to be *unknown* positive constants. Since both  $a_0 x_1$  and  $a_2 |x_1| x_1$  tend to damp out the motion these two expressions should be exploited in the control design and therefore not canceled out. On the contrary, the destabilizing term  $a_1 x_1^2$  must be perfectly compensated for or dominated by adding a nonlinear damping term proportional to  $x_1^3$  (remember that  $z_1 = x_1$ ).

Nonlinear damping suggests the following candidate for the stabilizing function:

$$\alpha_1 = \underbrace{-k_1 z_1}_{\text{linear damping}} \quad \underbrace{-\kappa_1 z_1^3}_{\text{nonlinear damping}} \quad (13.265)$$

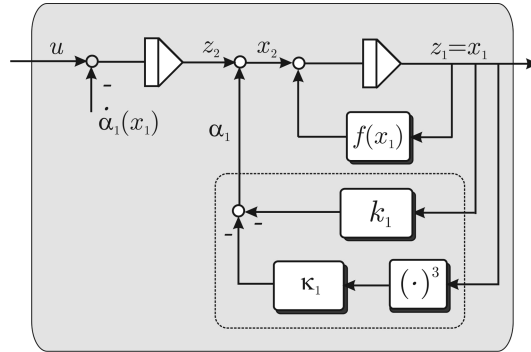


**Figure 13.14** Domination of destabilizing terms by adding nonlinear damping.

where  $k_1 > 0$  and  $\kappa_1 > 0$  (see Figure 13.14). Hence,

$$\begin{aligned}
 \dot{z}_1 &= f(z_1) + (\alpha_1 + z_2) \\
 &= -a_0 z_1 - a_1 z_1^2 - a_2 |z_1| z_1 - (k_1 + \kappa_1 z_1^2) z_1 + z_2 \\
 &= -(\underbrace{a_0 + a_2 |z_1|}_{\text{good damping}} + k_1) z_1 - \underbrace{a_1 z_1^2}_{\text{bad damping}} - \kappa_1 z_1^3 + z_2
 \end{aligned} \tag{13.266}$$

Consider the CLF:

$$V_1 = \frac{1}{2} z_1^2 \tag{13.267}$$

$$\dot{V}_1 = -(a_0 + a_2 |z_1| + k_1) z_1^2 - a_1 z_1^3 - \kappa_1 z_1^4 + z_1 z_2 \tag{13.268}$$

In the next step it is seen that

$$\begin{aligned}
 V_2 &= V_1 + \frac{1}{2} z_2^2 \\
 \dot{V}_2 &= -(\underbrace{a_0 + a_2 |z_1| + k_1}_{\text{energy dissipation}}) z_1^2 - \underbrace{a_1 z_1^3}_{\text{energy dissipation/generation}} - \kappa_1 z_1^4 + z_2(z_1 + u - \dot{\alpha}_1)
 \end{aligned}$$

From this expression it can be concluded that the good damping terms contribute to the energy dissipation. The bad damping term, however, must be dominated by the nonlinear damping term. Choosing

$$u = \dot{\alpha}_1 - k_2 z_2 - z_1 \tag{13.269}$$

finally yields

$$\dot{V}_2 = -(a_0 + a_2 |z_1| + k_1) z_1^2 - a_1 z_1^3 - \kappa_1 z_1^4 - k_2 z_2^2 \tag{13.270}$$

This expression can be rewritten by *completing the squares*. Consider the expression

$$\left( \frac{1}{2\sqrt{\kappa_1}}x + \sqrt{\kappa_1}y \right)^2 = \frac{1}{4\kappa_1}x^2 + xy + \kappa_1y^2 \geq 0 \quad (13.271)$$

⇓

$$-xy - \kappa_1y^2 = - \left( \frac{1}{2\sqrt{\kappa_1}}x + \sqrt{\kappa_1}y \right)^2 + \frac{1}{4\kappa_1}x^2 \quad (13.272)$$

Equation (13.270) with  $x = a_1z_1$  and  $y = z_1^2$  yields

$$\dot{V}_2 = - \left( \frac{a_1}{2\sqrt{\kappa_1}}z_1 + \sqrt{\kappa_1}z_1^2 \right)^2 + \frac{a_1^2}{4\kappa_1}z_1^2 - (a_0 + a_2|z_1| + k_1)z_1^2 - k_2z_2^2 \quad (13.273)$$

Since

$$\begin{aligned} - \left( \frac{a_1}{2\sqrt{\kappa_1}}z_1 + \sqrt{\kappa_1}z_1^2 \right)^2 &\leq 0 \\ -a_2|z_1| &\leq 0 \end{aligned} \quad (13.274)$$

it then follows that

$$\dot{V}_2 \leq - \left( a_0 + k_1 - \frac{a_1^2}{4\kappa_1} \right) z_1^2 - k_2 z_2^2 \quad (13.275)$$

Hence, by choosing the controller gains according to

$$\kappa_1 > 0 \quad (13.276)$$

$$k_1 > \frac{a_1^2}{4\kappa_1} - a_0 \quad (13.277)$$

$$k_2 > 0 \quad (13.278)$$

our design goal to render  $\dot{V}_2 < 0$  is satisfied. Notice that the controller (13.269) with (13.265) is implemented without using the unknown parameters  $a_0$ ,  $a_1$  and  $a_2$ . Hence, a robust nonlinear controller is derived by using backstepping. This result differs from feedback linearization, which is based on model cancelation.

### 13.3.3 Backstepping of SISO Mass–Damper–Spring Systems

The results of Section 13.3.2 can be generalized to the following class of SISO mechanical systems:

$$\dot{x} = v \quad (13.279)$$

$$m\dot{v} + d(v)v + k(x)x = \tau \quad (13.280)$$

$$y = x \quad (13.281)$$

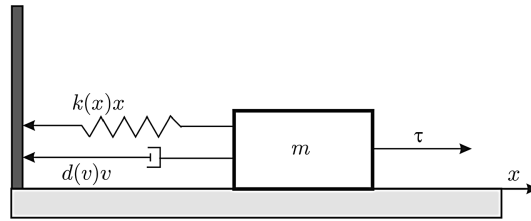


**Figure 13.15** Nonlinear mass–damper–spring system.

where \$x\$ is the position, \$v\$ is the velocity and

$$\begin{aligned} m &= \text{mass (positive)} \\ d(v) &= \text{nonlinear damper (non-negative)} \\ k(x) &= \text{nonlinear spring (non-negative)} \end{aligned}$$

The nonlinear mass–damper–spring system is shown in Figure 13.15.

### Nonlinear Trajectory-Tracking Control

Backstepping of the mass–damper–spring can be performed by choosing the output

$$e = y - y_d \quad (13.282)$$

where \$e\$ is the tracking error and \$y\_d(t) \in C^r\$ is an \$r\$ times differentiable (smooth) and bounded reference trajectory (see Section 10.2.1). Regulation of \$y = x\$ to zero is obtained by choosing \$\dot{y}\_d = y\_d = 0\$. Time differentiation of \$e\$ yields the following model:

$$\dot{e} = v - \dot{y}_d \quad (13.283)$$

$$m\dot{v} = \tau - d(v)v - k(x)x \quad (13.284)$$

The backstepping control law solving this problem is derived in two recursive steps similar to the integrator backstepping example in Section 13.3.2.

**Step 1:** Let \$z\_1 = e = y - y\_d\$, such that

$$\dot{z}_1 = v - \dot{y}_d \quad (13.285)$$

Taking \$v\$ as *virtual control*,

$$v = \alpha_1 + z_2 \quad (13.286)$$

where \$z\_2\$ is a new state variable to be interpreted later, yields

$$\dot{z}_1 = \alpha_1 + z_2 - \dot{y}_d \quad (13.287)$$

Next, the stabilizing function \$\alpha\_1\$ is chosen as

$$\alpha_1 = \dot{y}_d - [k_1 + n_1(z_1)]z_1 \quad (13.288)$$

where  $k_1 > 0$  is a feedback gain and  $n_1(z_1) \geq 0$  is a nonlinear damping term, for instance a nonlinear nondecreasing function  $n_1(z_1) = \kappa_1 |z_1|^{n_1}$  with  $n_1 > 0$  and  $\kappa_1 \geq 0$ . This yields

$$\dot{z}_1 = -[k_1 + n_1(z_1)]z_1 + z_2 \quad (13.289)$$

A CLF for  $z_1$  is

$$V_1 = \frac{1}{2}z_1^2 \quad (13.290)$$

$$\begin{aligned} \dot{V}_1 &= z_1 \dot{z}_1 \\ &= -[k_1 + n_1(z_1)]z_1^2 + z_1 z_2 \end{aligned} \quad (13.291)$$

**Step 2:** The second step stabilizes the  $z_2$  dynamics. Moreover, from (13.286) it is seen that

$$\begin{aligned} m\dot{z}_2 &= m\dot{v} - m\dot{\alpha}_1 \\ &= \tau - d(v)v - k(x)x - m\dot{\alpha}_1 \end{aligned} \quad (13.292)$$

Let  $V_2$  be the second CLF, which is chosen to reflect the kinetic energy  $\frac{1}{2}mv^2$  of the system. However, it makes sense to replace the velocity  $v$  with  $z_2$  in order to solve the trajectory-tracking control problem. This is usually referred to as “pseudo-kinetic energy”. Consider

$$V_2 = V_1 + \frac{1}{2}mz_2^2 \quad (13.293)$$

$$\begin{aligned} \dot{V}_2 &= \dot{V}_1 + m z_2 \dot{z}_2 \\ &= -[k_1 + n_1(z_1)]z_1^2 + z_1 z_2 + z_2[\tau - d(v)v - k(x)x - m\dot{\alpha}_1] \end{aligned} \quad (13.294)$$

Since the input  $\tau$  appears in  $\dot{V}_2$ , a value for  $\tau$  can be prescribed such that  $\dot{V}_2$  becomes negative definite. For instance:

$$\tau = m\dot{\alpha}_1 + d(v)v + k(x)x - z_1 - k_2 z_2 - n_2(z_2)z_2 \quad (13.295)$$

where  $k_2 > 0$  and  $n_2(z_2) = \kappa_2 |z_2|^{n_2} \geq 0$  with  $n_2 > 0$  can be specified by the designer. This yields

$$\dot{V}_2 = -[k_1 + n_1(z_1)]z_1^2 - [k_2 + n_2(z_2)]z_2^2 \quad (13.296)$$

When implementing the control law,  $\dot{\alpha}_1$  is computed by taking the time derivative of  $\alpha_1$  along the trajectories of  $y_d$  and  $z_1$ , see (13.288), to obtain

$$\dot{\alpha}_1 = \frac{\partial \alpha_1}{\partial \ddot{y}_d} \ddot{y}_d - \frac{\partial \alpha_1}{\partial z_1} \dot{z}_1 = \ddot{y}_d - \frac{\partial \alpha_1}{\partial z_1} (v - \dot{y}_d) \quad (13.297)$$

Hence, the state derivatives are avoided in the control law. Notice that the desired state  $y_d$  is assumed to be smooth such that  $\dot{y}_d$  and  $\ddot{y}_d$  exist.

### Error Dynamics

The resulting error dynamics is written

$$\begin{aligned} \begin{bmatrix} 1 & 0 \\ 0 & m \end{bmatrix} \begin{bmatrix} \dot{z}_1 \\ \dot{z}_2 \end{bmatrix} &= - \begin{bmatrix} k_1 + n_1(z_1) & 0 \\ 0 & k_2 + n_2(z_2) \end{bmatrix} \begin{bmatrix} z_1 \\ z_2 \end{bmatrix} + \begin{bmatrix} 0 & 1 \\ -1 & 0 \end{bmatrix} \begin{bmatrix} z_1 \\ z_2 \end{bmatrix} \\ &\Downarrow \\ M\dot{z} &= -K(z)z + Sz \end{aligned} \quad (13.298)$$

where  $z = [z_1, z_2]^\top$  and

$$M = \text{diag}\{1, m\}$$

$$K(z) = \text{diag}\{k_1 + n_1(z_1), k_2 + n_2(z_2)\}$$

$$S = \begin{bmatrix} 0 & 1 \\ -1 & 0 \end{bmatrix}$$

Hence, the equilibrium point  $(z_1, z_2) = (0, 0)$  is GES. This can be seen from  $V_2(z) = \frac{1}{2}z^\top Mz$ , which after time differentiation yields  $\dot{V}_2(z) = -z^\top Kz$  since  $z^\top Sz = 0, \forall z$ . Notice that kinetic energy has been applied in the Lyapunov analysis to achieve this.

### Setpoint Regulation

Setpoint regulation is obtained by choosing  $\dot{y}_d = y_d = 0$ . For simplicity let  $n_1(z_1) = n_2(z_2) = 0$  such that

$$z_1 = x$$

$$\alpha_1 = -k_1 z_1$$

and

$$\tau = m\dot{\alpha}_1 + d(v)v + k(x)x - z_1 - k_2 z_2 \quad (13.299)$$

### Nonlinear PD Control

The backstepping control law (13.299) can also be viewed as a nonlinear PD control law:

$$u = -K_p(x)x - K_d(v)v \quad (13.300)$$

by writing (13.299) as

$$\begin{aligned} u &= [d(v) - mk_1]v + [k(x) - 1]x - k_2(v + k_1x) \\ &= [d(v) - mk_1 - k_2]v + [k(x) - 1 - k_1k_2]x \end{aligned} \quad (13.301)$$

Hence,

$$K_p(x) = k_1 k_2 + 1 - k(x) \quad (13.302)$$

$$K_d(v) = m k_1 + k_2 - d(v) \quad (13.303)$$

### Nonlinear PID Control

The nonlinear PD controller (13.300) can be extended to include integral action by using *constant parameter adaptation* or by *augmenting an additional integrator* to the plant. More specifically

1. *Constant parameter adaptation*: An unknown constant (or slowly varying) disturbance is added to the dynamic model. This constant or bias is estimated online by using adaptive control. The resulting system with parameter estimator can be shown to be UGAS for the case of regulation and trajectory-tracking control (Fossen *et al.*, 2001).
2. *Integrator augmentation*: An additional integrator is augmented on the right-hand side of the integrator chain in order to obtain zero steady-state errors. The resulting system is proven to be GES.

The methods are presented in Sections 13.3.4 and 13.3.5.

#### 13.3.4 Integral Action by Constant Parameter Adaptation

The constant parameter adaptation technique is based on Fossen *et al.* (2001). For simplicity a mass–damper–spring system is considered. Hence, adaptive backstepping results in a control law of PID type.

Consider the system:

$$\dot{x} = v \quad (13.304)$$

$$m\dot{v} + d(v)v + k(x)x = \tau + w \quad (13.305)$$

$$\dot{w} = 0 \quad (13.306)$$

The trajectory-tracking control law can be designed by considering the tracking error

$$z_1 = x - x_d \quad (13.307)$$

with

$$\begin{aligned} \dot{z}_1 &= \dot{x} - \dot{x}_d \\ &= v - \dot{x}_d \\ &= (\alpha_1 + z_2) - v_d \end{aligned} \quad (13.308)$$

where  $z_2$  is a new state variable and  $v := \alpha_1 + z_2$  is the virtual control for  $z_1$ . Choosing the stabilizing function

$$\alpha_1 = \dot{x}_d - k_1 z_1 \quad (13.309)$$

yields

$$\dot{z}_1 = -k_1 z_1 + z_2 \quad (13.310)$$

The definition  $z_2 := v - \alpha_1$  implies that

$$\dot{z}_2 = \dot{v} - \ddot{x}_d + k_1(v - \dot{x}_d) \quad (13.311)$$

$$m\dot{z}_2 = \tau - d(v)v - k(x)x + w - m\ddot{x}_d + mk_1(v - \dot{x}_d) \quad (13.312)$$

Consider the CLF:

$$V_1 = \frac{1}{2}z_1^2 + \frac{1}{2p}\tilde{w}^2, \quad p > 0 \quad (13.313)$$

$$\begin{aligned} \dot{V}_1 &= z_1\dot{z}_1 + \frac{1}{p}\tilde{w}\dot{\tilde{w}} \\ &= z_1z_2 - k_1z_1^2 + \frac{1}{p}\tilde{w}\dot{\tilde{w}} \end{aligned} \quad (13.314)$$

where  $\tilde{w} = \hat{w} - w$  is the parameter estimation error. Next, consider the CLF:

$$V_2 = V_1 + \frac{1}{2}mz_2^2 \quad (13.315)$$

$$\begin{aligned} \dot{V}_2 &= \dot{V}_1 + z_2(m\dot{z}_2) \\ &= z_1z_2 - k_1z_1^2 + \frac{1}{p}\tilde{w}\dot{\tilde{w}} \\ &\quad + z_2[\tau - d(v)v - k(x)x + w - m\ddot{x}_d + mk_1(v - \dot{x}_d)] \end{aligned} \quad (13.316)$$

where it is noticed that  $\tilde{w} = \dot{\hat{w}}$ . Choosing the control law as

$$\tau = d(v)\alpha_1 + k(x)x - \hat{w} + m\ddot{x}_d - mk_1(v - \dot{x}_d) - z_1 - k_2z_2 \quad (13.317)$$

where  $\alpha_1 = v - z_2$ , yields

$$\dot{V}_2 = -k_1z_1^2 - [k_2 + d(v)]z_2^2 + \tilde{w} \left( \frac{1}{p}\dot{\hat{w}} - z_2 \right) \quad (13.318)$$

Choosing the update law as

$$\dot{w} = pz_2 \quad (13.319)$$

finally yields

$$\dot{V}_2 = -k_1 z_1^2 - [k_2 + d(v)]z_2^2 \quad (13.320)$$

The error dynamics takes the form

$$\begin{bmatrix} \dot{z}_1 \\ \dot{z}_2 \end{bmatrix} = \begin{bmatrix} -k_1 & 1 \\ -1 & -k_2 - d(v) \end{bmatrix} \begin{bmatrix} z_1 \\ z_2 \end{bmatrix} + \begin{bmatrix} 0 \\ -1 \end{bmatrix} \tilde{w} \quad (13.321)$$

$$\dot{\tilde{w}} = -p \begin{bmatrix} 0 & -1 \end{bmatrix} \begin{bmatrix} z_1 \\ z_2 \end{bmatrix} \quad (13.322)$$

$\Updownarrow$

$$\dot{z} = \mathbf{h}(z, t) + \mathbf{b}\tilde{w} \quad (13.323)$$

$$\dot{\tilde{w}} = -p\mathbf{b}^\top \left( \frac{\partial W(z, t)}{\partial z} \right)^\top \quad (13.324)$$

Notice that the dissipative term  $d(v) = d(z_2 + \alpha_1) = d(z_2 - k_1 z_1 + \dot{x}_d(t)) > 0$ ,  $\forall v$  has not been “canceled out” in order to exploit this as good damping in the error dynamics. The price for exploiting the so-called *good nonlinearities* in the design is that the error dynamics becomes *nonautonomous*. Since the feedback gains are assumed to be positive, that is  $k_1 > 0$  and  $k_2 > 0$ ,  $p > 0$ ,  $\mathbf{b} = [0, -1]^\top$  and  $\mathbf{b}^\top \mathbf{b} = 1 > 0$ , Theorem A.6 with  $W(z) = \frac{1}{2}z^\top z$  guarantees that the nonautonomous systems (13.321)–(13.322) is UGAS.

Notice that if a feedback linearizing controller is applied instead of (13.317), replacing the damping term  $d(v)\alpha_1$  with  $d(v)v$ , the control input becomes

$$\tau = d(v)v + k(x)x - \hat{w} + m\dot{x}_d - mk_1(v - \dot{x}_d) - z_1 - k_2 z_2 \quad (13.325)$$

The error dynamics

$$\begin{bmatrix} \dot{z}_1 \\ \dot{z}_2 \end{bmatrix} = \begin{bmatrix} -k_1 & 1 \\ -1 & -k_2 \end{bmatrix} \begin{bmatrix} z_1 \\ z_2 \end{bmatrix} + \begin{bmatrix} 0 \\ -1 \end{bmatrix} \tilde{w} \quad (13.326)$$

is *autonomous*. In this case, *Krasovskii–LaSalle’s invariant set theorem* (Theorem A.2) can be used to prove GAS.

### 13.3.5 Integrator Augmentation Technique

Consider the second-order mass–damper–spring system:

$$\dot{x} = v \quad (13.327)$$

$$m\dot{v} + d(v)v + k(x)x = \tau + w \quad (13.328)$$

$$y = x \quad (13.329)$$

where  $w$  is a constant *unknown* disturbance. Let  $e$  denote the tracking error

$$e = y - y_d \quad (13.330)$$

where  $y_d$  is the desired output. Hence,

$$\dot{e} = v - \dot{y}_d \quad (13.331)$$

$$m\dot{v} + d(v)v + k(x)x = \tau + w \quad (13.332)$$

#### Nonlinear PD Control

If  $w = 0$ , backstepping results in a nonlinear control law of PD type similar to the result in Section 13.3.3. However, by augmenting the plant with an additional integrator at the right end of the integrator chain, as illustrated in Figure 13.16, nonlinear PID control can be obtained.

#### Nonlinear PID Control

Augmentation of an additional integrator  $\dot{e}_I = e$  to the second-order plant (13.331)–(13.332) yields

$$\dot{e}_I = e \quad (13.333)$$

$$\dot{e} = v - \dot{y}_d \quad (13.334)$$

$$m\dot{v} + d(v)v + k(x)x = \tau + w \quad (13.335)$$

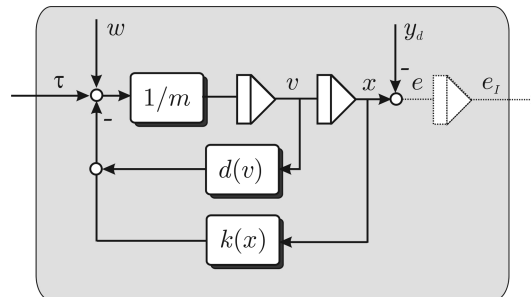


**Figure 13.16** Augmentation of an additional integrator.

For simplicity let us first assume that  $w = 0$ . Hence, backstepping with  $z_1 = e_I$  results in three steps:

### Step 1:

$$\begin{aligned}\dot{z}_1 &= e \\ &= \alpha_1 + z_2\end{aligned}\tag{13.336}$$

Choosing the stabilizing function  $\alpha_1 = -k_1 z_1$  yields

$$\dot{z}_1 = -k_1 z_1 + z_2\tag{13.337}$$

Hence,

$$V_1 = \frac{1}{2} z_1^2\tag{13.338}$$

$$\begin{aligned}\dot{V}_1 &= z_1 \dot{z}_1 \\ &= -k_1 z_1^2 + z_1 z_2\end{aligned}\tag{13.339}$$

### Step 2:

$$\begin{aligned}\dot{z}_2 &= \dot{e} - \dot{\alpha}_1 \\ &= v - \dot{y}_d - \dot{\alpha}_1 \\ &= (\alpha_2 + z_3) - \dot{y}_d - \dot{\alpha}_1\end{aligned}\tag{13.340}$$

Hence,

$$V_2 = V_1 + \frac{1}{2} z_2^2\tag{13.341}$$

$$\begin{aligned}\dot{V}_2 &= -k_1 z_1^2 + z_1 z_2 + z_2 \dot{z}_2 \\ &= -k_1 z_1^2 + z_2(z_1 + \alpha_2 + z_3 - \dot{y}_d - \dot{\alpha}_1)\end{aligned}\tag{13.342}$$

Choosing the stabilizing function  $\alpha_2 = \dot{\alpha}_1 + \dot{y}_d - k_2 z_2 - z_1$  yields

$$\dot{z}_2 = -z_1 - k_2 z_2 + z_3\tag{13.343}$$

$$\dot{V}_2 = -k_1 z_1^2 - k_2 z_2^2 + z_2 z_3\tag{13.344}$$

### Step 3:

$$\begin{aligned}m \dot{z}_3 &= m \dot{v} - m \dot{\alpha}_2 \\ &= \tau + w - d(v)v - k(x)x - m \dot{\alpha}_2 \\ &= \tau - d(v)\alpha_2 - d(v)z_3 - k(x)x - m \dot{\alpha}_2\end{aligned}\tag{13.345}$$

Let

$$V_3 = V_2 + \frac{1}{2}mz_3^2 \quad (13.346)$$

$$\begin{aligned} \dot{V}_3 &= -k_1z_1^2 - k_2z_2^2 + z_3(z_2 + m\dot{z}_3) \\ &= -k_1z_1^2 - k_2z_2^2 + z_3(z_2 + \tau - d(v)\alpha_2 - d(v)z_3 - k(x)x - m\dot{\alpha}_2) \end{aligned} \quad (13.347)$$

Choosing the control law as

$$\tau = m\dot{\alpha}_2 + d(v)\alpha_2 + k(x)x - z_2 - k_3z_3 \quad (13.348)$$

yields

$$\dot{V}_3 = -k_1z_1^2 - k_2z_2^2 - (d(v) + k_3)z_3^2 < 0, \forall z_1 \neq 0, z_2 \neq 0, z_3 \neq 0 \quad (13.349)$$

and

$$m\dot{z}_3 = -[d(v) + k_3]z_3 - z_2 \quad (13.350)$$

### Error Dynamics

For the undisturbed case  $w = 0$ , the error dynamics takes the form

$$\begin{bmatrix} 1 & 0 & 0 \\ 0 & 1 & 0 \\ 0 & 0 & m \end{bmatrix} \begin{bmatrix} \dot{z}_1 \\ \dot{z}_2 \\ \dot{z}_3 \end{bmatrix} = - \begin{bmatrix} k_1 & 0 & 0 \\ 0 & k_2 & 0 \\ 0 & 0 & d(v) + k_3 \end{bmatrix} \begin{bmatrix} z_1 \\ z_2 \\ z_3 \end{bmatrix} + \begin{bmatrix} 0 & 1 & 0 \\ -1 & 0 & 1 \\ 0 & -1 & 0 \end{bmatrix} \begin{bmatrix} z_1 \\ z_2 \\ z_3 \end{bmatrix} \quad (13.351)$$

Hence, the equilibrium point  $(z_1, z_2, z_3) = (0, 0, 0)$  is GES and therefore the tracking error  $e$  converges to zero. If  $w = \text{constant}$ , the error dynamics takes the form

$$\begin{bmatrix} 1 & 0 & 0 \\ 0 & 1 & 0 \\ 0 & 0 & m \end{bmatrix} \begin{bmatrix} \dot{z}_1 \\ \dot{z}_2 \\ \dot{z}_3 \end{bmatrix} = - \begin{bmatrix} k_1 & 0 & 0 \\ 0 & k_2 & 0 \\ 0 & 0 & d(v) + k_3 \end{bmatrix} \begin{bmatrix} z_1 \\ z_2 \\ z_3 \end{bmatrix} + \begin{bmatrix} 0 & 1 & 0 \\ -1 & 0 & 1 \\ 0 & -1 & 0 \end{bmatrix} \begin{bmatrix} z_1 \\ z_2 \\ z_3 \end{bmatrix} + \begin{bmatrix} 0 \\ 0 \\ 1 \end{bmatrix} w$$

Hence, in the steady state ( $\dot{z} = \mathbf{0}$  and  $d(v) = 0$ )

$$z_2 = k_1z_1 = e - \alpha_1 = e + k_1z_1 \Rightarrow e = 0 \quad (13.352)$$

The equilibrium point for  $w = \text{constant}$  is

$$\begin{bmatrix} z_1 \\ z_2 \\ z_3 \end{bmatrix} = \begin{bmatrix} k_1 & -1 & 0 \\ 1 & k_2 & -1 \\ 0 & 1 & k_3 \end{bmatrix}^{-1} \begin{bmatrix} 0 \\ 0 \\ 1 \end{bmatrix} w = \frac{1}{k_1k_2k_3 + k_1 + k_3} \begin{bmatrix} 1 \\ k_1 \\ 1 + k_1k_2 \end{bmatrix} w \quad (13.353)$$

Therefore it can be concluded that for the case  $w = \text{constant}$  the equilibrium point  $(z_1, z_2, z_3)$  is GES but  $(z_1, z_2, z_3)$  will converge to the constant nonzero values given by (13.353), even though  $e = 0$ . This shows that augmentation of an additional integrator when performing backstepping leads to zero steady-state errors in the case of regulation under the assumption of a constant disturbance  $w$ .

### Implementation Considerations

The integrator augmentation technique is particularly interesting for implementation in mechanical systems since the integral term is computed by integrating  $z_1 = y - y_d$  which for a mechanical system is the position tracking error. This corresponds to applying a PID controller on a second-order system. On the contrary, when using *constant parameter adaptation* the integral term will be the integral of a linear combination of the state tracking errors; see (13.322). For a mechanical system this implies that both the position and velocity tracking errors are used to provide integral action. In many cases it is difficult to measure the velocity with the same accuracy as the position. This implies that the adaptive method will be more sensitive to measurement noise than the *integrator augmentation technique*. A comparative study of the different backstepping integral techniques is found in Skjetne and Fossen (2004).

#### 13.3.6 Case Study: Backstepping of MIMO Mass–Damper–Spring Systems

The concept of vectorial backstepping was first introduced by Fossen and Berge (1997) and Fossen and Grøvlen (1998). Consider a MIMO nonlinear mass–damper–spring system in the form

$$\dot{\mathbf{x}} = \mathbf{v} \quad (13.354)$$

$$\mathbf{M}\dot{\mathbf{v}} + \mathbf{D}(\mathbf{v})\mathbf{v} + \mathbf{K}(\mathbf{x})\mathbf{x} = \mathbf{B}\mathbf{u} \quad (13.355)$$

where  $\mathbf{x} \in \mathbb{R}^n$  is the position vector,  $\mathbf{v} \in \mathbb{R}^n$  is the velocity vector,  $\mathbf{u} \in \mathbb{R}^r$  ( $r \geq n$ ) is the control input vector,  $\mathbf{D}(\mathbf{v}) \in \mathbb{R}^{n \times n}$  represents a matrix of damping coefficients,  $\mathbf{K}(\mathbf{x}) \in \mathbb{R}^{n \times n}$  is a matrix of spring coefficients,  $\mathbf{M} \in \mathbb{R}^{n \times n}$  is the inertia matrix and  $\mathbf{B} \in \mathbb{R}^{n \times r}$  is the input matrix. Hence, backstepping can be performed in *two vectorial steps*.

**Step 1:** For the first system (13.354) consider  $\mathbf{v}$  as the control and let

$$\mathbf{v} = \mathbf{s} + \boldsymbol{\alpha}_1 \quad (13.356)$$

where

$\mathbf{s} = \tilde{\mathbf{v}} + \boldsymbol{\Lambda} \tilde{\mathbf{x}}$       New state vector used for tracking control

$\boldsymbol{\alpha}_1$       Stabilizing vector field to be defined later

Here  $\tilde{\mathbf{v}} = \mathbf{v} - \mathbf{v}_d$  and  $\tilde{\mathbf{x}} = \mathbf{x} - \mathbf{x}_d$  are the velocity and position tracking errors, respectively, and  $\boldsymbol{\Lambda} > 0$  is a diagonal matrix of positive elements. The definition of the  $\mathbf{s}$  vector is motivated by Slotine and Li (1987), who introduced  $\mathbf{s}$  as a measure of tracking when designing their adaptive robot controller. It turns out that this transformation has the nice property of transforming the nonlinear state-space model (13.354)–(13.355) to the form

$$\begin{aligned} \mathbf{M}\dot{\mathbf{s}} + \mathbf{D}(\mathbf{v})\mathbf{s} &= \mathbf{M}\dot{\mathbf{v}} + \mathbf{D}(\mathbf{v})\mathbf{v} - \mathbf{M}\dot{\mathbf{v}}_r - \mathbf{D}(\mathbf{v})\mathbf{v}_r \\ &= \mathbf{B}\mathbf{u} - \mathbf{M}\dot{\mathbf{v}}_r - \mathbf{D}(\mathbf{v})\mathbf{v}_r - \mathbf{K}(\mathbf{x})\mathbf{x} \end{aligned} \quad (13.357)$$

where  $\mathbf{v}_r$  can be interpreted as a “virtual” reference trajectory:

$$\begin{aligned}\mathbf{v}_r &= \mathbf{v} - \mathbf{s} \\ &= \mathbf{v}_d - \mathbf{\Lambda} \tilde{\mathbf{x}}\end{aligned}\quad (13.358)$$

The position error dynamics of Step 1 can therefore be written

$$\begin{aligned}\dot{\tilde{\mathbf{x}}} &= \mathbf{v} - \mathbf{v}_d \\ &= s + \boldsymbol{\alpha}_1 - \mathbf{v}_d \quad (\boldsymbol{\alpha}_1 = \mathbf{v}_r = \mathbf{v} - \mathbf{s}) \\ &= -\mathbf{\Lambda} \tilde{\mathbf{x}} + s\end{aligned}\quad (13.359)$$

Hence,

$$V_1 = \frac{1}{2} \tilde{\mathbf{x}}^\top \mathbf{K}_p \tilde{\mathbf{x}}, \quad \mathbf{K}_p = \mathbf{K}_p^\top > 0 \quad (13.360)$$

and

$$\begin{aligned}\dot{V}_1 &= \tilde{\mathbf{x}}^\top \mathbf{K}_p \dot{\tilde{\mathbf{x}}} \\ &= \tilde{\mathbf{x}}^\top \mathbf{K}_p (-\mathbf{\Lambda} \tilde{\mathbf{x}} + s) \\ &= -\tilde{\mathbf{x}}^\top \mathbf{K}_p \mathbf{\Lambda} \tilde{\mathbf{x}} + s^\top \mathbf{K}_p \tilde{\mathbf{x}}\end{aligned}\quad (13.361)$$

**Step 2:** In the second step, a CLF motivated by *pseudo-kinetic energy* is chosen according to

$$V_2 = \frac{1}{2} \mathbf{s}^\top \mathbf{M} \mathbf{s} + V_1, \quad \mathbf{M} = \mathbf{M}^\top > 0 \quad (13.362)$$

$$\begin{aligned}\dot{V}_2 &= \mathbf{s}^\top \mathbf{M} \dot{\mathbf{s}} + \dot{V}_1 \\ &= \mathbf{s}^\top (\mathbf{B} \mathbf{u} - \mathbf{M} \dot{\mathbf{v}}_r - \mathbf{D}(\mathbf{v}) \mathbf{v}_r - \mathbf{K}(\mathbf{x}) \mathbf{x} - \mathbf{D}(\mathbf{v}) \mathbf{s}) - \tilde{\mathbf{x}}^\top \mathbf{K}_p \mathbf{\Lambda} \tilde{\mathbf{x}} + s^\top \mathbf{K}_p \tilde{\mathbf{x}} \\ &= \mathbf{s}^\top (\mathbf{B} \mathbf{u} - \mathbf{M} \dot{\mathbf{v}}_r - \mathbf{D}(\mathbf{v}) \mathbf{v}_r - \mathbf{K}(\mathbf{x}) \mathbf{x} - \mathbf{D}(\mathbf{v}) \mathbf{s} + \mathbf{K}_p \tilde{\mathbf{x}}) - \tilde{\mathbf{x}}^\top \mathbf{K}_p \mathbf{\Lambda} \tilde{\mathbf{x}}\end{aligned}\quad (13.363)$$

This suggests that the control law is chosen as

$$\mathbf{B} \mathbf{u} = \mathbf{M} \dot{\mathbf{v}}_r + \mathbf{D}(\mathbf{v}) \mathbf{v}_r + \mathbf{K}(\mathbf{x}) \mathbf{x} - \mathbf{K}_p \tilde{\mathbf{x}} - \mathbf{K}_d \mathbf{s}, \quad \mathbf{K}_d > 0 \quad (13.364)$$

which results in

$$\dot{V}_2 = -\mathbf{s}^\top (\mathbf{D}(\mathbf{v}) + \mathbf{K}_d) \mathbf{s} - \tilde{\mathbf{x}}^\top \mathbf{K}_p \mathbf{\Lambda} \tilde{\mathbf{x}}$$

Since  $V_2$  is positive definite and  $\dot{V}_2$  is negative definite it follows from Theorem A.3 that the equilibrium point  $(\tilde{\mathbf{x}}, \mathbf{s}) = (\mathbf{0}, \mathbf{0})$  is GES. Moreover, convergence of  $\mathbf{s} \rightarrow \mathbf{0}$  and  $\tilde{\mathbf{x}} \rightarrow \mathbf{0}$  implies that  $\tilde{\mathbf{v}} \rightarrow \mathbf{0}$ . When implementing the control law (13.364) it is assumed that  $\mathbf{B}$  has an inverse:

$$\mathbf{B}^\dagger = \mathbf{B}^\top (\mathbf{B} \mathbf{B}^\top)^{-1} \quad (13.365)$$

or simply  $\mathbf{B}^{-1}$  for the square case  $r = n$ .

### Nonlinear Mass–Damper–Spring System with Actuator Dynamics

Consider the mass–damper–spring system of the previous section with actuator dynamics:

$$\dot{\mathbf{x}} = \mathbf{v} \quad (13.366)$$

$$\mathbf{M}\dot{\mathbf{v}} + \mathbf{D}(\mathbf{v})\mathbf{v} + \mathbf{K}(\mathbf{x})\mathbf{x} = \mathbf{B}\mathbf{u} \quad (13.367)$$

$$\mathbf{T}\dot{\mathbf{u}} + \mathbf{u} = \mathbf{u}_c \quad (13.368)$$

where  $\mathbf{T} \in \mathbb{R}^{r \times r}$  is a diagonal matrix of actuator time constants and  $\mathbf{u}_c \in \mathbb{R}^r$  is a vector of actuator commands. Instead of choosing the controller  $\mathbf{u}$  in Step 2,  $\mathbf{u}_c$  is treated as the control input to be specified in Step 3. Recall that

$$\dot{V}_2 = \mathbf{s}^\top (\mathbf{B}\mathbf{u} - \mathbf{M}\dot{\mathbf{v}}_r - \mathbf{D}(\mathbf{v})\mathbf{v}_r - \mathbf{K}(\mathbf{x})\mathbf{x} - \mathbf{D}(\mathbf{v})\mathbf{s} + \mathbf{K}_p \tilde{\mathbf{x}}) - \tilde{\mathbf{x}}^\top \mathbf{K}_p \mathbf{\Lambda} \tilde{\mathbf{x}} \quad (13.369)$$

**Step 3:** Let  $\mathbf{Bu}$  be the virtual control vector of Step 3. Hence,

$$\mathbf{Bu} = \mathbf{z} + \boldsymbol{\alpha}_2 \quad (13.370)$$

$$\boldsymbol{\alpha}_2 = \mathbf{M}\dot{\mathbf{v}}_r + \mathbf{D}(\mathbf{v})\mathbf{v}_r + \mathbf{K}(\mathbf{x})\mathbf{x} - \mathbf{K}_p \tilde{\mathbf{x}} - \mathbf{K}_d \mathbf{s} \quad (13.371)$$

where  $\mathbf{z}$  is a new state variable. This results in

$$\dot{V}_2 = \mathbf{s}^\top \mathbf{z} - \mathbf{s}^\top (\mathbf{D}(\mathbf{v}) + \mathbf{K}_d)\mathbf{s} - \tilde{\mathbf{x}}^\top \mathbf{K}_p \mathbf{\Lambda} \tilde{\mathbf{x}} \quad (13.372)$$

Choose

$$V_3 = \frac{1}{2}\mathbf{z}^\top \mathbf{z} + V_2 \quad (13.373)$$

$$\begin{aligned} \dot{V}_3 &= \mathbf{z}^\top \mathbf{K}\dot{\mathbf{z}} + \dot{V}_2 \\ &= \mathbf{z}^\top (\mathbf{B}\dot{\mathbf{u}} - \dot{\boldsymbol{\alpha}}_2) + \mathbf{s}^\top \mathbf{z} - \mathbf{s}^\top (\mathbf{D}(\mathbf{v}) + \mathbf{K}_d)\mathbf{s} - \tilde{\mathbf{x}}^\top \mathbf{K}_p \mathbf{\Lambda} \tilde{\mathbf{x}} \\ &= \mathbf{z}^\top (\mathbf{B}\mathbf{T}^{-1}(\mathbf{u}_c - \mathbf{u}) - \dot{\boldsymbol{\alpha}}_2 + \mathbf{s}) - \mathbf{s}^\top (\mathbf{D}(\mathbf{v}) + \mathbf{K}_d)\mathbf{s} - \tilde{\mathbf{x}}^\top \mathbf{K}_p \mathbf{\Lambda} \tilde{\mathbf{x}} \end{aligned} \quad (13.374)$$

The control law

$$\mathbf{u}_c = \mathbf{u} + \mathbf{T}\mathbf{B}^\dagger(\dot{\boldsymbol{\alpha}}_2 - \mathbf{s} - \mathbf{K}_z \mathbf{z}) \quad (13.375)$$

yields

$$\dot{V}_3 = -\mathbf{z}^\top \mathbf{K}_z \mathbf{z} - \mathbf{s}^\top (\mathbf{D}(\mathbf{v}) + \mathbf{K}_d)\mathbf{s} - \tilde{\mathbf{x}}^\top \mathbf{K}_p \mathbf{\Lambda} \tilde{\mathbf{x}} \quad (13.376)$$

Again GES is guaranteed. The main drawback of including the actuator dynamic is that  $\dot{\alpha}_2$  must be computed. The expression for  $\dot{\alpha}_2$  will not depend of the state derivatives since

$$\dot{\alpha}_2 = \sum_{i=1}^n \frac{\partial \alpha_2}{\partial (\text{state})_i} (\text{state})_i$$

$(\text{state})_i$  = system equation depending on the states only

**Example 13.5 (MIMO Backstepping of Robots)**

This example is based on the results of Fossen and Berge (1997). Consider the nonlinear robot model (Sciavicco and Siciliano, 1996):

$$\dot{q} = v \quad (13.377)$$

$$M(q)\dot{v} + C(q, v)v + g(q) = \tau \quad (13.378)$$

where  $M(q) = M^\top(q) > 0$  is the inertia matrix,  $C(q, v)$  is a matrix of Coriolis and centripetal forces defined in terms of the Christoffel symbols and  $g(q)$  is a vector of gravitational forces and moments.  $q \in \mathbb{R}^n$  is a vector of joint angles,  $v \in \mathbb{R}^n$  is a vector of joint angular rates and  $\tau \in \mathbb{R}^n$  is a vector of control torques. Vectorial backstepping of a robot manipulator (see Figure 13.17) can be done in two steps:

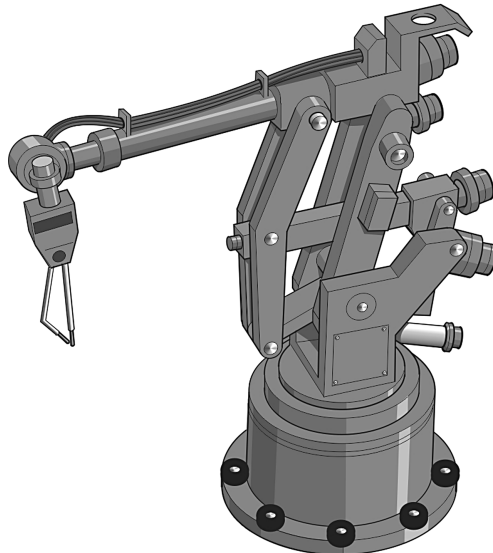


**Figure 13.17** Robot manipulator.

**Step 1:** Define the virtual control vector

$$\dot{\mathbf{q}} = \mathbf{v} := \mathbf{s} + \boldsymbol{\alpha}_1 \quad (13.379)$$

where  $\mathbf{s}$  is a new state variable and  $\boldsymbol{\alpha}_1$  is stabilizing vector field, which can be chosen as

$$\boldsymbol{\alpha}_1 = \mathbf{v}_r, \quad \mathbf{v}_r = \mathbf{v}_d - \mathbf{\Lambda} \tilde{\mathbf{q}} \quad (13.380)$$

where  $\mathbf{\Lambda} > 0$  is a diagonal design matrix and  $\tilde{\mathbf{q}} = \mathbf{q} - \mathbf{q}_d$  is the tracking error. Combining (13.379) and (13.380) yields

$$\tilde{\mathbf{v}} = -\mathbf{\Lambda} \tilde{\mathbf{q}} + \mathbf{s} \quad (13.381)$$

where  $\dot{\tilde{\mathbf{q}}} = \tilde{\mathbf{v}}$ .

**Step 2:** Consider the CLF:

$$V = \frac{1}{2} (\mathbf{s}^\top \mathbf{M}(\mathbf{q}) \mathbf{s} + \tilde{\mathbf{q}}^\top \mathbf{K}_q \tilde{\mathbf{q}}) > 0, \quad \forall \mathbf{s} \neq \mathbf{0}, \tilde{\mathbf{q}} \neq \mathbf{0} \quad (13.382)$$

$$\begin{aligned} \dot{V} &= \mathbf{s}^\top \mathbf{M}(\mathbf{q}) \dot{\mathbf{s}} + \frac{1}{2} \mathbf{s}^\top \dot{\mathbf{M}}(\mathbf{q}) \mathbf{s} + \tilde{\mathbf{q}}^\top \mathbf{K}_q \tilde{\mathbf{v}} \\ &= \mathbf{s}^\top \mathbf{M}(\mathbf{q}) \dot{\mathbf{s}} + \frac{1}{2} \mathbf{s}^\top \dot{\mathbf{M}}(\mathbf{q}) \mathbf{s} - \tilde{\mathbf{q}}^\top \mathbf{K}_q \mathbf{\Lambda} \tilde{\mathbf{q}} + \tilde{\mathbf{q}}^\top \mathbf{K}_q \mathbf{s} \end{aligned} \quad (13.383)$$

Equations (13.379) and (13.380) can be combined to give

$$\begin{aligned} \mathbf{M}(\mathbf{q}) \dot{\mathbf{s}} &= \mathbf{M}(\mathbf{q}) \dot{\mathbf{v}} - \mathbf{M}(\mathbf{q}) \dot{\boldsymbol{\alpha}} \\ &= \boldsymbol{\tau} - \mathbf{M}(\mathbf{q}) \dot{\mathbf{v}}_r - \mathbf{C}(\mathbf{q}, \mathbf{v}) \mathbf{v}_r - \mathbf{g}(\mathbf{q}) - \mathbf{C}(\mathbf{q}, \mathbf{v}) \mathbf{s} \end{aligned} \quad (13.384)$$

Substituting (13.384) into (13.383) yields

$$\begin{aligned} \dot{V} &= \mathbf{s}^\top (\boldsymbol{\tau} - \mathbf{M}(\mathbf{q}) \dot{\mathbf{v}}_r - \mathbf{C}(\mathbf{q}, \mathbf{v}) \mathbf{v}_r - \mathbf{g}(\mathbf{q}) + \mathbf{K}_q \tilde{\mathbf{q}}) \\ &\quad + \mathbf{s}^\top \left( \frac{1}{2} \dot{\mathbf{M}}(\mathbf{q}) - \mathbf{C}(\mathbf{q}, \mathbf{v}) \right) \mathbf{s} - \tilde{\mathbf{q}}^\top \mathbf{K}_q \mathbf{\Lambda} \tilde{\mathbf{q}} \\ &= \mathbf{s}^\top (\boldsymbol{\tau} - \mathbf{M}(\mathbf{q}) \dot{\mathbf{v}}_r - \mathbf{C}(\mathbf{q}, \mathbf{v}) \mathbf{v}_r - \mathbf{g}(\mathbf{q}) + \mathbf{K}_q \tilde{\mathbf{q}}) - \tilde{\mathbf{q}}^\top \mathbf{K}_q \mathbf{\Lambda} \tilde{\mathbf{q}} \end{aligned} \quad (13.385)$$

Here the skew-symmetric property  $\mathbf{s}^\top (\frac{1}{2} \dot{\mathbf{M}}(\mathbf{q}) - \mathbf{C}(\mathbf{q}, \mathbf{v})) \mathbf{s} = \mathbf{0}$ ,  $\forall \mathbf{s}$  has been applied. The backstepping control law is chosen as

$$\boldsymbol{\tau} = \mathbf{M}(\mathbf{q}) \dot{\mathbf{v}}_r + \mathbf{C}(\mathbf{q}, \mathbf{v}) \mathbf{v}_r + \mathbf{g}(\mathbf{q}) - \mathbf{K}_d \mathbf{s} - \mathbf{K}_q \tilde{\mathbf{q}} \quad (13.386)$$

where  $\mathbf{K}_d = \mathbf{K}_d^\top > 0$  and  $\mathbf{K}_q = \mathbf{K}_q^\top > 0$  are design matrices. This finally yields

$$\dot{V} = -\mathbf{s}^\top \mathbf{K}_d \mathbf{s} - \tilde{\mathbf{q}}^\top \mathbf{K}_q \mathbf{\Lambda} \tilde{\mathbf{q}} < 0, \quad \forall \mathbf{s} \neq \mathbf{0}, \tilde{\mathbf{q}} \neq \mathbf{0} \quad (13.387)$$

and GES follows. The control law (13.386) is equivalent to the control law of Slotine and Li (1987) with perfectly known parameters (nonadaptive case) except for the additional feedback term  $\mathbf{K}_q \tilde{\mathbf{q}}$  which is necessary to obtain GES.

### 13.3.7 Case Study: MIMO Backstepping for Fully Actuated Ships

Conventional ship control systems are designed under the assumption that the kinematic and kinetic equations can be linearized such that gain-scheduling techniques and optimal control theory can be applied (see Fossen, 1994). This is not a good assumption for tracking applications where the surge and sway positions ( $N, E$ ) and yaw angle  $\psi$  must be controlled simultaneously. The main reason for this is that the rotation matrix in yaw must be linearized. In addition to this, assumptions such as linear damping and negligible Coriolis and centripetal forces are only good for low-speed maneuvering and stationkeeping. These limitations clearly motivate a nonlinear design. MIMO nonlinear backstepping designs can be used for this purpose by exploiting nonlinear system properties such as symmetry of the inertia matrix, dissipative damping and skew-symmetry of the Coriolis and centripetal matrix (see Fossen and Fjellstad, 1995).

A MIMO nonlinear backstepping technique for marine craft where the nonlinear system properties are exploited is presented below (Fossen and Strand, 1998). An alternative reference is Fossen and Strand (1999a).

#### Vectorial Backstepping of Marine Craft in 6 DOF

Consider a marine craft described by the following equations of motion:

$$\dot{\boldsymbol{\eta}} = \mathbf{J}_\Theta(\boldsymbol{\eta})\mathbf{v} \quad (13.388)$$

$$\mathbf{M}\dot{\mathbf{v}} + \mathbf{C}(\mathbf{v})\mathbf{v} + \mathbf{D}(\mathbf{v})\mathbf{v} + \mathbf{g}(\boldsymbol{\eta}) = \boldsymbol{\tau} \quad (13.389)$$

$$\boldsymbol{\tau} = \mathbf{B}\mathbf{u} \quad (13.390)$$

This model describes the motion of a craft in 6 DOF. It is assumed that the craft is fully actuated such that  $\mathbf{B}\mathbf{B}^\top$  is invertible. The system (13.388)–(13.390) satisfies the following properties:

- (i)  $\mathbf{M} = \mathbf{M}^\top > 0$ ,  $\dot{\mathbf{M}} = \mathbf{0}$
- (ii)  $\mathbf{C}(\mathbf{v}) = -\mathbf{C}^\top(\mathbf{v})$
- (iii)  $\mathbf{D}(\mathbf{v}) > 0$
- (iv)  $\mathbf{B}\mathbf{B}^\top$  is nonsingular
- (v)  $\mathbf{J}_\Theta(\boldsymbol{\eta})$  = Euler angle transformation matrix (not defined for  $\theta = \pm 90^\circ$ )

#### New State Variables

Assume that the reference trajectories given by  $\boldsymbol{\eta}_d^{(3)}$ ,  $\ddot{\boldsymbol{\eta}}_d$ ,  $\dot{\boldsymbol{\eta}}_d$  and  $\boldsymbol{\eta}_d$  are smooth and bounded. The virtual reference trajectories in BODY and NED coordinates are defined as

$$\dot{\boldsymbol{\eta}}_r := \dot{\boldsymbol{\eta}}_d - \boldsymbol{\Lambda} \tilde{\boldsymbol{\eta}} \quad (13.391)$$

$$\mathbf{v}_r := \mathbf{J}_\Theta^{-1}(\boldsymbol{\eta})\dot{\boldsymbol{\eta}}_r, \quad \theta \neq \pm 90^\circ \quad (13.392)$$

where  $\tilde{\boldsymbol{\eta}} = \boldsymbol{\eta} - \boldsymbol{\eta}_d$  is the tracking error and  $\boldsymbol{\Lambda} > 0$  is a diagonal design matrix. Furthermore, let

$$s = \dot{\boldsymbol{\eta}} - \dot{\boldsymbol{\eta}}_r = \dot{\tilde{\boldsymbol{\eta}}} + \boldsymbol{\Lambda} \tilde{\boldsymbol{\eta}} \quad (13.393)$$

The marine craft dynamics (13.388)–(13.389) can be written (Fossen, 1993)

$$\mathbf{M}^*(\boldsymbol{\eta})\ddot{\boldsymbol{\eta}} + \mathbf{C}^*(\mathbf{v}, \boldsymbol{\eta})\dot{\boldsymbol{\eta}} + \mathbf{D}^*(\mathbf{v}, \boldsymbol{\eta})\dot{\boldsymbol{\eta}} + \mathbf{g}^*(\boldsymbol{\eta}) = \mathbf{J}_\Theta^{-\top}(\boldsymbol{\eta})\boldsymbol{\tau} \quad (13.394)$$

where

$$\begin{aligned}\mathbf{M}^*(\eta) &= \mathbf{J}_\Theta^{-\top}(\eta) \mathbf{M} \mathbf{J}_\Theta^{-1}(\eta) \\ \mathbf{C}^*(\mathbf{v}, \eta) &= \mathbf{J}_\Theta^{-\top}(\eta) [\mathbf{C}(\mathbf{v}) - \mathbf{M} \mathbf{J}_\Theta^{-1}(\eta) \dot{\mathbf{J}}_\Theta(\eta)] \mathbf{J}_\Theta^{-1}(\eta) \\ \mathbf{D}^*(\mathbf{v}, \eta) &= \mathbf{J}_\Theta^{-\top}(\eta) \mathbf{D}(\mathbf{v}) \mathbf{J}_\Theta^{-1}(\eta) \\ \mathbf{g}^*(\eta) &= \mathbf{J}_\Theta^{-\top}(\eta) \mathbf{g}(\eta)\end{aligned}$$

Hence,

$$\begin{aligned}\mathbf{M}^*(\eta) \dot{s} &= -\mathbf{C}^*(\mathbf{v}, \eta) s - \mathbf{D}^*(\mathbf{v}, \eta) s + \mathbf{J}_\Theta^{-\top}(\eta) \mathbf{B} u \\ &\quad - \mathbf{M}^*(\eta) \ddot{\eta}_r - \mathbf{C}^*(\mathbf{v}, \eta) \dot{\eta}_r - \mathbf{D}^*(\mathbf{v}, \eta) \dot{\eta}_r - \mathbf{g}^*(\eta)\end{aligned}\quad (13.395)$$

or equivalently

$$\begin{aligned}\mathbf{M}^*(\eta) \dot{s} &= -\mathbf{C}^*(\mathbf{v}, \eta) s - \mathbf{D}^*(\mathbf{v}, \eta) s \\ &\quad + \mathbf{J}_\Theta^{-\top}(\eta) [\mathbf{B} u - \mathbf{M} \dot{\mathbf{v}}_r - \mathbf{C}(\mathbf{v}) \mathbf{v}_r - \mathbf{D}(\mathbf{v}) \mathbf{v}_r - \mathbf{g}(\eta)]\end{aligned}\quad (13.396)$$

**Step 1:** Consider the error dynamics

$$\dot{\eta} - \dot{\eta}_d = \mathbf{J}_\Theta(\eta)(\mathbf{v} - \mathbf{v}_d) \quad (13.397)$$

Let  $\mathbf{v}$  be the virtual control vector

$$\mathbf{J}_\Theta(\eta) \mathbf{v} := s + \boldsymbol{\alpha}_1 \quad (13.398)$$

The position error dynamics can therefore be written

$$\begin{aligned}\dot{\tilde{\eta}} &= \mathbf{J}_\Theta(\eta)(\mathbf{v} - \mathbf{v}_d) \\ &= s + \boldsymbol{\alpha}_1 - \mathbf{J}_\Theta(\eta) \mathbf{v}_d \quad \{\boldsymbol{\alpha}_1 = \dot{\eta}_r = \dot{\eta}_d - \boldsymbol{\Lambda} \tilde{\eta}, \quad \dot{\eta}_d = \mathbf{J}_\Theta(\eta) \mathbf{v}_d\} \\ &= -\boldsymbol{\Lambda} \tilde{\eta} + s\end{aligned}\quad (13.399)$$

Hence, a CLF is

$$V_1 = \frac{1}{2} \tilde{\eta}^\top \mathbf{K}_p \tilde{\eta}, \quad \mathbf{K}_p = \mathbf{K}_p^\top > 0 \quad (13.400)$$

resulting in

$$\begin{aligned}\dot{V}_1 &= \tilde{\eta}^\top \mathbf{K}_p \dot{\tilde{\eta}} \\ &= \tilde{\eta}^\top \mathbf{K}_p (-\boldsymbol{\Lambda} \tilde{\eta} + s) \\ &= -\tilde{\eta}^\top \mathbf{K}_p \boldsymbol{\Lambda} \tilde{\eta} + s^\top \mathbf{K}_p \tilde{\eta}\end{aligned}\quad (13.401)$$

**Step 2:** In the second step a CLF motivated by the *pseudo-kinetic energy* is chosen:

$$V_2 = \frac{1}{2} s^\top \mathbf{M}^*(\eta) s + V_1, \quad \mathbf{M}^* = (\mathbf{M}^*)^\top > 0 \quad (13.402)$$

$$\begin{aligned}
\dot{V}_2 &= s^\top \mathbf{M}^*(\eta) \dot{s} + \frac{1}{2} s^\top \dot{\mathbf{M}}^*(\eta) s + \dot{V}_1 \\
&= -s^\top [C^*(v, \eta) + D^*(v, \eta)] s \\
&\quad + s^\top J_{\Theta}^{-\top}(\eta) [\mathbf{B}u - \mathbf{M}\dot{v}_r - \mathbf{C}(v)v_r - \mathbf{D}(v)v_r - g(\eta)] \\
&\quad + \frac{1}{2} s^\top \dot{\mathbf{M}}^*(\eta) s - \tilde{\eta}^\top \mathbf{K}_p \Lambda \tilde{\eta} + s^\top \mathbf{K}_p \tilde{\eta}
\end{aligned} \tag{13.403}$$

Using the skew-symmetric property

$$s^\top (\dot{\mathbf{M}}^*(\eta) - 2C^*(v, \eta)) s = 0, \quad \forall v, \eta, s \tag{13.404}$$

yields

$$\begin{aligned}
\dot{V}_2 &= s^\top J_{\Theta}^{-\top}(\eta) [\mathbf{B}u - \mathbf{M}\dot{v}_r - \mathbf{C}(v)v_r - \mathbf{D}(v)v_r - g(\eta) + J_{\Theta}^\top(\eta) \mathbf{K}_p \tilde{\eta}] \\
&\quad - s^\top D^*(v, \eta) s - \tilde{\eta}^\top \mathbf{K}_p \Lambda \tilde{\eta}
\end{aligned} \tag{13.405}$$

Hence, the control law can be chosen as (see Figure 13.18)

$$\tau = \mathbf{M}\dot{v}_r + \mathbf{C}(v)v_r + \mathbf{D}(v)v_r + g(\eta) - J_{\Theta}^\top(\eta) \mathbf{K}_p \tilde{\eta} - J_{\Theta}^\top(\eta) \mathbf{K}_d s \tag{13.406}$$

$$u = \mathbf{B}^\dagger \tau \tag{13.407}$$

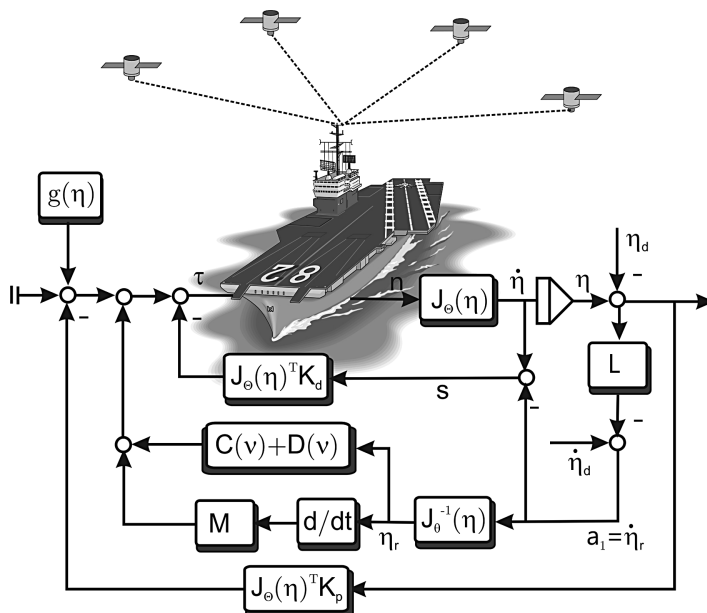


**Figure 13.18** Nonlinear MIMO backstepping controller for 6 DOF trajectory-tracking control.

where  $\mathbf{K}_d > 0$ . This results in

$$\dot{V}_2 = -\mathbf{s}^\top (\mathbf{D}^*(\mathbf{v}, \boldsymbol{\eta}) + \mathbf{K}_d)\mathbf{s} - \tilde{\boldsymbol{\eta}}^\top \mathbf{K}_p \mathbf{\Lambda} \tilde{\boldsymbol{\eta}}$$

Since  $V_2$  is positive definite and  $\dot{V}_2$  is negative definite it follows from Theorem A.3 that the equilibrium point  $(\tilde{\boldsymbol{\eta}}, \mathbf{s}) = (\mathbf{0}, \mathbf{0})$  is GES. In addition, it follows from convergence of  $\mathbf{s} \rightarrow \mathbf{0}$  and  $\tilde{\boldsymbol{\eta}} \rightarrow \mathbf{0}$  that  $\dot{\tilde{\boldsymbol{\eta}}} \rightarrow \mathbf{0}$ .

### Vectorial Backstepping in 3 DOF

Vectorial backstepping in 3 DOF (surge, sway and yaw) is a special case of the general 6 DOF solution which can be applied for surface vessels. Typical applications are stationkeeping and low-speed maneuvering of ships, semi-submersibles and high-speed craft (see Figure 13.19).

In this case the Euler angle transformation matrix  $\mathbf{J}_\Theta(\boldsymbol{\eta})$  reduces to (see (2.40) in Section 2.2):

$$\mathbf{J}_\Theta(\boldsymbol{\eta}) \in \mathbb{R}^{6 \times 6} \rightarrow \mathbf{R}(\psi) \in SO(3) \quad (13.408)$$

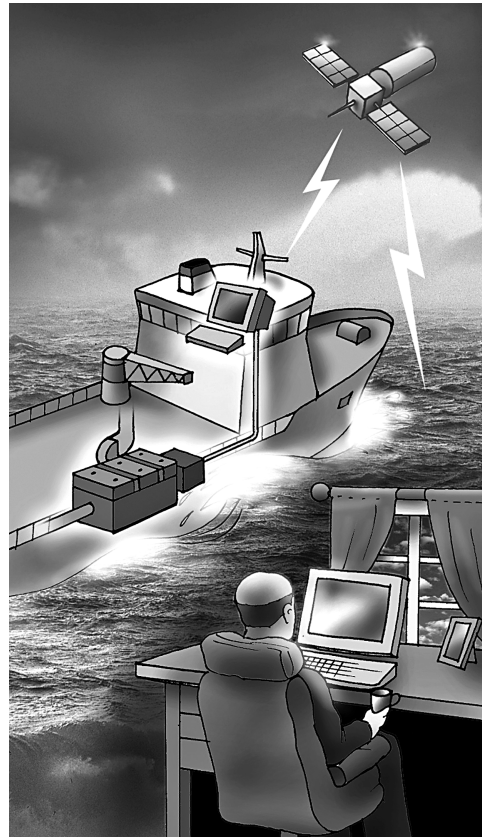


**Figure 13.19** Dynamic positioning of a supply vessel using measurements from a global navigation satellite system. Illustration by Bjarne Stenberg/Department of Marine Technology, NTNU.

which is the rotation matrix in yaw. This implies that

$$\mathbf{R}^{-1}(\psi) = \mathbf{R}^\top(\psi) \quad (13.409)$$

The equations of motion (13.394) therefore become

$$\mathbf{M}^*(\psi)\ddot{\eta} + \mathbf{C}^*(v, \psi)\dot{\eta} + \mathbf{D}^*(v, \psi)\dot{\eta} = \mathbf{R}(\psi)\tau \quad (13.410)$$

where the gravitational and buoyancy forces are assumed to outbalance each other such that  $\mathbf{g}(\eta) = \mathbf{0}$ , and

$$\begin{aligned}\mathbf{M}^*(\psi) &= \mathbf{R}(\psi)\mathbf{M}\mathbf{R}^\top(\psi) \\ \mathbf{C}^*(v, \psi) &= \mathbf{R}(\psi)[\mathbf{C}(v) - \mathbf{M}\mathbf{R}^\top(\psi)\dot{\mathbf{R}}(\psi)]\mathbf{R}^\top(\psi) \\ \mathbf{D}^*(v, \psi) &= \mathbf{R}(\psi)\mathbf{D}(v)\mathbf{R}^\top(\psi)\end{aligned}$$

### 13.3.8 Case Study: MIMO Backstepping Design with Acceleration Feedback for Fully Actuated Ships

The results of the previous section can be extended to include acceleration feedback. A surface vessel in surge, sway and yaw will be used to illustrate the design procedure. For simplicity a PD control law will be designed. Integral action can easily be included by using adaptive backstepping or integral augmentation techniques as explained in Sections 13.3.4 and 13.3.5.

Consider the 3 DOF maneuvering model:

$$\dot{\eta} = \mathbf{R}(\psi)v \quad (13.411)$$

$$\mathbf{M}\dot{v} + \mathbf{C}(v)v + \mathbf{D}(v)v = \tau \quad (13.412)$$

where

$$\mathbf{M} = \begin{bmatrix} m - X_{\dot{u}} & 0 & 0 \\ 0 & m - Y_{\dot{v}} & mx_g - Y_{\dot{r}} \\ 0 & mx_g - N_{\dot{v}} & I_z - N_{\dot{r}} \end{bmatrix} \quad (13.413)$$

Conventional accelerometers measure linear accelerations along the body axes. Hence, the signals  $\dot{u}$  and  $\dot{v}$  can be fed back using the control law

$$\tau = \tau_{PD} - \mathbf{K}_m\dot{v} - \mathbf{C}_m(v)v \quad (13.414)$$

where

$$\mathbf{K}_m = \begin{bmatrix} K_{11} & K_{12} & 0 \\ K_{21} & K_{22} & 0 \\ K_{31} & K_{32} & 0 \end{bmatrix} \quad (13.415)$$

$$\mathbf{C}_m(v) = \begin{bmatrix} 0 & 0 & -K_{21}u - K_{22}v \\ 0 & 0 & K_{11}u + K_{12}v \\ K_{21}u + K_{22}v & -K_{11}u - K_{12}v & 0 \end{bmatrix} \quad (13.416)$$

The expression for  $\mathbf{C}_m(\mathbf{v})$  in (13.414) is based on (6.43). Consequently, the system inertia matrix after acceleration feedback becomes

$$\mathbf{H} = \mathbf{M} + \mathbf{K}_m = \begin{bmatrix} m - X_{\dot{u}} + K_{11} & K_{12} & 0 \\ K_{21} & m - Y_{\dot{v}} + K_{22} & mx_g - Y_{\dot{r}} \\ K_{31} & mx_g - N_{\dot{v}} + K_{32} & I_z - N_{\dot{r}} \end{bmatrix} \quad (13.417)$$

and

$$\mathbf{C}_H(\mathbf{v}) = \mathbf{C}(\mathbf{v}) + \mathbf{C}_m(\mathbf{v}) \quad (13.418)$$

The feedback term  $\mathbf{C}_m(\mathbf{v})\mathbf{v}$  is necessary to ensure that

$$\mathbf{s}^\top [\dot{\mathbf{H}}^*(\psi) - 2\mathbf{C}_H^*(\mathbf{v}, \psi)]\mathbf{s} = 0, \quad \mathbf{s} \neq \mathbf{0} \quad (13.419)$$

where

$$\mathbf{H}^*(\psi) = \mathbf{R}(\psi)\mathbf{H}\mathbf{R}^\top(\psi) \quad (13.420)$$

$$\mathbf{C}_H^*(\mathbf{v}, \psi) = \mathbf{R}(\psi)[\mathbf{C}_H(\mathbf{v}) - \mathbf{H}\mathbf{R}^\top(\psi)\dot{\mathbf{R}}(\psi)]\mathbf{R}^\top(\psi) \quad (13.421)$$

The control law (13.414) gives us some flexibility since the acceleration feedback terms  $K_{11}$ ,  $K_{12}$ ,  $K_{21}$ ,  $K_{22}$ ,  $K_{31}$  and  $K_{32}$  can be chosen such that  $\mathbf{H} = \mathbf{H}^\top > 0$ . A symmetric inertia matrix is obtained by requiring that

$$\mathbf{K}_m = \begin{bmatrix} K_{11} & K_{12} & 0 \\ K_{21} & K_{22} & 0 \\ K_{31} & K_{32} & 0 \end{bmatrix} := \begin{bmatrix} X_{\dot{u}} + \Delta K_{11} & 0 & 0 \\ 0 & Y_{\dot{v}} + \Delta K_{22} & 0 \\ 0 & N_{\dot{v}} - Y_{\dot{r}} & 0 \end{bmatrix} \quad (13.422)$$

where  $\Delta K_{11}$  and  $\Delta K_{22}$  can be treated as additional design parameters for the mass in the  $x$  and  $y$  directions. The resulting expression is

$$\mathbf{H} = \begin{bmatrix} m + \Delta K_{11} & 0 & 0 \\ 0 & m + \Delta K_{22} & mx_g - Y_{\dot{r}} \\ 0 & mx_g - Y_{\dot{r}} & I_z - N_{\dot{r}} \end{bmatrix} \quad (13.423)$$

If  $\Delta K_{11} = \Delta K_{22}$ , the mass in the  $x$  and  $y$  directions is equal. Hence, the PID controller will be independent of the heading angle, which is advantageous when tuning dynamic positioning systems, for instance.

The resulting dynamics after acceleration feedback is

$$\mathbf{H}\dot{\mathbf{v}} + \mathbf{C}_H(\mathbf{v})\mathbf{v} + \mathbf{D}(\mathbf{v})\mathbf{v} = \boldsymbol{\tau}_{\text{PD}} \quad (13.424)$$

Consider the CLF:

$$V_1 = \frac{1}{2}\mathbf{z}_1^\top \mathbf{K}_p \mathbf{z}_1, \quad \mathbf{z}_1 = \boldsymbol{\eta}_d - \boldsymbol{\eta} \quad (13.425)$$

$$V_2 = V_1 + \frac{1}{2}\mathbf{v}^\top \mathbf{H}\mathbf{v} \quad (13.426)$$

where  $V_1$  and  $V_2$  represent the potential and kinetic energy, respectively.

## New State Variables

Assume that the reference trajectories  $\eta_d^{(3)}, \ddot{\eta}_d, \dot{\eta}_d$  and  $\eta_d$  are smooth and bounded. A virtual reference trajectory is defined as

$$\dot{\eta}_r := \dot{\eta}_d - \Lambda \tilde{\eta}, \quad v_r := R^\top(\psi) \dot{\eta}_r \quad (13.427)$$

where  $\tilde{\eta} = \eta - \eta_d$  is the tracking error and  $\Lambda > 0$  is a diagonal design matrix. Furthermore, let

$$s = \dot{\eta} - \dot{\eta}_r = \dot{\tilde{\eta}} + \Lambda \tilde{\eta} \quad (13.428)$$

The marine craft dynamics (13.411)–(13.424) can be transformed to

$$H^*(\psi) \ddot{\eta} + C_H^*(v, \psi) \dot{\eta} + D^*(v, \psi) \eta = R(\psi) \tau_{PD} \quad (13.429)$$

Hence,

$$\begin{aligned} H^*(\psi) \dot{s} &= -C_H^*(v, \psi) s - D^*(v, \psi) s + R(\psi) \tau_{PD} \\ &\quad - H^*(\psi) \ddot{\eta}_r - C_H^*(v, \psi) \dot{\eta}_r - D^*(v, \psi) \eta_r \end{aligned} \quad (13.430)$$

or equivalently

$$H^*(\psi) \dot{s} + C_H^*(v, \psi) s + D^*(v, \psi) s = R(\psi) [\tau_{PD} - H \dot{v}_r - C_H(v) v_r - D(v) v_r] \quad (13.431)$$

**Step 1:** Consider the error dynamics:

$$\dot{\eta} - \dot{\eta}_d = R(\psi) [v - v_d] \quad (13.432)$$

Let  $R(\psi)v$  be the virtual control vector  $R(\psi)v := s + \alpha_1$ . The position error dynamics can therefore be written

$$\begin{aligned} \dot{\tilde{\eta}} &= R(\psi) [v - v_d] \\ &= s + \alpha_1 - R(\psi) v_d, \quad \{\alpha_1 = \dot{\eta}_r = \dot{\eta}_d - \Lambda \tilde{\eta}, \quad \dot{\eta}_d = R(\psi) v_d\} \\ &= -\Lambda \tilde{\eta} + s \end{aligned} \quad (13.433)$$

Hence,

$$V_1 = \frac{1}{2} \tilde{\eta}^\top K_p \tilde{\eta}, \quad K_p = K_p^\top > 0 \quad (13.434)$$

and

$$\begin{aligned} \dot{V}_1 &= \tilde{\eta}^\top K_p \dot{\tilde{\eta}} \\ &= \tilde{\eta}^\top K_p (-\Lambda \tilde{\eta} + s) \\ &= -\tilde{\eta}^\top K_p \Lambda \tilde{\eta} + s^\top K_p \tilde{\eta} \end{aligned} \quad (13.435)$$

**Step 2:** In the second step, a CLF is motivated by *pseudo-kinetic energy* is chosen according to

$$V_2 = \frac{1}{2} s^\top H^*(\psi) s + V_1 \quad (13.436)$$

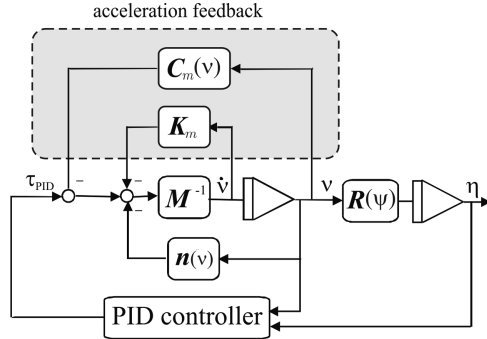


**Figure 13.20** Acceleration feedback and PID controller.

$$\begin{aligned}
 \dot{V}_2 &= s^\top H^*(\psi)\dot{s} + \frac{1}{2}s^\top \dot{H}^*(\psi)s + \dot{V}_1 \\
 &= s^\top [-C_H^*(v, \psi)s - D^*(v, \psi)s + R(\psi)[\tau_{PD} - H\dot{v}_r - C_H(v)v_r - D(v)v_r]] \\
 &\quad + \frac{1}{2}s^\top \dot{H}^*(\psi)s - \tilde{\eta}^\top K_p \Lambda \tilde{\eta} + s^\top K_p \tilde{\eta}
 \end{aligned} \tag{13.437}$$

Using the skew-symmetric property  $s^\top [\dot{H}^*(\psi) - 2C_H^*(v, \psi)]s = 0$  yields

$$\begin{aligned}
 \dot{V}_2 &= s^\top R(\psi)[\tau_{PD} - H\dot{v}_r - C_H(v)v_r - D(v)v_r + R^\top(\psi)K_p \tilde{\eta}] \\
 &\quad - s^\top D^*(v, \psi)s - \tilde{\eta}^\top K_p \Lambda \tilde{\eta}
 \end{aligned} \tag{13.438}$$

Consequently, the 3 DOF control law

$$\tau_{PD} = H\dot{v}_r + C_H(v)v_r + D(v)v_r - R^\top(\psi)[K_p \tilde{\eta} + K_d s] \tag{13.439}$$

results in

$$\dot{V}_2 = -s^\top (D^*(v, \psi) + K_d)s - \tilde{\eta}^\top K_p \Lambda \tilde{\eta}$$

Since  $V_2$  is positive definite and  $\dot{V}_2$  is negative definite it follows that the equilibrium point  $(\tilde{\eta}, s) = (\mathbf{0}, \mathbf{0})$  is GES. Moreover, convergence of  $s \rightarrow \mathbf{0}$  and  $\tilde{\eta} \rightarrow \mathbf{0}$  implies that  $\dot{\tilde{\eta}} \rightarrow \mathbf{0}$ . The PD controller can easily be replaced by a PID controller (see Sections 13.3.4 and 13.3.5). In this case only UGAS is guaranteed.

### 13.3.9 Case Study: Nonlinear Separation Principle for PD Controller-Observer Design

For the motion control systems presented so far, slowly varying environmental forces have been compensated for by adding integral action in the controller. In this section it is demonstrated how a globally converging observer and a PD control law plus a nonlinear term of observer bias estimates can be combined to compensate for slowly varying environmental disturbances (Loria *et al.*, 2000). Moreover, the

integral term is removed in the controller and replaced by a bias estimate. The stability proof is based on a *separation principle*, which holds for nonlinear systems. The separation principle is theoretically supported by results on cascaded nonlinear systems and standard Lyapunov theory, and it is validated in practice by experimentation with a model ship.

The controller–observer is designed in three steps:

1. Design a UGAS state estimator.
2. Design the control law as if the whole state  $\mathbf{x}$  and bias term  $\mathbf{b}$  were known (measured) and free of noise.
3. Implement the control law with the observer estimates  $\hat{\mathbf{x}}$  and  $\hat{\mathbf{b}}$  and show that the observer–controller error dynamics is GAS.

The stability proof of this approach requires that the separation principle hold for nonlinear systems. The method in this section relies on Lyapunov theorems for stability of cascaded time-varying systems to prove UGAS (Panteley and Loria, 1998).

### Cascaded Systems

Consider the time-varying systems  $\Sigma_1$  and  $\Sigma_2$  (Loria *et al.*, 2000):

$$\Sigma_1 : \dot{\mathbf{x}}_1 = \mathbf{f}_1(t, \mathbf{x}_1) + \mathbf{G}(t, \mathbf{x})\mathbf{x}_2 \quad (13.440)$$

$$\Sigma_2 : \dot{\mathbf{x}}_2 = \mathbf{f}_2(t, \mathbf{x}_2) \quad (13.441)$$

where  $\mathbf{x}_1 \in \mathbb{R}^n$ ,  $\mathbf{x}_2 \in \mathbb{R}^m$  and  $\mathbf{x} = [\mathbf{x}_1^\top, \mathbf{x}_2^\top]^\top$ . The function  $\mathbf{f}_1(t, \mathbf{x}_1)$  is continuously differentiable in  $(t, \mathbf{x}_1)$ , while  $\mathbf{f}_2(t, \mathbf{x}_2)$  and  $\mathbf{G}(t, \mathbf{x})$  are continuous in their arguments, and locally Lipschitz. The two subsystems  $\Sigma_1$  and  $\Sigma_2$  will represent the controller and observer error dynamics, respectively, while  $\mathbf{G}(t, \mathbf{x})\mathbf{x}_2$  is the interaction term coupling these two subsystems together. A growth rate condition on  $\mathbf{G}(t, \mathbf{x})$  is needed in order to prevent the controller error dynamics  $\Sigma_1$  from becoming unstable when the true states are replaced with observer estimates.

The cascaded system (13.440)–(13.441) can be proven to be UGAS by reformulating Theorems 1 and 2 in Panteley and Loria (1998) according to:

#### **Theorem 13.1 (UGAS for Cascaded Systems)**

The cascaded system (13.440)–(13.441) is UGAS if Assumptions A1–A3 are satisfied:

A1. The system

$$\dot{\mathbf{x}}_1 = \mathbf{f}_1(t, \mathbf{x}_1) \quad (13.442)$$

is UGAS with a Lyapunov function  $V(t, \mathbf{x}_1)$ ,  $V : \mathbb{R}_{\geq 0} \times \mathbb{R}^n \rightarrow \mathbb{R}_{\geq 0}$ , positive definite, that is  $V(t, \mathbf{0}) = \mathbf{0}$  and  $V(t, \mathbf{x}_1) > 0$  for all  $\mathbf{x}_1 \neq \mathbf{0}$ , and proper (radially unbounded), which satisfies

$$\left\| \frac{\partial V}{\partial \mathbf{x}_1} \right\| \|\mathbf{x}_1\| \leq c_1 V(t, \mathbf{x}_1), \quad \forall \|\mathbf{x}_1\| \geq \mu \quad (13.443)$$

where  $c_1, \mu > 0$ . It is also assumed that  $(\partial V / \partial \mathbf{x}_1)(t, \mathbf{x}_1)$  is bounded uniformly in  $t$  for all  $\|\mathbf{x}_1\| < \mu$ ; that is there exists a constant  $c_2 > 0$  such that for all  $t \geq t_0 \geq 0$ :

$$\left\| \frac{\partial V}{\partial \mathbf{x}_1} \right\| \leq c_2, \quad \forall \|\mathbf{x}_1\| \leq \mu \quad (13.444)$$

A2. The function  $\mathbf{G}(t, \mathbf{x})$  satisfies

$$\|\mathbf{G}(t, \mathbf{x})\| \leq \theta_1(\|\mathbf{x}_2\|) + \theta_2(\|\mathbf{x}_2\|)\|\mathbf{x}_1\| \quad (13.445)$$

where  $\theta_1, \theta_2 : \mathbb{R}_{\geq 0} \rightarrow \mathbb{R}_{\geq 0}$  are continuous.

A3. Equation  $\dot{\mathbf{x}}_2 = \mathbf{f}_2(t, \mathbf{x}_2)$  is UGAS, and for all  $t_0 \geq 0$ :

$$\int_{t_0}^{\infty} \|\mathbf{x}_2(t)\| dt \leq \phi(\|\mathbf{x}_2(t_0)\|) \quad (13.446)$$

where the function  $\phi(\cdot)$  is a class  $\mathcal{K}$  function.

### DP Control System

Consider the nonlinear DP model:

$$\dot{\boldsymbol{\eta}} = \mathbf{R}(\psi)\mathbf{v} \quad (13.447)$$

$$\mathbf{M}\dot{\mathbf{v}} + \mathbf{D}\mathbf{v} = \boldsymbol{\tau} + \mathbf{R}^T(\psi)\mathbf{b} \quad (13.448)$$

$$\dot{\mathbf{b}} = \mathbf{0} \quad (13.449)$$

$$\mathbf{y} = \boldsymbol{\eta} + \boldsymbol{\eta}_w \quad (13.450)$$

where  $\mathbf{b} \in \mathbb{R}^3$  is a bias term representing slowly varying environmental forces and  $\mathbf{y} \in \mathbb{R}^3$  represent the measurements. Instead of using integral action to compensate for  $\mathbf{b}$ , a PD controller

$$\boldsymbol{\tau} = -\mathbf{R}^T(\psi)\mathbf{K}_p\mathbf{e} - \mathbf{K}_d\mathbf{v} - \mathbf{R}^T(\psi)\mathbf{b}, \quad \mathbf{e} = \boldsymbol{\eta} - \boldsymbol{\eta}_d \quad (13.451)$$

can be implemented under the assumption that  $\mathbf{b}$  is known (perfect compensation) and  $\dot{\boldsymbol{\eta}}_d = \mathbf{0}$ . However, it is impossible to measure  $\mathbf{b}$  so a state observer is needed. For this purpose the passive observer (11.128)–(11.132) in Section 11.4.1 can be used to generate estimates of  $\boldsymbol{\eta}$ ,  $\mathbf{v}$  and  $\mathbf{b}$ , and at the same time provide wave filtering. Application of a nonlinear separation principle implies that the controller can be implemented using the estimated states  $\hat{\boldsymbol{\eta}}$ ,  $\hat{\mathbf{v}}$  and  $\hat{\mathbf{b}}$ ; that is

$$\boldsymbol{\tau} = -\mathbf{R}^T(\psi)\mathbf{K}_p\hat{\mathbf{e}} - \mathbf{K}_d\hat{\mathbf{v}} - \mathbf{R}^T(\psi)\hat{\mathbf{b}}, \quad \hat{\mathbf{e}} = \hat{\boldsymbol{\eta}} - \boldsymbol{\eta}_d \quad (13.452)$$

The proof needed to show that the passive observer with the controller (13.452) is UGAS is done in three steps corresponding to Assumptions A1–A3 in Theorem 13.1.

### Step 1: Observer Error Dynamics

Since the observer error dynamics

$$\Sigma_2 : \dot{\mathbf{x}}_2 = \mathbf{f}_2(t, \mathbf{x}_2) \quad (13.453)$$

is UGES and consequently UGAS when considering the passive observer in Section 11.4.1, there exist positive constants  $\lambda_1$  and  $\lambda_2$  such that

$$\|\mathbf{x}_2(t)\| \leq \lambda_1 \|\mathbf{x}_2(t_0)\| e^{-\lambda_2(t-t_0)} \quad (13.454)$$

Therefore Assumption A3 in Theorem 13.1 is satisfied with  $\phi(\|\mathbf{x}_2(t_0)\|) = (\lambda_1/\lambda_2) \|\mathbf{x}_2(t_0)\|$ .

### Step 2: Regulator Error Dynamics

The *full-state* feedback controller (13.451) when applied to (13.447)–(13.448) results in

$$\dot{\mathbf{e}} = \mathbf{R}(\psi)\mathbf{v} \quad (13.455)$$

$$\mathbf{M}\dot{\mathbf{v}} + (\mathbf{D} + \mathbf{K}_d)\mathbf{v} + \mathbf{R}^\top(\psi)\mathbf{K}_p\mathbf{e} = \mathbf{0} \quad (13.456)$$

This system is GAS according to LaSalle–Krasovskii's theorem since

$$V = \frac{1}{2} (\mathbf{v}^\top \mathbf{M} \mathbf{v} + \mathbf{e}^\top \mathbf{K}_p \mathbf{e}) > 0, \quad \forall \mathbf{v} \neq \mathbf{0}, \mathbf{e} \neq \mathbf{0} \quad (13.457)$$

and

$$\dot{V} = -\mathbf{v}^\top (\mathbf{D} + \mathbf{K}_d) \mathbf{v} \leq 0 \quad (13.458)$$

This implies that the first condition on the system  $\dot{\mathbf{x}}_1 = f_1(t, \mathbf{x}_1)$ , Assumption A1 in Theorem 13.1, is satisfied. Next, a constant  $c_1$  is easily found by considering

$$\left\| \frac{\partial V}{\partial \mathbf{x}_1} \right\| \|\mathbf{x}_1\| \leq \max\{m_M, k_M, 1\} \|\mathbf{x}_1\|^2, \quad \forall \|\mathbf{x}_1\| \geq \mu \quad (13.459)$$

where  $m_M = \lambda_{\max}(\mathbf{M})$  and  $k_M = \lambda_{\max}(\mathbf{K}_p)$ . Hence, (13.443) is satisfied with

$$c_1 = \frac{\max\{m_M, k_M, 1\}}{\min\{m_m, k_m, 1\}} \quad (13.460)$$

where  $m_m = \lambda_{\min}(\mathbf{M})$  and  $k_m = \lambda_{\min}(\mathbf{K}_p)$ . Also from (13.459) it is clear that (13.444) is satisfied by

$$c_2 = \max\{m_M, k_M, 1\}\mu \quad (13.461)$$

### Step 3: Growth Rate Condition

Finally, it can be shown that the growth rate condition (13.445) on  $\mathbf{x}_1$ , Assumption A2 in Theorem 13.1, is satisfied by choosing  $\theta_1 = \text{constant}$  and  $\theta_2 = 0$  such that

$$\|\mathbf{G}(t, \mathbf{x})\| \leq \theta_1 (\|\mathbf{x}_2\|) \quad (13.462)$$

The details in this analysis is found in Loria *et al.* (2000).

### Experimental Results

The nonlinear controller (13.452) and passive observer of Section 11.4.1 have been tested experimentally using a model ship. In this experiment wind and wave forces were generated using a fan and a wave maker. More details regarding the experiment are found in Loria *et al.* (2000).

In the experiments the desired position and heading of the ship during DP were chosen as

$$x_d = 208 \text{ m} \quad (13.463)$$

$$y_d = 334 \text{ m} \quad (13.464)$$

$$\psi_d = -150 \text{ deg} \quad (13.465)$$

The experiment was carried out for a ship scale 1:70, but the results have been transformed to full scale. The development of the experiment is as follows:

1. During the first 350 seconds there are no environmental forces perturbing the ship.

*Comments:* From Figure 13.22 it is seen that the bias estimate  $\hat{b}$  and the WF estimate  $\hat{\eta}_w$  are both approximately zero, as expected, in the first 350 seconds. The nonzero values of  $\hat{b}$  are due to the water motion generated by the propellers. It is also seen that the regulation and estimation errors are very small during this phase; see upper plots in Figures 13.21 and 13.23.

2. After 350 seconds wind forces are generated by using a ducted fan directed approximately 30 degrees off the port side bow of the ship.

*Comments:* When turned on, the fan produces a step input disturbance to the system; notice the peaks in Figures 13.21 and 13.23. This step is an unrealistic situation (in full-scale applications, no abrupt changes in the bias occur). However, it can be generated in the laboratory to show the performance of the observer-based controller. The bias estimates  $\hat{b}$  from the observer are used in the output feedback control law to obtain perfect regulation, which verifies the separation principle (see Figure 13.23). Most of the wind force is compensated by the control input, and therefore the regulation errors converge to zero in 100–150 seconds; see the first three plots of Figure 13.21. However, since the wind force is a step, the observer needs some time for the bias estimate to converge to its true value, after which the controller compensates for the bias, hence keeping the ship almost still.

3. After 800 seconds the wave generator is turned on.

*Comments:* This results in an oscillatory WF motion  $\eta_w$  which builds up over time. The estimated wave frequency motion  $\hat{\eta}_w$  is shown in the upper plots of Figure 13.22. Their effect in the position measurements is shown in the upper plots of Figure 13.21. In order to avoid  $\hat{\eta}_w$  entering the feedback loop, this signal is filtered out from the position measurement. This results in smooth controls; see the bottom plots of Figure 13.22. The LF estimates are clearly shown in the upper plots of Figure 13.21.

4. After 1700 seconds both the wind and wave generators are turned off.

*Comments:* Turning off the fan produces a second step input disturbance while the wave-induced motion decays more slowly. It is seen from Figure 13.22 that the bias estimates drop to approximately their initial values in 100–150 seconds while the amplitudes of the WF motion estimates drop quite slowly. Again, almost perfect regulation to zero is obtained as soon as the bias estimates have converged to their true values. This clearly demonstrates the separation principle. In a full-scale implementation the wind force will build up quite slowly. Hence the step inputs do not constitute a problem.

### 13.3.10 Case Study: Weather Optimal Position Control for Ships and Floating Structures

Conventional DP systems for ships and free-floating rigs are usually designed for stationkeeping by specifying a desired constant position ( $N_d, E_d$ ) and a desired constant heading angle  $\psi_d$ . In order to minimize the ship fuel consumption, the desired heading  $\psi_d$  should in many operations be chosen such that the yaw moment is zero. For vessels with port/starboard symmetry, this means that the mean environmental forces due to wind, waves and ocean currents act through the centerline of the vessel. Then the ship must be rotated until the yaw moment is zero.

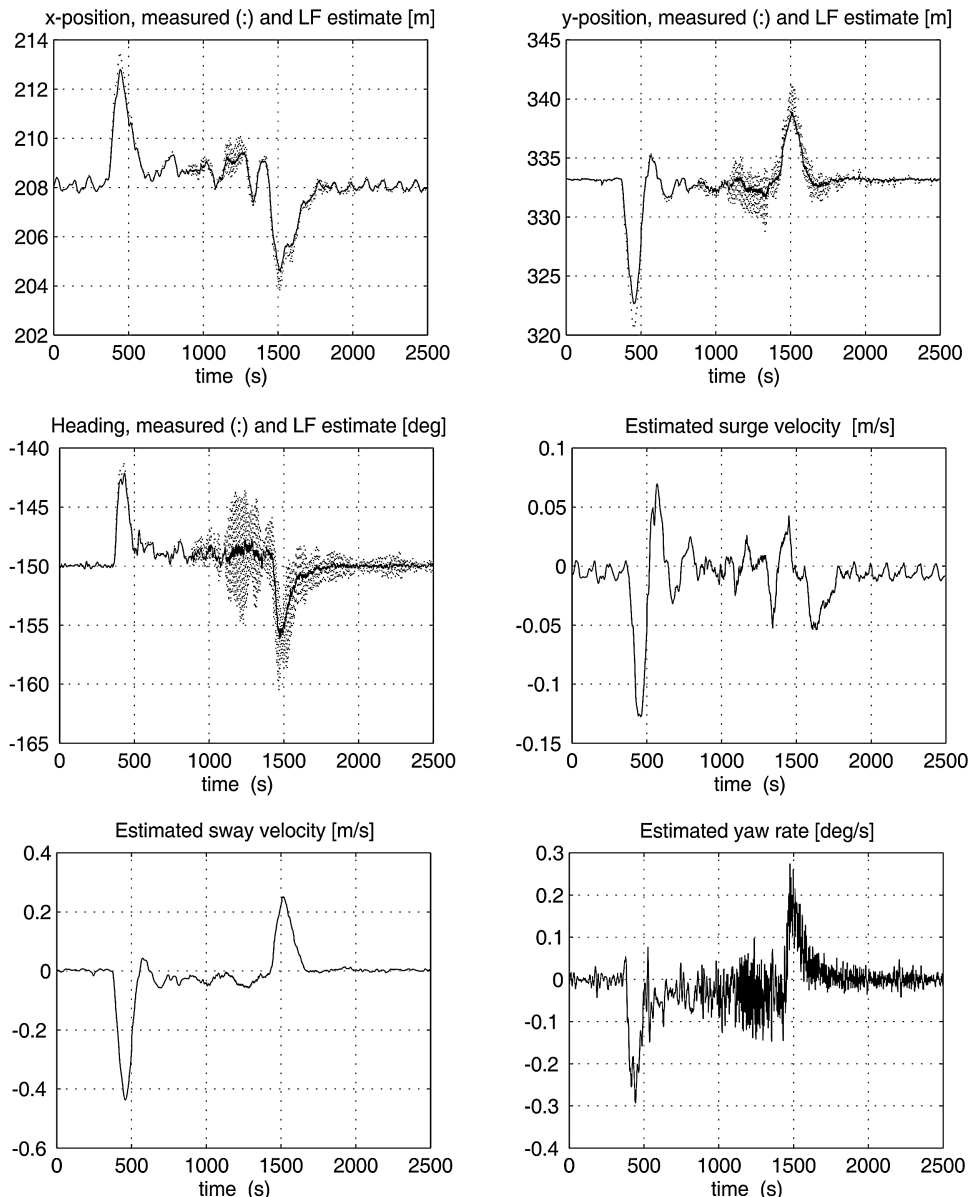


**Figure 13.21** Plots 1–3 show the three components of the measurement vector  $\mathbf{y} = [x + x_w, y + y_w, \psi + \psi_w]$  and the LF estimates. Plots 4–6 show the estimated LF velocity components  $\hat{\mathbf{v}} = [\hat{u}, \hat{v}, \hat{r}]^\top$  versus time.

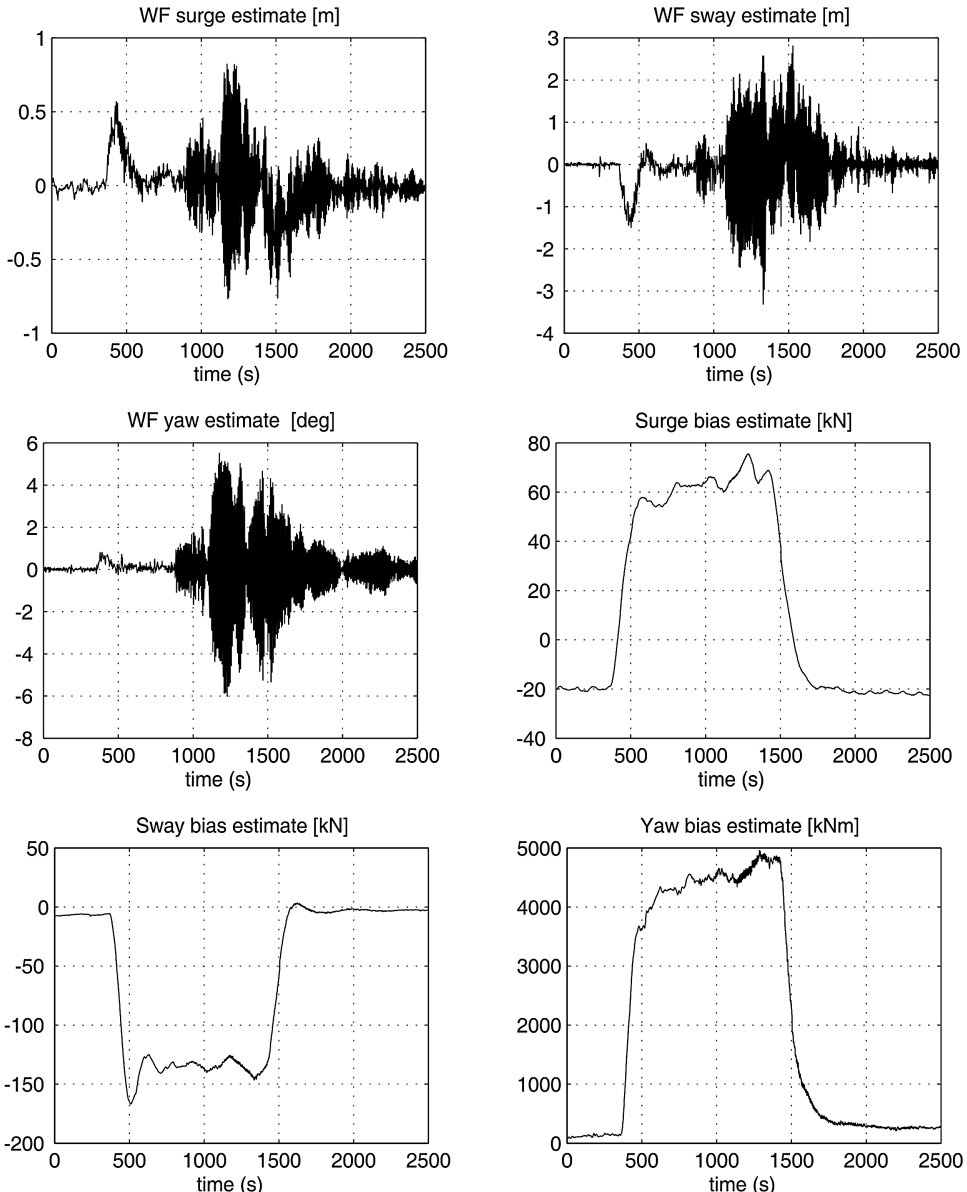


**Figure 13.22** Plots 1–3 show the estimated WF motion components  $\hat{\eta}_w = [\hat{x}_w, \hat{y}_w, \hat{\psi}_w]^\top$  while plots 4–6 show the bias estimates  $\hat{b} = [\hat{b}_1, \hat{b}_2, \hat{b}_3]^\top$  versus time.

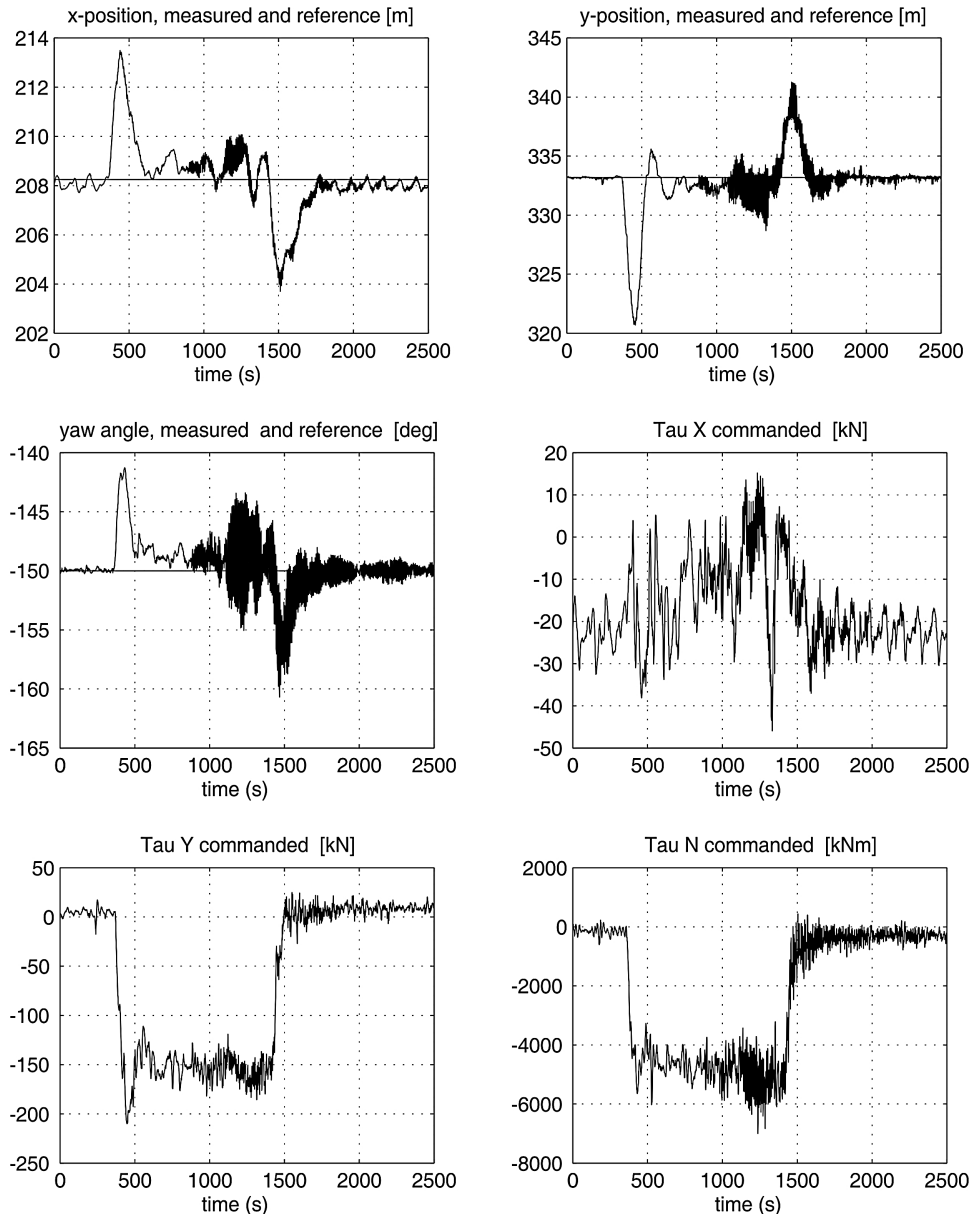


**Figure 13.23** Plots 1–3 show the three components of the measured position  $\mathbf{y} = [x + x_w, y + y_w, \psi + \psi_w]^\top$  together with the desired position  $\mathbf{\eta}_d = [x_d, y_d, \psi_d]^\top$  while plots 4–6 are the control inputs  $\boldsymbol{\tau} = [\tau_1, \tau_2, \tau_3]^\top$  versus time.

Unfortunately, it is impossible to measure or compute the direction of the mean environmental force with sufficient accuracy. Hence, the desired heading  $\psi_d$  is usually taken to be the measurement of the mean wind direction, which can be easily measured. In practice, however, this can result in large offsets from the true mean direction of the total environmental force. The main reason for this is the unmeasured ocean current force component and waves that do not coincide with the wind direction. Hence, the DP system can be operated under highly nonoptimal conditions if fuel saving is the issue. A small offset in the optimal heading angle will result in a large use of thrust.

One popular method for computing the weather optimal heading  $\psi_d$  is to monitor the resulting thruster forces in the  $x$  and  $y$  directions. Hence, the bow of the ship can be turned in one direction until the thruster force in the  $y$  direction approaches zero. This method is appealing but the main catch in doing this is that the total resulting thruster forces in the  $x$  and  $y$  directions have to be computed since there are no sensors doing this job directly. The sensors only measure the angular speed and pitch angle of the propellers. Hence, the thrust for each propeller must be computed by using a model of the thruster characteristic, resulting in a fairly rough estimate of the total thruster force in each direction.

Another principle, proposed by Pinkster (1971) and Pinkster and Nienhuis (1986), is to control the  $x$  and  $y$  positions using a PID feedback controller, in addition to feedback from the yaw velocity, such that the vessel tends toward the optimal heading. This principle, however, requires that the rotation point of the vessel is located a certain distance forward of the center of gravity, or even fore of the bow, and it also puts restrictions on the thruster configuration and the number of thrusters installed.

This section describes the weather optimal position controller (WOPC) by Fossen and Strand (2001). The control objective is that the vessel heading should adjust automatically to the mean environmental forces (wind, waves and ocean currents) such that a minimum amount of energy is used in order to save fuel and reduce  $\text{NO}_x/\text{CO}_x$  emissions without using any environmental sensors. This is particularly useful for shuttle tankers and FPSOs, which can be located at the same position for a long time. Also DP-operated supply vessels that must keep their position for days in loading/off-loading operations have a great WOPC fuel-saving potential.

The ship can be exponentially stabilized on a circle arc with constant radius by letting the bow of the ship point toward the origin of the circle. In order to maintain a fixed position at the same time, a translatory circle center control law is designed. The circle center is translated such that the Cartesian position is constant, while the bow of the ship is automatically turned up against the mean environmental force to obtain weathervaning. This approach is motivated by a pendulum in the gravity field where gravity is the unmeasured quantity. The circular motion of the controlled ship, where the mean environmental force can be interpreted as an unknown force field, copies the dynamics of a pendulum in the gravity field (see Figure 13.24).

### 3 DOF Equations of Motion using Polar Coordinates

Consider a marine craft in 3 DOF:

$$\dot{\eta} = \mathbf{R}(\psi)\mathbf{v} \quad (13.466)$$

$$\mathbf{M}\dot{\mathbf{v}} + \mathbf{C}(\mathbf{v})\mathbf{v} + \mathbf{D}(\mathbf{v})\mathbf{v} = \boldsymbol{\tau} + \mathbf{w} \quad (13.467)$$

where the North-East positions ( $N, E$ ) and heading  $\psi$  are represented by  $\eta = [N, E, \psi]^\top$  and the body-fixed velocities are represented by  $\mathbf{v} = [u, v, r]^\top$ . It is assumed that  $\mathbf{M} = \mathbf{M}^\top > 0$ ,  $\dot{\mathbf{M}} = \mathbf{0}$  and  $\mathbf{D}(\mathbf{v}) > 0$ . Unmodeled external forces and moment due to wind, ocean currents and waves are lumped together into a body-fixed disturbance vector  $\mathbf{w} \in \mathbb{R}^3$  to be interpreted later.

The Cartesian coordinates ( $N, E$ ) are related to the *polar coordinates* by

$$N = N_0 + \rho \cos(\gamma), \quad E = E_0 + \rho \sin(\gamma) \quad (13.468)$$

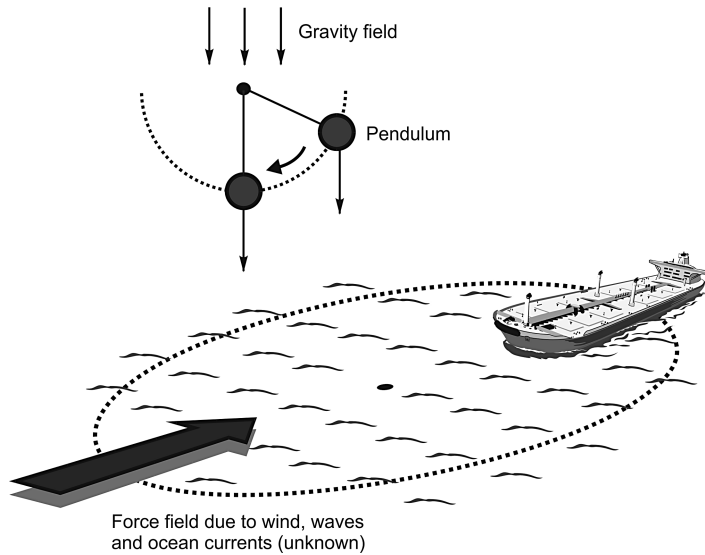


**Figure 13.24** The principle of WOPC using the equivalence to a pendulum in the gravity field where gravity is the unmeasured quantity.

where  $(N_0, E_0)$  is the origin of a circle with radius  $\rho$  and polar angle  $\gamma$  given by

$$\rho = \sqrt{(N - N_0)^2 + (E - E_0)^2} \quad \gamma = \text{atan2}((E - E_0), (N - N_0)) \quad (13.469)$$

Time differentiation of (13.468) yields

$$\dot{N} = \dot{N}_0 + \dot{\rho} \cos(\gamma) - \rho \sin(\gamma)\dot{\gamma} \quad (13.470)$$

$$\dot{E} = \dot{E}_0 + \dot{\rho} \sin(\gamma) + \rho \cos(\gamma)\dot{\gamma} \quad (13.471)$$

Define the state vectors:

$$\mathbf{p}_0 := [N_0, E_0]^\top, \quad \mathbf{x} := [\rho, \gamma, \psi]^\top \quad (13.472)$$

From (13.470) and (13.471) a new kinematic relationship can be derived in terms of the vectors  $\mathbf{p}_0$  and  $\mathbf{x}$  as

$$\dot{\eta} = \mathbf{R}(\gamma)\mathbf{H}(\rho)\dot{\mathbf{x}} + \mathbf{L}\dot{\mathbf{p}}_0 \quad (13.473)$$

$$\mathbf{H}(\rho) = \begin{bmatrix} 1 & 0 & 0 \\ 0 & \rho & 0 \\ 0 & 0 & 1 \end{bmatrix}, \quad \mathbf{L} = \begin{bmatrix} 1 & 0 \\ 0 & 1 \\ 0 & 0 \end{bmatrix} \quad (13.474)$$

From (13.473) the Cartesian kinematics (13.466) can be replaced by a differential equation for the polar coordinates:

$$\dot{\mathbf{x}} = \mathbf{T}(\mathbf{x})\mathbf{v} - \mathbf{T}(\mathbf{x})\mathbf{R}^\top(\psi)\mathbf{L}\dot{\mathbf{p}}_0 \quad (13.475)$$

$$\mathbf{T}(\mathbf{x}) = \mathbf{H}^{-1}(\rho) \underbrace{\mathbf{R}^\top(\gamma)\mathbf{R}(\psi)}_{\mathbf{R}^\top(\gamma-\psi)} \quad (13.476)$$

Note that the conversion between Cartesian and polar coordinates is only a local diffeomorphism, since the radius must be kept larger than a minimum value, that is  $\rho > \rho_{\min} > 0$ , in order to avoid the singular point  $\rho = 0$ .

### Marine Craft Model Transformation

The marine craft model (13.467) can be expressed in polar coordinates by using (13.475) and substituting

$$\mathbf{v} = \mathbf{T}^{-1}(\mathbf{x})\dot{\mathbf{x}} + \mathbf{R}^\top\mathbf{L}\dot{\mathbf{p}}_0 \quad (13.477)$$

$$\dot{\mathbf{v}} = \mathbf{T}^{-1}(\mathbf{x})\ddot{\mathbf{x}} + \dot{\mathbf{T}}^{-1}(\mathbf{x})\dot{\mathbf{x}} + \mathbf{R}^\top\mathbf{L}\ddot{\mathbf{p}}_0 + \dot{\mathbf{R}}^\top\mathbf{L}\dot{\mathbf{p}}_0 \quad (13.478)$$

such that

$$\begin{aligned} \mathbf{M}\dot{\mathbf{v}} + \mathbf{C}(\mathbf{v})\mathbf{v} + \mathbf{D}(\mathbf{v})\mathbf{v} &= \boldsymbol{\tau} + \mathbf{w} \\ \Updownarrow \rho > 0 \\ \mathbf{M}_x(\mathbf{x})\ddot{\mathbf{x}} + \mathbf{C}_x(\mathbf{v}, \mathbf{x})\dot{\mathbf{x}} + \mathbf{D}_x(\mathbf{v}, \mathbf{x})\dot{\mathbf{x}} &= \mathbf{T}^{-\top}[\mathbf{q}(\mathbf{v}, \mathbf{x}, \dot{\mathbf{p}}_0, \ddot{\mathbf{p}}_0) + \boldsymbol{\tau} + \mathbf{w}] \end{aligned} \quad (13.479)$$

where

$$\mathbf{M}_x(\mathbf{x}) = \mathbf{T}^{-\top}(\mathbf{x})\mathbf{M}\mathbf{T}^{-1}(\mathbf{x})$$

$$\mathbf{C}_x(\mathbf{v}, \mathbf{x}) = \mathbf{T}^{-\top}(\mathbf{x}) (\mathbf{C}(\mathbf{v}) - \mathbf{M}\mathbf{T}^{-1}(\mathbf{x})\dot{\mathbf{T}}(\mathbf{x})) \mathbf{T}^{-1}(\mathbf{x})$$

$$\mathbf{D}_x(\mathbf{v}, \mathbf{x}) = \mathbf{T}^{-\top}(\mathbf{x})\mathbf{D}(\mathbf{v})\mathbf{T}^{-1}(\mathbf{x})$$

$$\mathbf{q}(\mathbf{v}, \mathbf{x}, \dot{\mathbf{p}}_0, \ddot{\mathbf{p}}_0) = -\mathbf{M}\mathbf{R}^\top(\psi)\mathbf{L}\ddot{\mathbf{p}}_0 - \mathbf{M}\dot{\mathbf{R}}^\top(\psi)\mathbf{L}\dot{\mathbf{p}}_0 - [\mathbf{C}(\mathbf{v}) + \mathbf{D}(\mathbf{v})]\mathbf{R}^\top(\psi)\mathbf{L}\dot{\mathbf{p}}_0$$

Here  $\mathbf{M}_x(\mathbf{x})$ ,  $\mathbf{C}_x(\mathbf{v}, \mathbf{x})$  and  $\mathbf{D}_x(\mathbf{v}, \mathbf{x})$  can be shown to satisfy

$$\mathbf{M}_x(\mathbf{x}) = \mathbf{M}_x^\top(\mathbf{x}) > 0, \quad \mathbf{D}_x(\mathbf{v}, \mathbf{x}) > 0, \quad \forall \mathbf{x}$$

The marine craft dynamics also satisfy the skew-symmetric property:

$$\mathbf{z}^\top (\dot{\mathbf{M}}_x - 2\mathbf{C}_x) \mathbf{z} = 0, \quad \forall \mathbf{z}, \mathbf{x} \quad (13.480)$$

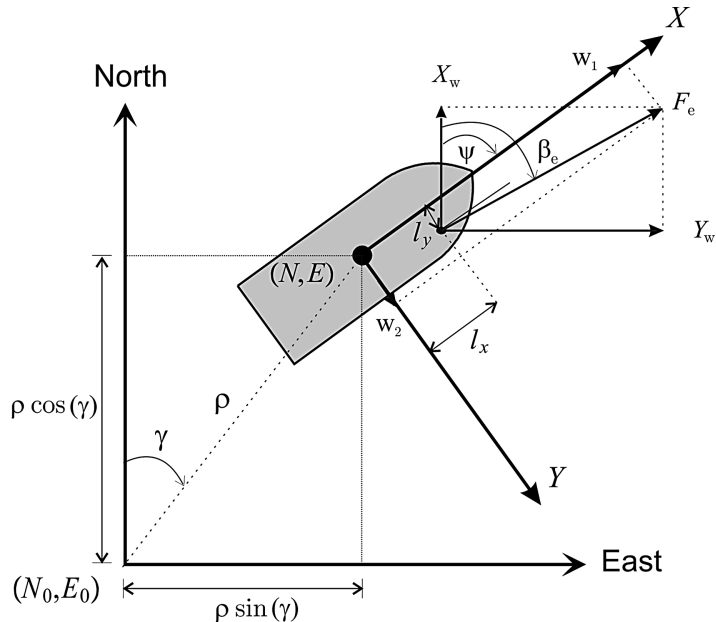


**Figure 13.25** Environmental force  $F_e$  decomposed into components  $w_1$  and  $w_2$ .

### Weather Optimal Control Objectives

The steady-state LF motion of the craft and also the craft's equilibrium position depend on the *unknown* environmental forces acting on the hull. Let the environmental forces due to *wind*, *waves* and *ocean currents* be represented by:

- A slowly varying mean force  $F_e$  that attacks the craft at a point  $(l_x, l_y)$  in body-fixed coordinates.
- A slowly varying mean direction  $\beta_e$  relative to the Earth-fixed frame (see Figure 13.25).

The WF motion is assumed to be filtered out of the measurements by using a wave filter (see Chapter 11). Since there are no sensors that can be used to measure  $(F_e, \beta_e)$  and  $(l_x, l_y)$  with sufficient accuracy, it is impossible to use feedforward from the environmental forces. This leads to the following assumptions:

**A1:** *The unknown mean environmental force  $F_e$  and its direction  $\beta_e$  are assumed to be constant or at least slowly varying.*

**A2:** *The unknown attack point  $(l_x, l_y)$  is constant for each constant  $F_e$ .*

**Discussion:** *These are good assumptions since the motion control system is only supposed to counteract the slowly varying motion components of the environmental forces.*

From Figure 13.25 the body-fixed environmental force vector  $\mathbf{w} \in \mathbb{R}^3$  can be expressed as

$$\mathbf{w} = \begin{bmatrix} w_1(\psi) \\ w_2(\psi) \\ w_3(\psi) \end{bmatrix} = \begin{bmatrix} F_e \cos(\beta_e - \psi) \\ F_e \sin(\beta_e - \psi) \\ l_x F_e \sin(\beta_e - \psi) - l_y F_e \cos(\beta_e - \psi) \end{bmatrix} \quad (13.481)$$

Notice that the environmental forces vary with the heading angle  $\psi$  of the craft. Consequently,

$$F_e = \sqrt{w_1^2 + w_2^2}, \quad \beta_e = \psi + \tan^{-1}(w_2/w_1) \quad (13.482)$$

The environmental forces  $X_w$  and  $Y_w$  with attack point  $(l_x(\psi), l_y(\psi))$  are shown in Figure 13.25. Note that the attack point will change with the yaw angle  $\psi$ . This relationship will be a complicated function of hull and superstructure geometries. However, the weather optimal control objectives can be satisfied by using the following definitions (Fossen and Strand, 2001):

#### **Definition 13.3 (Weather Optimal Heading)**

*The weather optimal heading angle  $\psi_{\text{opt}}$  is given by the equilibrium state where the yaw moment  $w_3(\psi_{\text{opt}}) = 0$  at the same time as the bow of the craft is turned up against weather (mean environmental forces); that is  $w_2(\psi_{\text{opt}}) = 0$ . This implies that  $\psi_{\text{opt}} = \beta_e$ ,  $l_x(\psi_{\text{opt}}) = \text{constant}$  and  $l_y(\psi_{\text{opt}}) = 0$  such that*

$$\mathbf{w}(\psi_{\text{opt}}) = \begin{bmatrix} w_1(\psi_{\text{opt}}) \\ w_2(\psi_{\text{opt}}) \\ w_3(\psi_{\text{opt}}) \end{bmatrix} = \begin{bmatrix} -F_e \\ 0 \\ 0 \end{bmatrix}$$

*Hence, the mean environmental force attacks the craft in the bow, which has the minimum drag coefficient for water and wind loads.*

#### **Definition 13.4 (Weather Optimal Positioning)**

*Weather optimal positioning (stationkeeping) is defined as the equilibrium state where  $\psi_{\text{opt}}$  satisfies*

$$w_1(\psi_{\text{opt}}) = -F_e, \quad w_2(\psi_{\text{opt}}) = w_3(\psi_{\text{opt}}) = l_y(\psi_{\text{opt}}) = 0 \quad (13.483)$$

*and the position  $(N, E) = (N_d, E_d)$  is kept constant.*

These definitions motivate the following two control objectives:

- **Weather Optimal Heading Control (WOHC):** This is obtained by restricting the craft's movement to a circle with constant radius  $\rho = \rho_d$  and at the same time force the craft's bow to point towards the center of the circle until the weather optimal heading angle  $\psi = \psi_{\text{opt}}$  is reached (see Figure 13.26). An analogy to this is a pendulum in a gravity field (see Figure 13.24). The position  $(N, E) = (N_0 + \rho \cos(\gamma), E_0 + \rho \sin(\gamma))$  will vary until the weather optimal heading angle is reached. This is obtained by specifying the control objective in polar coordinates according to

$$\rho_d = \text{constant}, \quad \dot{\gamma}_d = 0, \quad \psi_d = \pi + \gamma \quad (13.484)$$

**Discussion:** The requirement  $\rho_d = \text{constant}$  implies that the craft follows a circular arc with a constant radius. The second requirement  $\dot{\gamma}_d = 0$  implies that the tangential speed  $\rho\dot{\gamma}$  is kept small while the last requirement  $\psi_d = \pi + \gamma$  ensures that the craft's bow points toward the center of the circle.

- **Weather Optimal Positioning Control (WOPC):** In order to maintain a fixed Earth-fixed position  $(N, E) = (N_d, E_d)$ , the circle center  $\mathbf{p}_0 = [N_0, E_0]^\top$  must be moved simultaneously as control objective O1 is satisfied. This is referred to as *translatory circle center control*.

#### **Nonlinear and Adaptive Control Design**

The WOPC positioning controller is derived by using the polar coordinate representation. The backstepping design methodology (Krstic *et al.*, 1995) with extension to integral control (Fossen *et al.*, 2001) is

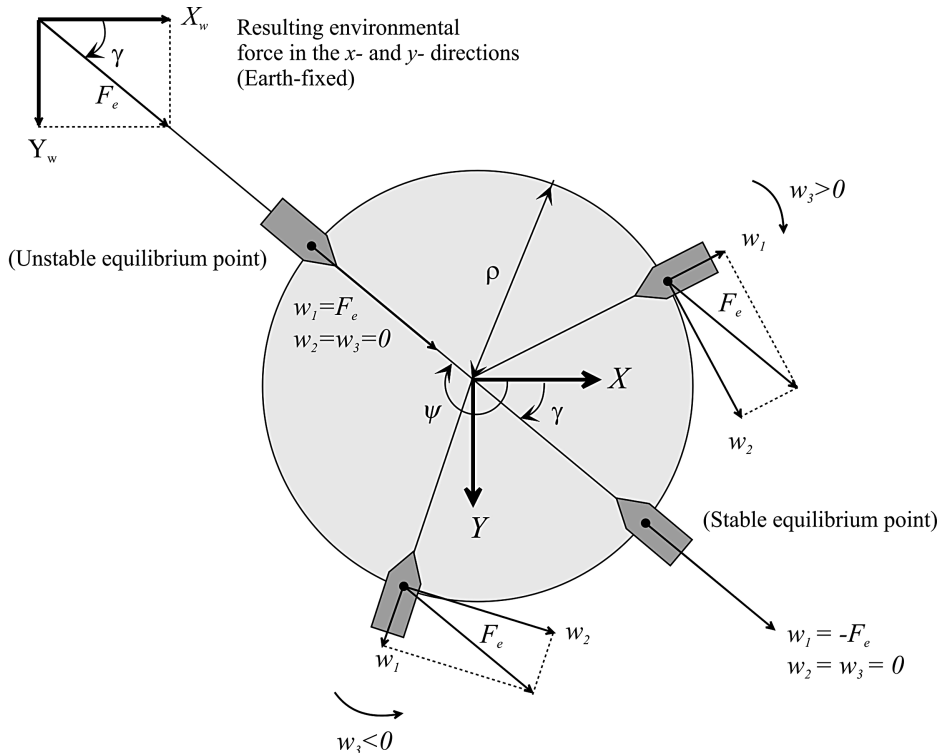


**Figure 13.26** Stable and unstable equilibrium points for WOPC.

used to derive the feedback controller (see Section 13.3). Notice that conventional PID control can be used as well. It is assumed that all states can be measured.

The WOPC controller will be derived in three successive steps:

1. *Nonlinear backstepping (PD control):* The ship is forced to move along a circular arc with desired radius  $\rho_d$ , with minimum tangential velocity  $\rho\dot{\gamma}$  and desired heading  $\psi_d$ .
2. *Adaptive backstepping (PID control):* This is necessary to compensate for the unknown environmental force  $F_e$ .
3. *Translational control of the circle center:* The circle center  $(N_0, E_0)$  is translated such that the ship maintains a constant position  $(N_d, E_d)$  even though it is moving along a virtual circular arc. Hence, the captain of the ship will only notice that the ship is rotating a yaw angle  $\psi$  about a constant position  $(N_d, E_d)$  until the weather optimal heading  $\psi_{opt}$  is reached.

### Nonlinear Backstepping (PD Control)

A general positioning controller is derived by using vectorial backstepping (Fossen and Grøvlen, 1998). The tracking objective is specified in polar coordinates using a smooth reference trajectory  $\mathbf{x}_d = [\rho_d, \gamma_d, \psi_d]^\top \in C^3$  where

$$\mathbf{x}_d, \dot{\mathbf{x}}_d, \ddot{\mathbf{x}}_d \in \mathcal{L}_\infty$$

Since the transformed system (13.479) is of order 2, backstepping is performed in two *vectorial steps*, resulting in a nonlinear PD control law. First, a *virtual reference trajectory* is defined as:

$$\dot{\mathbf{x}}_r := \dot{\mathbf{x}}_d - \boldsymbol{\Lambda} z_1 \quad (13.485)$$

where  $z_1 = \mathbf{x} - \mathbf{x}_d$  is the tracking error and  $\boldsymbol{\Lambda} > 0$  is a diagonal design matrix. Furthermore, let  $z_2$  denote a measure of tracking defined according to

$$z_2 := \dot{\mathbf{x}} - \dot{\mathbf{x}}_r = \dot{z}_1 + \boldsymbol{\Lambda} z_1 \quad (13.486)$$

From (13.486), the following expressions are obtained:

$$\dot{\mathbf{x}} = z_2 + \dot{z}_r, \quad \ddot{\mathbf{x}} = \dot{z}_2 + \ddot{z}_r \quad (13.487)$$

This implies that the marine craft model (13.479) can be expressed in terms of  $z_2$ ,  $\dot{\mathbf{x}}_r$  and  $\ddot{\mathbf{x}}_r$  as

$$\mathbf{M}_x \dot{z}_2 + \mathbf{C}_x z_2 + \mathbf{D}_x z_2 = \mathbf{T}^{-\top} \boldsymbol{\tau} + \mathbf{T}^{-\top} \mathbf{q}(\cdot) - \mathbf{M}_x \ddot{\mathbf{x}}_r - \mathbf{C}_x \dot{\mathbf{x}}_r - \mathbf{D}_x \dot{\mathbf{x}}_r + \mathbf{T}^{-\top} \mathbf{w} \quad (13.488)$$

**Step 1:** Let  $z_1$  be the first error variable, which from (13.486) has the dynamics

$$\dot{z}_1 = -\boldsymbol{\Lambda} z_1 + z_2 \quad (13.489)$$

A CLF for the first step is

$$V_1 = \frac{1}{2} z_1^\top \mathbf{K}_p z_1 \quad (13.490)$$

$$\dot{V}_1 = -z_1^\top \mathbf{K}_p \boldsymbol{\Lambda} z_1 + z_1^\top \mathbf{K}_p z_2 \quad (13.491)$$

where  $\mathbf{K}_p = \mathbf{K}_p^\top > 0$  is a constant design matrix.

**Step 2:** In the second step the CLF is motivated by the “pseudo-kinetic energy”:

$$V_2 = V_1 + \frac{1}{2} z_2^\top \mathbf{M}_x z_2, \quad \mathbf{M}_x = \mathbf{M}_x^\top > 0 \quad (13.492)$$

Time differentiation of  $V_2$  along the trajectories of  $z_1$  and  $z_2$  gives

$$\dot{V}_2 = \dot{V}_1 + z_2^\top \mathbf{M}_x \dot{z}_2 + \frac{1}{2} z_2^\top \dot{\mathbf{M}}_x z_2 \quad (13.493)$$

which by substitution of (13.491) and (13.488) gives

$$\begin{aligned} \dot{V}_2 = & -z_1^\top \mathbf{K}_p \boldsymbol{\Lambda} z_1 + \frac{1}{2} z_2^\top (\dot{\mathbf{M}}_x - 2\mathbf{C}_x) z_2 - z_2^\top \mathbf{D}_x z_2 + z_2^\top \mathbf{T}^{-\top} \mathbf{w} \\ & + z_2^\top (\mathbf{K}_p z_1 + \mathbf{T}^{-\top} \boldsymbol{\tau} + \mathbf{T}^{-\top} \mathbf{q}(\cdot) - \mathbf{M}_x \ddot{\mathbf{x}}_r - \mathbf{C}_x \dot{\mathbf{x}}_r - \mathbf{D}_x \dot{\mathbf{x}}_r) \end{aligned} \quad (13.494)$$

By using the property (13.480) and choosing the nonlinear PD control law as

$$\boldsymbol{\tau} = \mathbf{T}^\top (\mathbf{M}_x \ddot{\mathbf{x}}_r + \mathbf{C}_x \dot{\mathbf{x}}_r + \mathbf{D}_x \dot{\mathbf{x}}_r - \mathbf{K}_p z_1 - \mathbf{K}_d z_2) - \mathbf{q}(\cdot) \quad (13.495)$$

where  $\mathbf{K}_d > 0$  is a strictly positive design matrix, it is seen that

$$\dot{V}_2 = -z_1^\top \mathbf{K}_p \boldsymbol{\Lambda} z_1 - z_2^\top (\mathbf{K}_d + \mathbf{D}_x) z_2 + z_2^\top \mathbf{T}^{-\top} \mathbf{w} \quad (13.496)$$

Notice that the dissipative term  $\mathbf{z}_2^\top \mathbf{D}_x \mathbf{z}_2 > 0, \forall \mathbf{z}_2 \neq \mathbf{0}$  is exploited in the design as it appears in the expression for  $\dot{V}_2$ . With the control law (13.495) the closed-loop dynamics becomes

$$\mathbf{M}_x \dot{\mathbf{z}}_2 + (\mathbf{C}_x + \mathbf{D}_x + \mathbf{K}_d) \mathbf{z}_2 + \mathbf{K}_p \mathbf{z}_1 = \mathbf{T}^{-\top} \mathbf{w} \quad (13.497)$$

**Error dynamics:** The error dynamics of the resulting system becomes *nonautonomous* since

$$\begin{aligned} \begin{bmatrix} \mathbf{K}_p & \mathbf{0}_{3 \times 3} \\ \mathbf{0}_{3 \times 3} & \mathbf{M}_x \end{bmatrix} \begin{bmatrix} \dot{\mathbf{z}}_1 \\ \dot{\mathbf{z}}_2 \end{bmatrix} &= - \begin{bmatrix} \mathbf{K}_p \mathbf{\Lambda} & \mathbf{0}_{3 \times 3} \\ \mathbf{0}_{3 \times 3} & \mathbf{C}_x + \mathbf{D}_x + \mathbf{K}_d \end{bmatrix} \begin{bmatrix} \mathbf{z}_1 \\ \mathbf{z}_2 \end{bmatrix} \\ &\quad + \begin{bmatrix} \mathbf{0}_{3 \times 3} & \mathbf{K}_p \\ -\mathbf{K}_p & \mathbf{0}_{3 \times 3} \end{bmatrix} \begin{bmatrix} \mathbf{z}_1 \\ \mathbf{z}_2 \end{bmatrix} + \begin{bmatrix} \mathbf{0}_{3 \times 1} \\ \mathbf{T}^{-\top} \end{bmatrix} \mathbf{w} \\ &\Downarrow \\ \mathcal{M}(\mathbf{x}) \dot{\mathbf{z}} &= -\mathcal{K}(\mathbf{x}, \mathbf{v}) \mathbf{z} + \mathcal{S} \mathbf{z} + \bar{\mathcal{B}}(\mathbf{x}) \mathbf{w} \end{aligned} \quad (13.498)$$

where the different matrices are defined as

$$\begin{aligned} \mathcal{M}(\mathbf{x}) = \mathcal{M}^T(\mathbf{x}) &= \begin{bmatrix} \mathbf{K}_p & \mathbf{0}_{3 \times 3} \\ \mathbf{0}_{3 \times 3} & \mathbf{M}_x(\mathbf{x}) \end{bmatrix} \\ \mathcal{K}(\mathbf{x}, \mathbf{v}) &= \begin{bmatrix} \mathbf{K}_p \mathbf{\Lambda} & \mathbf{0}_{3 \times 3} \\ \mathbf{0}_{3 \times 3} & \mathbf{C}_x(\mathbf{x}, \mathbf{v}) + \mathbf{D}_x(\mathbf{x}, \mathbf{v}) + \mathbf{K}_d \end{bmatrix} > 0 \\ \mathcal{S} = -\mathcal{S}^T &= \begin{bmatrix} \mathbf{0}_{3 \times 3} & \mathbf{K}_p \\ -\mathbf{K}_p & \mathbf{0}_{3 \times 3} \end{bmatrix}, \quad \bar{\mathcal{B}}(\mathbf{x}) = \begin{bmatrix} \mathbf{0}_{3 \times 1} \\ \mathbf{T}^{-\top}(\mathbf{x}) \end{bmatrix} \end{aligned}$$

In the absence of disturbances,  $\mathbf{w} \equiv \mathbf{0}$ , the origin  $\mathbf{z} = \mathbf{0}$  is uniformly locally exponentially stable (ULES) according to Lyapunov. Global results cannot be achieved due to the local diffeomorphism between the Cartesian and polar coordinates; that is the transformation matrix  $\mathbf{T}(\mathbf{x})$  is singular for  $\rho = 0$ .

With disturbances  $\mathbf{w} \neq \mathbf{0}$ , the closed-loop system is input-to-state stable (ISS). In the next section, it is shown how adaptive backstepping (backstepping with integral action) can be used to obtain ULES for the case of a nonzero disturbance vector  $\mathbf{w} \neq \mathbf{0}$ .

### Adaptive Backstepping (PID Control)

Since the mean disturbance  $\mathbf{w}$  is nonzero this will result in a steady-state offset when using the PD controller from the previous section. The craft is, however, restricted to move along a circular arc with  $\mathbf{w}$  as a force field. Therefore there will be a stable and an unstable equilibrium point on the circle arc (similar to a pendulum in the gravity field); see Figure 13.24. The stable equilibrium point is given by

$$\mathbf{w} = \phi F_e = [-1, 0, 0]^\top F_e \quad (13.499)$$

Since the disturbance  $F_e$  is assumed to be slowly varying, adaptive backstepping can be applied to obtain an integral effect in the system. Thus, in the analysis it will be assumed that  $\dot{F}_e = 0$ . Let the estimate of  $F_e$  be denoted as  $\hat{F}_e$  and  $\tilde{F}_e = \hat{F}_e - F_e$ . An additional step in the derivation of the backstepping control law must be performed in order to obtain an adaptive update law for  $\hat{F}_e$ .

**Step 3:** The adaptive update law is found by adding the square parameter estimation error to  $V_2$ . Consequently,

$$V_3 = V_2 + \frac{1}{2\sigma} \tilde{F}_e^2, \quad \sigma > 0 \quad (13.500)$$

$$\dot{V}_3 = \dot{V}_2 + \frac{1}{\sigma} \dot{\tilde{F}}_e \tilde{F}_e \quad (13.501)$$

The nonlinear control law (13.495) is modified to

$$\tau = \mathbf{T}^\top (\mathbf{M}_x \ddot{\mathbf{x}}_r + \mathbf{C}_x \dot{\mathbf{x}}_r + \mathbf{D}_x \dot{\mathbf{x}}_r - \mathbf{K}_p z_1 - \mathbf{K}_d z_2) - \mathbf{q}(\cdot) - \boldsymbol{\phi} \hat{F}_e \quad (13.502)$$

where the last term  $\boldsymbol{\phi} \hat{F}_e$  provides integral action. Hence, the  $z_2$  dynamics becomes

$$\mathbf{M}_x \dot{z}_2 + (\mathbf{C}_x + \mathbf{D}_x + \mathbf{K}_d) z_2 + \mathbf{K}_p z_1 = -\mathbf{T}^{-\top} \boldsymbol{\phi} \hat{F}_e \quad (13.503)$$

This implies that

$$\begin{aligned} \dot{V}_3 &= -z_1^\top \mathbf{K}_p \mathbf{A} z_1 - z_2^\top (\mathbf{K}_d + \mathbf{D}_x) z_2 - z_2^\top \mathbf{T}^{-\top} \boldsymbol{\phi} \hat{F}_e + \frac{1}{\sigma} \dot{\tilde{F}}_e \tilde{F}_e \\ &= -z_1^\top \mathbf{K}_p \mathbf{A} z_1 - z_2^\top (\mathbf{K}_d + \mathbf{D}_x) z_2 + \hat{F}_e (-\boldsymbol{\phi}^\top \mathbf{T}^{-1} z_2 + \frac{1}{\sigma} \dot{\tilde{F}}_e) \end{aligned} \quad (13.504)$$

The adaptive law  $\dot{\hat{F}}_e = \dot{\tilde{F}}_e$  is chosen as

$$\dot{\hat{F}}_e = \sigma \boldsymbol{\phi}^\top \mathbf{T}^{-1} z_2, \quad \sigma > 0 \quad (13.505)$$

such that

$$\dot{V}_3 = -z_1^\top \mathbf{K}_p \mathbf{A} z_1 - z_2^\top (\mathbf{K}_d + \mathbf{D}_x) z_2 \leq 0 \quad (13.506)$$

### Error Dynamics

The nonautonomous error dynamics for the adaptive backstepping controller can be written

$$\mathcal{M}(\mathbf{x}) \dot{\mathbf{z}} = [-\mathcal{K}(\mathbf{x}, \mathbf{v}) + \mathcal{S}] \mathbf{z} + \mathcal{B}(\mathbf{x}) \tilde{F}_e \quad (13.507)$$

$$\dot{\tilde{F}}_e = -\sigma \mathcal{B}^\top(\mathbf{x}) \mathbf{z} \quad (13.508)$$

where

$$\mathcal{B}(\mathbf{x}) = \begin{bmatrix} \mathbf{0}_{3 \times 1} \\ -\mathbf{T}^{-\top}(\mathbf{x}) \boldsymbol{\phi} \end{bmatrix} \quad (13.509)$$

In order to satisfy *control objective O1*, the controller gains must be chosen according to

$$\mathbf{K}_p = \begin{bmatrix} k_{p1} & 0 & 0 \\ 0 & 0 & 0 \\ 0 & 0 & k_{p3} \end{bmatrix}, \quad \mathbf{K}_d = \begin{bmatrix} k_{d1} & 0 & 0 \\ 0 & k_{d2} & 0 \\ 0 & 0 & k_{d3} \end{bmatrix}, \quad \boldsymbol{\Lambda} = \begin{bmatrix} \lambda_1 & 0 & 0 \\ 0 & 0 & 0 \\ 0 & 0 & \lambda_3 \end{bmatrix} \quad (13.510)$$

Notice that  $k_{p2} = \lambda_2 = 0$ . This implies that the craft is free to move along the circular arc with tangential velocity  $\rho\dot{\psi}$ . The gain  $k_{d2} > 0$  is used to increase the tangential damping (D control) while the radius  $\rho$  and heading  $\psi$  are stabilized by using PID control.

### Semi-Definite Matrices

Since the controller gains  $k_{p2}$  and  $\lambda_2$  are chosen to be zero, the matrices

$$\mathbf{K}_p \geq 0, \quad \boldsymbol{\Lambda} \geq 0 \quad (13.511)$$

are only positive semi-definite. Hence,  $V_3$  is positive semi-definite. Uniform local asymptotic stability (ULAS) of the equilibrium  $(z, \tilde{F}_e) = (\mathbf{0}, 0)$  can, however, be proven since the error dynamics  $(z_1, z_2)$  is ISS. Consider the reduced order system  $(z_{1r}, z_2)$  given by

$$z_{1r} = \mathbf{E}z_1, \quad \mathbf{E} = \begin{bmatrix} 1 & 0 & 0 \\ 0 & 0 & 1 \end{bmatrix} \quad (13.512)$$

This implies that

$$\begin{aligned} \dot{z}_{1r} &= -\mathbf{E}\boldsymbol{\Lambda}z_1 + \mathbf{E}z_2 \\ &= -(\mathbf{E}\boldsymbol{\Lambda}\mathbf{E}^\top)z_{1r} + \mathbf{E}z_2 \end{aligned} \quad (13.513)$$

Notice that the last step is possible since the diagonal matrices  $\boldsymbol{\Lambda} = \text{diag}\{\lambda_1, 0, \lambda_3\}$  satisfy

$$\boldsymbol{\Lambda}\mathbf{E}^\top z_{1r} = \boldsymbol{\Lambda}z_1 \quad (13.514)$$

Hence, the error dynamics (13.507)–(13.508) can be transformed to

$$\mathcal{M}_r(\mathbf{x})\dot{z}_r = [-\mathcal{K}_r(\mathbf{x}, \mathbf{v}) + \mathcal{S}_r]z_r + \mathcal{B}_r(\mathbf{x})\tilde{F}_e \quad (13.515)$$

$$\dot{\tilde{F}}_e = -\sigma\mathcal{B}_r^\top(\mathbf{x})z_r \quad (13.516)$$

where  $z_r = [z_{1r}^\top, z_2^\top]^\top$  and

$$\begin{aligned} \mathcal{M}_r(\mathbf{x}) = \mathcal{M}_r^\top(\mathbf{x}) &= \begin{bmatrix} \mathbf{E}\mathbf{K}_p\mathbf{E}^\top & \mathbf{0}_{2 \times 3} \\ \mathbf{0}_{3 \times 2} & \mathbf{M}_x(\mathbf{x}) \end{bmatrix} \\ \mathcal{K}_r(\mathbf{x}, \mathbf{v}) &= \begin{bmatrix} (\mathbf{E}\mathbf{K}_p\mathbf{E}^\top)(\mathbf{E}\boldsymbol{\Lambda}\mathbf{E}^\top) & \mathbf{0}_{2 \times 3} \\ \mathbf{0}_{3 \times 2} & \mathbf{C}_x(\mathbf{x}, \mathbf{v}) + \mathbf{D}_x(\mathbf{x}, \mathbf{v}) + \mathbf{K}_d \end{bmatrix} > 0 \\ \mathcal{S}_r &= -\mathcal{S}_r^\top = \begin{bmatrix} \mathbf{0}_{2 \times 2} & \mathbf{E}\mathbf{K}_p \\ -\mathbf{K}_p\mathbf{E}^\top & \mathbf{0}_{3 \times 3} \end{bmatrix}, \quad \mathcal{B}_r(\mathbf{x}) = \begin{bmatrix} \mathbf{0}_{2 \times 1} \\ \mathbf{T}^{-\top}(\mathbf{x})\boldsymbol{\phi} \end{bmatrix} \end{aligned}$$

where the fact that  $\mathbf{K}_p\mathbf{E}^\top z_{1r} = \mathbf{K}_p z_1$  for  $\mathbf{K}_p = \text{diag}\{k_{p1}, 0, k_{p3}\}$  has been applied.

### Nonautonomous Lyapunov Analysis

Even though the Lyapunov function  $V_3$  corresponding to the states  $(z_1, z_2)$  is only positive semi-definite (since  $\mathbf{K}_p$  is positive semi-definite) the Lyapunov function  $V_{3r}$  corresponding to the new output  $(z_{1r}, z_2)$  is positive definite. Using the fact that the closed-loop system governed by  $(z_1, z_2)$  is ISS, asymptotic tracking is guaranteed by

$$V_{3r} = \frac{1}{2} \left[ z_{1r}^\top (\mathbf{E} \mathbf{K}_p \mathbf{E}^\top) z_{1r} + z_2^\top \mathbf{M}_x z_2 + \frac{1}{\sigma} \tilde{F}_e^2 \right] > 0 \quad (13.517)$$

$$\dot{V}_{3r} = -z_{1r}^\top (\mathbf{E} \mathbf{K}_p \mathbf{E}^\top) (\mathbf{E} \Lambda \mathbf{E}^\top) z_{1r} - z_2^\top (\mathbf{K}_d + \mathbf{D}_x) z_2 \leq 0 \quad (13.518)$$

where  $\mathbf{E} \mathbf{K}_p \mathbf{E}^\top > 0$  and  $\mathbf{E} \Lambda \mathbf{E}^\top > 0$ . Hence,  $z_{1r}, z_2, \tilde{F}_e \in \mathcal{L}_\infty$ . Notice that  $\dot{V}_3$  is only negative semi-definite since a negative term proportional to  $-\tilde{F}_e^2$  is missing in the expression for  $\dot{V}_3$ . ULES of the equilibrium point  $(z_{1r}, z_2, \tilde{F}_e) = (\mathbf{0}, \mathbf{0}, 0)$  follows by using the stability theorem of Fossen *et al.* (2001) for nonlinear *nonautonomous* systems (see Appendix A.2.4). Since, the closed-loop system  $(z_1, z_2)$  is ISS it is sufficient to consider the reduced order system  $(z_{1r}, z_2)$  with output  $z_{1r} = \mathbf{E} z_1$  in the stability analysis. According to Appendix A.2.4, we can choose  $\mathbf{x}_1 = [z_{1r}^\top, z_2^\top]^\top$ ,  $\mathbf{x}_2 = \tilde{F}_e$ ,  $\mathbf{P} = \sigma$  and  $W(\mathbf{x}_1, t) = \frac{1}{2} \mathbf{x}_1^\top \mathbf{x}_1$ . Then the equilibrium point  $(z_{1r}, z_2, \tilde{F}_e) = (\mathbf{0}, \mathbf{0}, 0)$  of the nonlinear error system (13.507)–(13.508) is ULES since

$$\text{rank}\{(\mathcal{M}_r^{-1}(\mathbf{x}) \mathcal{B}_r(\mathbf{x}))^\top (\mathcal{M}_r^{-1}(\mathbf{x}) \mathcal{B}_r(\mathbf{x}))\} = 1, \forall \mathbf{x}$$

and

$$\begin{aligned} \max \{\|\mathbf{h}(\mathbf{x}_1, t)\|, \|\mathbf{x}_1\|\} &= \max \left\{ \left\| \mathcal{M}_r^{-1}(\mathbf{x}) [-\mathcal{K}_r(\mathbf{x}, \mathbf{v}) + \mathcal{S}_r] \mathbf{x}_1 \right\|, \|\mathbf{x}_1\| \right\} \\ &\leq \rho_1(\|\mathbf{x}_1\|) \|\mathbf{x}_1\| \\ \|\mathbf{B}(\mathbf{x}, t)\| &= \left\| \mathcal{M}_r^{-1}(\mathbf{x}) \mathcal{B}_r(\mathbf{x}) \right\| \leq \rho_2(\|\mathbf{x}_1\|) \\ \max \left\{ \left\| \frac{\partial \mathbf{B}(\mathbf{x}, t)}{\partial t} \right\|, \left\| \frac{\partial \mathbf{B}(\mathbf{x}, t)}{\partial \mathbf{x}_i} \right\| \right\} &= \max \left\{ \left\| \frac{\partial \mathcal{M}_r^{-1}(\mathbf{x}) \mathcal{B}_r(\mathbf{x})}{\partial \mathbf{x}_i} \right\| \right\} \leq \rho_3(\|\mathbf{x}_1\|) \end{aligned}$$

### Translational Control of the Circle Center

The adaptive backstepping controller satisfies a control objective O1, that is weather optimal heading control. Weather optimal position control (control objective O2) can be satisfied by moving the circle center  $\mathbf{p}_0 = [N_0, E_0]^\top$  online such that the craft maintains a constant position  $\mathbf{p} = [N, E]^\top$ .

In order to meet the fixed position control objective, an update law for the circle center  $\mathbf{p}_0$  must be derived. The Cartesian Earth-fixed position of the craft is given by

$$\mathbf{p} = \mathbf{L}^\top \boldsymbol{\eta} \quad (13.519)$$

where  $\mathbf{L}$  is defined in (13.474). Let  $\tilde{\mathbf{p}} = \mathbf{p} - \mathbf{p}_d$  denote the corresponding deviation from the desired position vector  $\mathbf{p}_d = [N_d, E_d]^\top$ . The desired position can either be constant (regulation) or a smooth time-varying reference trajectory. The control law for translation of the circle center is derived by considering

the following CLF:

$$V_p = \frac{1}{2} \tilde{\mathbf{p}}^\top \tilde{\mathbf{p}} \quad (13.520)$$

$$\dot{V}_p = \tilde{\mathbf{p}}^\top (\dot{\mathbf{p}} - \dot{\mathbf{p}}_d) = \tilde{\mathbf{p}}^\top (\mathbf{L}^\top \dot{\mathbf{q}} - \dot{\mathbf{p}}_d) \quad (13.521)$$

By using (13.473),  $\mathbf{L}^\top \mathbf{L} = \mathbf{I}_{2 \times 2}$  and  $\dot{\mathbf{x}} = \mathbf{z}_2 + \dot{\mathbf{x}}_r$  it is seen that

$$\begin{aligned} \dot{V}_p &= \tilde{\mathbf{p}}^\top [\mathbf{L}^\top (\mathbf{R}(\gamma) \mathbf{H}(\rho) \dot{\mathbf{x}} + \mathbf{L} \dot{\mathbf{p}}_0) - \dot{\mathbf{p}}_d] \\ &= \tilde{\mathbf{p}}^\top (\dot{\mathbf{p}}_0 - \dot{\mathbf{p}}_d + \mathbf{L}^\top \mathbf{R}(\gamma) \mathbf{H}(\rho) \dot{\mathbf{x}}_r) + \tilde{\mathbf{p}}^\top \mathbf{L}^\top \mathbf{R}(\gamma) \mathbf{H}(\rho) \mathbf{z}_2 \end{aligned} \quad (13.522)$$

Now, by choosing the circle center update law as

$$\dot{\mathbf{p}}_0 = \dot{\mathbf{p}}_d - \mathbf{L}^\top \mathbf{R}(\gamma) \mathbf{H}(\rho) \dot{\mathbf{x}}_r - k_0 \tilde{\mathbf{p}} \quad (13.523)$$

where  $k_0 > 0$ , it is seen that

$$\dot{V}_p = -k_0 \tilde{\mathbf{p}}^\top \tilde{\mathbf{p}} + \tilde{\mathbf{p}}^\top \mathbf{L}^\top \mathbf{R}(\gamma) \mathbf{H}(\rho) \mathbf{z}_2 \quad (13.524)$$

In (13.524) a cross-term in  $\tilde{\mathbf{p}}$  and  $\mathbf{z}_2$  is noted. In order to guarantee that the time derivative of the total system  $V_{\text{wopc}} = V_{3r} + V_p$  is negative semi-definite, the weather optimal controller (13.502) must be modified such that the cross-term in (13.524) is canceled.

### Weather Optimal Position Control (WOPC)

The cross-terms involving  $\tilde{\mathbf{p}}$  and  $\mathbf{z}_2$  in  $\dot{V}_p$  can be removed by modifying the nonlinear controller (13.502) to

$$\boldsymbol{\tau} = \mathbf{T}^\top (\mathbf{M}_x \ddot{\mathbf{x}}_r + \mathbf{C}_x \dot{\mathbf{x}}_r + \mathbf{D}_x \dot{\mathbf{x}}_r - \mathbf{K}_p \mathbf{z}_1 - \mathbf{K}_d \mathbf{z}_2) - \mathbf{q}(\cdot) - \boldsymbol{\phi} \hat{F}_e - \mathbf{T}^\top \mathbf{H}^\top(\rho) \mathbf{R}^\top(\gamma) \mathbf{L} \tilde{\mathbf{p}} \quad (13.525)$$

The last term in  $\boldsymbol{\tau}$  implies that

$$\dot{V}_{3r} = -\mathbf{z}_{1r}^\top (\mathbf{E} \mathbf{K}_p \mathbf{E}^\top) (\mathbf{E} \boldsymbol{\Lambda} \mathbf{E}^\top) \mathbf{z}_{1r} - \mathbf{z}_{2r}^\top (\mathbf{K}_d + \mathbf{D}_x) \mathbf{z}_2 - \tilde{\mathbf{p}}^\top \mathbf{L}^\top \mathbf{R}(\gamma) \mathbf{H}(\rho) \mathbf{z}_2 \quad (13.526)$$

Consider

$$V_{\text{wopc}} = V_{3r} + V_p \quad (13.527)$$

$$\dot{V}_{\text{wopc}} = -\mathbf{z}_{1r}^\top (\mathbf{E} \mathbf{K}_p \mathbf{E}^\top) (\mathbf{E} \boldsymbol{\Lambda} \mathbf{E}^\top) \mathbf{z}_{1r} - \mathbf{z}_{2r}^\top (\mathbf{K}_d + \mathbf{D}_x) \mathbf{z}_2 - k_0 \tilde{\mathbf{p}}^\top \tilde{\mathbf{p}} \quad (13.528)$$

and therefore the equilibrium point  $(\mathbf{z}_{1r}, \mathbf{z}_2, \hat{F}_e, \tilde{\mathbf{p}}) = (\mathbf{0}, \mathbf{0}, 0, \mathbf{0})$  is ULES. The term  $\tilde{\mathbf{p}}_0$  is needed in the expression for  $\mathbf{q}(\cdot)$ . This term is computed from (13.523) as

$$\ddot{\mathbf{p}}_0 = \ddot{\mathbf{p}}_d - k_0(\dot{\mathbf{p}} - \dot{\mathbf{p}}_d) - \mathbf{L}^\top \mathbf{R}(\gamma) \mathbf{H}(\rho) \dot{\mathbf{x}}_r \\ - \mathbf{L}^\top \dot{\mathbf{R}}(\gamma) \mathbf{H}(\rho) \dot{\mathbf{x}}_r - \mathbf{L}^\top \mathbf{R}(\gamma) \dot{\mathbf{H}}(\rho) \dot{\mathbf{x}}_r \quad (13.529)$$

### Experiment 1: Weather Optimal Heading Control (WOHC)

The proposed WOHC system has been implemented and tested experimentally using a model ship of scale 1:70. A ducted fan was used to generate wind forces. The length of the model ship is  $L_m = 1.19$  m and the mass is  $m_m = 17.6$  kg. The experimental results are scaled to full scale by considering a supply vessel with mass  $m_s = 4500$  tons using the bis system (see Section 7.2.5).

In the first experiment the ship was allowed to move on the circle arc and the circle center controller (13.523) was turned off; that is  $N_0 = \text{constant}$  and  $E_0 = \text{constant}$ . This is referred to as WOHC. The fixed origin and circle arc are shown in Figure 13.27. Notice that the initial heading is approximately 30 degrees (see Figure 13.28), while the position  $(N, E) \approx (13, -43)$ . These values are those obtained when the fan was initially directed at 210 degrees in the opposite direction of the ship heading.

After 3000 seconds the fan was slowly rotated to 165 degrees, corresponding to a weather optimal heading of -15 degrees (see Figure 13.28). During this process, the ship starts to move on the circle arc with heading towards the circle center until it is stabilized to its new heading at -15 degrees. The new position on the circle arc is  $(N, E) \approx (3, 20)$ . This clearly demonstrates that the ship heading converges to the optimal value by copying the dynamics of a pendulum in the gravity field. This is done without using any external wind sensor.

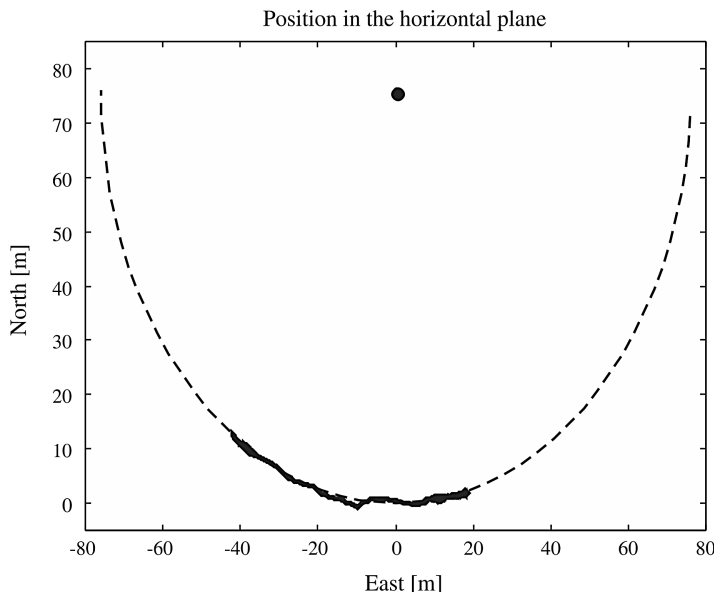


**Figure 13.27** WOHC experiment showing the circular motion of the ship when the circle center controller is turned off (WOHC).

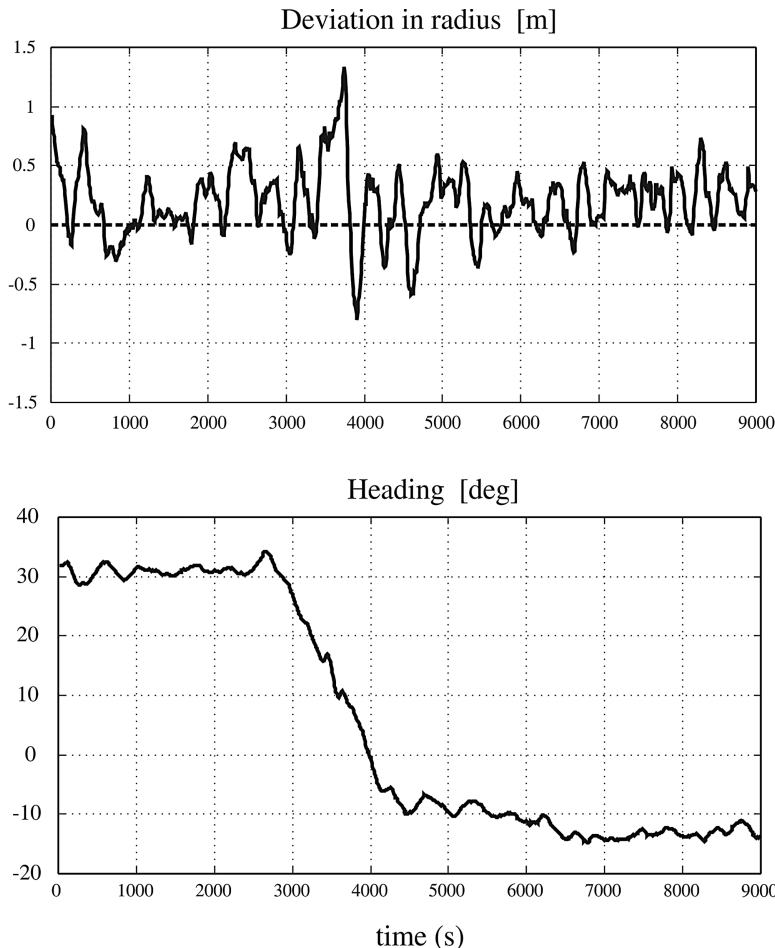


**Figure 13.28** WOHC experiment showing the performance of the radius regulator (upper plot) and weather optimal heading (lower plot) versus time (s).

In the next experiment, the circle center is translated online in order to obtain a constant position ( $N, E$ ).

### Experiment 2: Weather Optimal Position Control (WOPC)

In the second experiment the ship should maintain its position by activating the circle center controller (13.5.23). The performance during stationkeeping and translation of the circle is shown in Figures 13.29–13.31. The position controller works within an accuracy of  $\pm 1$  m, which is the accuracy of the GNSS system.

Again the weather optimal heading is changed from approximately 23 degrees to 2 degrees but this time without changing the position ( $N, E$ ) of the ship. The position deviations and the weather optimal heading are shown in Figure 13.30. These values are obtained by moving the fan from an initial angle of 203 degrees to 182 degrees.

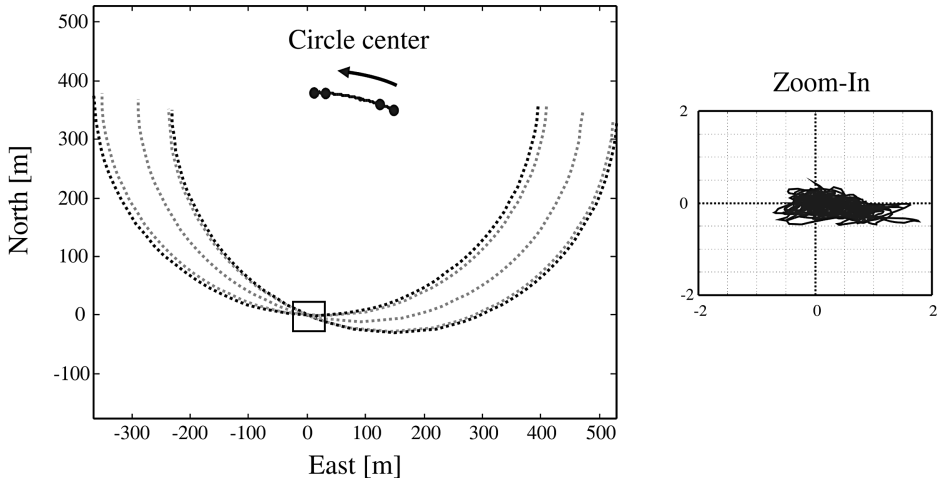


**Figure 13.29** WOPC experiment showing how the circle center is moved to obtain stationkeeping to  $(N_d, E_d) = (0, 0)$ .

### 13.3.11 Case Study: Heading Autopilot for Ships and Underwater Vehicles

A nonlinear backstepping controller can be designed by writing the autopilot model (7.53) in SISO strict feedback form:

$$\dot{\psi} = r \quad (13.530)$$

$$m\dot{r} + d(r)r = \delta \quad (13.531)$$

where  $m = T/K$  and  $d(r) = H_N(r)/K$ . The only nonlinearity in this model is due to the maneuvering characteristic  $H_N(r)$ .

In Section 13.3.3 it was shown that the backstepping controller for this system is

$$\delta = m\dot{\alpha}_1 + d(r)r - z_1 - k_2 z_2 - n_2(z_2)z_2 \quad (13.532)$$

$$\alpha_1 = r_d - [k_1 + n_1(z_1)]z_1 \quad (13.533)$$

where  $k_1 > 0$  and  $k_2 > 0$  are two feedback gains and  $n_i(z_i) \geq 0$  ( $i = 1, 2$ ) are two optional nonlinear damping terms, for instance chosen as nondecreasing functions  $n_i(z_i) = \kappa_i |z_i|^{n_i}$  with  $n_i \geq 1$  and  $\kappa_i \geq 0$  ( $i = 1, 2$ ) as design parameters. The following change of coordinates is needed to implement the controller:

$$z_1 = \psi - \psi_d \quad (13.534)$$

$$z_2 = r - \alpha_1 \quad (13.535)$$

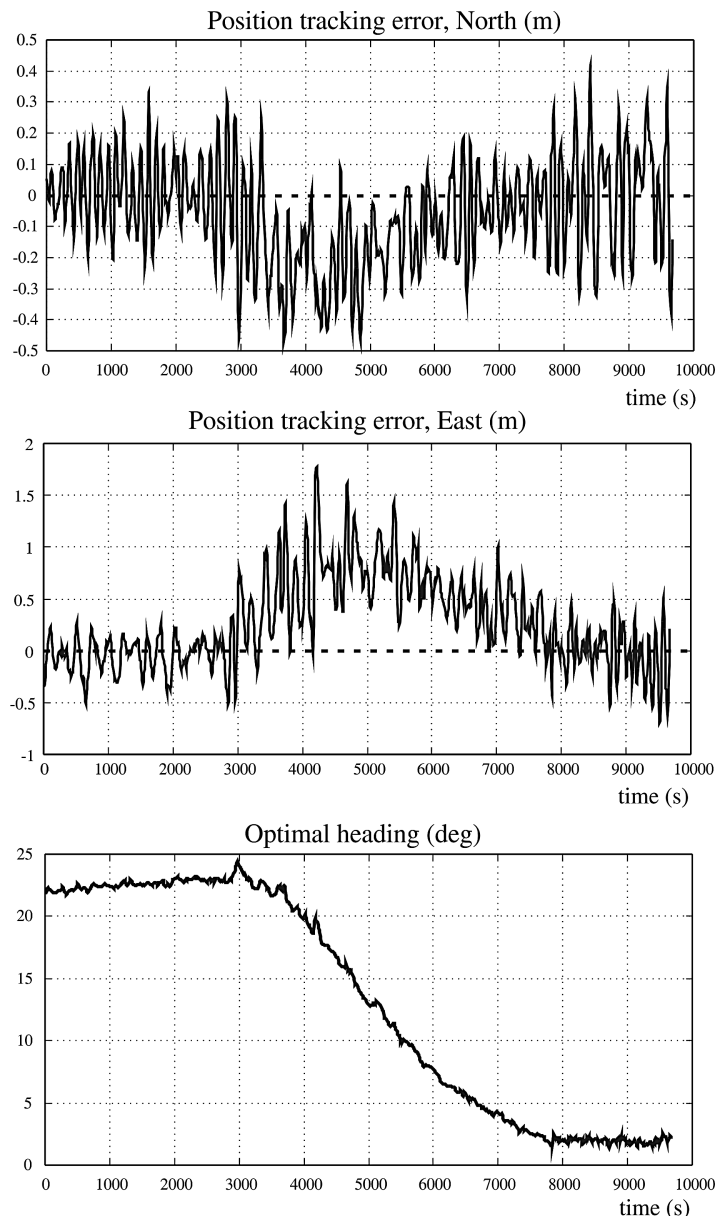


**Figure 13.30** WOPC experiment showing the North and East position accuracies (upper plots) and weather optimal heading (lower plot) versus time (seconds). The position accuracy is within  $\pm 1$  m while the heading changes from 23 degrees to 2 degrees as the fan is rotated.

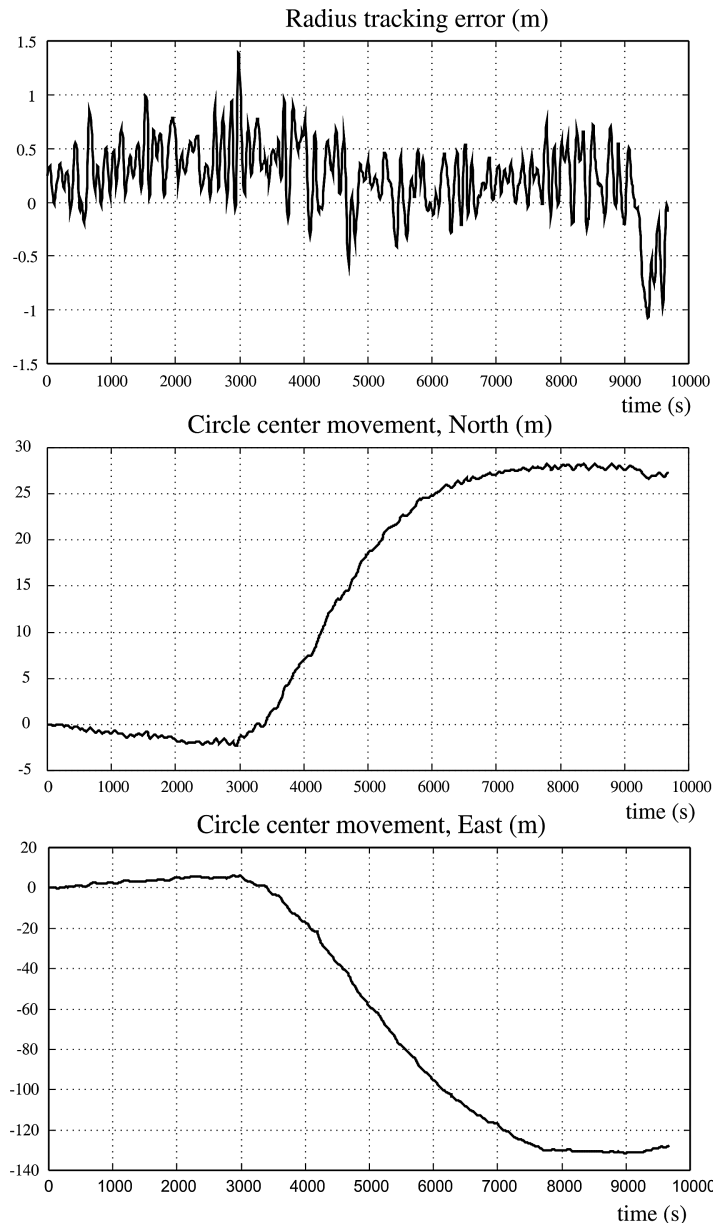


**Figure 13.31** WOPC experiment showing the deviation for the radius regulator (upper plot) and the translation of the circle center ( $N_0, E_0$ ) (lower plots) versus time in seconds. The radius deviation is within  $\pm 1$  m during the rotation of the fan.

The backstepping controller includes a PD term as well as reference feedforward. In addition the nonlinear damping terms  $n_i(z_i)$  ( $i = 1, 2$ ) can be used to improve the performance and stability of the closed-loop system.

When using feedback linearization all the nonlinearities in  $H_N(r)$  are compensated for. This requires that the dissipative terms are known with good accuracy, which is not true in many cases. The backstepping controller gives more design flexibility with respect to the damping terms. In fact, it is possible to exploit good damping terms such as  $n_3r^3$  and  $n_1r$  in  $H_N(r)$  instead of canceling them. This is straightforward in setpoint regulation; see Krstic *et al.* (1995), for instance. In trajectory-tracking control, however, it is not clear how good damping with respect to a time-varying reference trajectory should be defined. A discussion on backstepping versus feedback linearization is found in Section 13.3.2.

Extensions to integral action can be done by using the method of Loria *et al.* (1999) and Fossen *et al.* (2001), which is referred to as *backstepping with integral action*. Alternatively, an *integrator augmentation technique* can be applied. Both these methods are described in detail in Sections 13.3.4 and 13.3.5.

The actuator dynamics can be included in the design by using the approach of Fossen and Berge (1997) where backstepping is performed in three steps to include a first-order actuator model.

### 13.3.12 Case Study: Path-Following Controller for Underactuated Marine Craft

For floating rigs, semi-submersibles and supply vessels, trajectory-tracking control in *surge*, *sway* and *yaw* (3 DOF) is easily achieved since independent control forces and moments are simultaneously available in all degrees of freedom. For slow speed, this is referred to as DP and the craft is controlled by means of tunnel thrusters, azimuths and main propellers. Conventional craft, on the other hand, are usually equipped with one or two main propellers for forward speed control and rudders for turning control. The minimum configuration for waypoint tracking control is one main propeller and a single rudder. This means that only two controls are available, thus rendering the ship underactuated for the task of 3 DOF trajectory-tracking control (see Section 9.4).

Conventional waypoint guidance systems are usually designed by reducing the output space from 3 DOF position and heading to 2 DOF heading and surge (Healey and Marco, 1992). In its simplest form this involves the use of a classical autopilot system where the commanded yaw angle  $\psi_d$  is generated such that the *cross-track error* is minimized. A path-following control system is usually designed such that the ship moves forward with reference speed  $u_d$  at the same time as the cross-track error to the path is minimized. As a result,  $\psi_d$  and  $u_d$  are tracked using only two controls.

This section is based on Fossen *et al.* (2003a) and presents a maneuvering controller involving an LOS guidance system and a nonlinear feedback trajectory-tracking controller. The desired output is reduced from  $(x_d, y_d, \psi_d)$  to  $\psi_d$  and  $u_d$  using an LOS projection algorithm. The tracking task  $\psi(t) \rightarrow \psi_d(t)$  is then achieved using only one control (normally the rudder), while tracking of the speed assignment  $u_d$  is performed by the remaining control (the main propeller). Since we are dealing with segments of straight lines, the LOS projection algorithm will guarantee that the task of path-following is satisfied.

First, an LOS guidance procedure is derived. This includes a projection algorithm and a waypoint switching algorithm. To avoid large bumps in  $\psi_d$  when switching, and to provide the necessary derivatives of  $\psi_d$  to the controller, the commanded LOS heading is fed through a reference model. Second, a nonlinear 2 DOF tracking controller is derived using the backstepping technique. Three stabilizing functions  $\alpha := [\alpha_1, \alpha_2, \alpha_3]^\top$  are defined where  $\alpha_1$  and  $\alpha_3$  are specified to satisfy the tracking objectives in the controlled surge and yaw modes. The stabilizing function  $\alpha_2$  in the uncontrolled sway mode is left as a free design variable. By assigning dynamics to  $\alpha_2$ , the resulting controller becomes a dynamic feedback controller so that  $\alpha_2(t) \rightarrow v(t)$  during path following. This is an appealing idea that adds to the extensive theory of backstepping. The presented design technique results in a robust controller for underactuated ships since integral action can be implemented for both path-following and speed control.

### Problem Statement

The problem statement is stated as a maneuvering problem with the following two objectives (Skjetne *et al.*, 2004):

**LOS Geometric Task:** Force the marine craft position  $\mathbf{p} = [x, y]^\top$  to converge to a desired path by forcing the course angle  $\chi$  to converge to (see Section 10.3.2)

$$\chi_d = \text{atan2}(y_{\text{los}} - y, x_{\text{los}} - x) \quad (13.536)$$

where the LOS position  $p_{\text{los}} = [x_{\text{los}}, y_{\text{los}}]^\top$  is the point along the path to which the craft should be pointed. Notice that  $\psi = \chi - \beta$  and  $\psi_d = \chi_d - \beta$  implies that  $\bar{\psi} = \bar{\chi}$  when designing the controller.

**Dynamic Task:** Force the speed  $u$  to converge to a desired speed assignment  $u_d$  according to

$$\lim_{t \rightarrow \infty} [u(t) - u_d(t)] = 0 \quad (13.537)$$

where  $u_d$  is the desired speed composed along the body-fixed  $x$  axis.

A conventional trajectory-tracking control system for 3 DOF is usually implemented using a standard PID autopilot in series with an LOS algorithm. Hence, a state-of-the-art autopilot system can be modified to take the LOS reference angle as input (see Figure 12.20). This adds flexibility since the default commercial autopilot system can be used together with the LOS guidance system. The speed can be adjusted manually by the captain or automatically using the path speed profile.

Consider the 3 DOF nonlinear maneuvering model in the following form:

$$\dot{\boldsymbol{\eta}} = \mathbf{R}(\psi)\mathbf{v} \quad (13.538)$$

$$\mathbf{M}\dot{\mathbf{v}} + \mathbf{N}(\mathbf{v})\mathbf{v} = \begin{bmatrix} (1-t)T \\ Y_\delta\delta \\ N_\delta\delta \end{bmatrix} := \begin{bmatrix} \tau_1 \\ Y_\delta\delta \\ \tau_3 \end{bmatrix} \quad (13.539)$$

where  $\boldsymbol{\eta} = [N, E, \psi]^\top$ ,  $\mathbf{v} = [u, v, r]^\top$  and

$$\mathbf{R}(\psi) = \begin{bmatrix} \cos(\psi) & -\sin(\psi) & 0 \\ \sin(\psi) & \cos(\psi) & 0 \\ 0 & 0 & 1 \end{bmatrix} \quad (13.540)$$

The matrices  $\mathbf{M}$  and  $\mathbf{N}$  take the following form:

$$\mathbf{M} = \begin{bmatrix} m_{11} & 0 & 0 \\ 0 & m_{22} & m_{23} \\ 0 & m_{32} & m_{33} \end{bmatrix} = \begin{bmatrix} m - X_{\dot{u}} & 0 & 0 \\ 0 & m - Y_{\dot{v}} & mx_g - Y_{\dot{r}} \\ 0 & mx_g - N_{\dot{v}} & I_z - N_{\dot{r}} \end{bmatrix}$$

$$\mathbf{N}(\mathbf{v}) = \begin{bmatrix} n_{11} & 0 & 0 \\ 0 & n_{22} & n_{23} \\ 0 & n_{32} & n_{33} \end{bmatrix} = \begin{bmatrix} -X_u & 0 & 0 \\ 0 & -Y_v & mu - Y_r \\ 0 & -N_v & mx_g u - N_r \end{bmatrix}$$

The control force and moment in surge and yaw are denoted  $\tau_1$  and  $\tau_3$ , respectively, while sway is left uncontrolled. Notice that the rudder angle  $\delta$  affects the sway equation but it will not be used to actively

control sway. The controller computes  $\tau_1$  and  $\tau_3$  which can be allocated to thrust  $T$  and rudder angle  $\delta$  using

$$\tau_1 = (1 - t)T \quad (13.541)$$

$$\tau_3 = N_\delta \delta \quad (13.542)$$

where  $t$  is the thrust deduction number. This gives

$$T = \frac{1}{1-t} \tau_1 \quad (13.543)$$

$$\delta = \frac{1}{N_\delta} \tau_3 \quad (13.544)$$

### Backstepping Design

The design is based on the model (13.538)–(13.539) where  $\mathbf{M} = \mathbf{M}^\top > 0$ . Define the error signals  $z_1 \in S$  and  $z_2 \in \mathbb{R}^3$  according to

$$z_1 := \chi - \chi_d = \psi - \psi_d \quad (13.545)$$

$$z_2 := [z_{2,1}, z_{2,2}, z_{2,3}]^\top = \mathbf{v} - \boldsymbol{\alpha} \quad (13.546)$$

where  $\chi_d$  and its derivatives are provided by proper filtering of the LOS angle,  $u_d \in \mathcal{L}_\infty$  is the desired speed and  $\boldsymbol{\alpha} := [\alpha_1, \alpha_2, \alpha_3]^\top \in \mathbb{R}^3$  is a vector of stabilizing functions to be specified later. Next, let

$$\mathbf{h} = [0, 0, 1]^\top \quad (13.547)$$

such that

$$\begin{aligned} \dot{z}_1 &= r - r_d = \mathbf{h}^\top \mathbf{v} - r_d \\ &= \alpha_3 + \mathbf{h}^\top z_2 - r_d \end{aligned} \quad (13.548)$$

where  $r_d = \dot{\psi}_d$  and

$$\begin{aligned} \mathbf{M}\dot{z}_2 &= \mathbf{M}\dot{\mathbf{v}} - \mathbf{M}\dot{\boldsymbol{\alpha}} \\ &= \boldsymbol{\tau} - \mathbf{N}\mathbf{v} - \mathbf{M}\dot{\boldsymbol{\alpha}} \end{aligned} \quad (13.549)$$

Consider the CLF:

$$V = \frac{1}{2}z_1^2 + \frac{1}{2}z_2^\top \mathbf{M}z_2, \quad \mathbf{M} = \mathbf{M}^\top > 0 \quad (13.550)$$

Differentiating  $V$  along the trajectories of  $z_1$  and  $z_2$  yields

$$\begin{aligned} \dot{V} &= z_1 \dot{z}_1 + z_2^\top \mathbf{M} \dot{z}_2 \\ &= z_1(\alpha_3 + \mathbf{h}^\top z_2 - r_d) + z_2^\top (\boldsymbol{\tau} - \mathbf{N}\mathbf{v} - \mathbf{M}\dot{\boldsymbol{\alpha}}) \end{aligned}$$

Choosing the virtual control  $\alpha_3$  as

$$\alpha_3 = -cz_1 + r_d \quad (13.551)$$

while  $\alpha_1$  and  $\alpha_2$  are yet to be defined gives

$$\begin{aligned}\dot{V} &= -cz_1^2 + z_1 \mathbf{h}^\top \mathbf{z}_2 + \mathbf{z}_2^\top (\boldsymbol{\tau} - N\mathbf{v} - \mathbf{M}\dot{\boldsymbol{\alpha}}) \\ &= -cz_1^2 + \mathbf{z}_2^\top (\mathbf{h}z_1 + \boldsymbol{\tau} - N\mathbf{v} - \mathbf{M}\dot{\boldsymbol{\alpha}})\end{aligned}\quad (13.552)$$

Suppose we can assign

$$\boldsymbol{\tau} = \begin{bmatrix} \tau_1 \\ Y_\delta \delta \\ \tau_3 \end{bmatrix} = \mathbf{M}\dot{\boldsymbol{\alpha}} + N\mathbf{v} - \mathbf{K}\mathbf{z}_2 - \mathbf{h}z_1 \quad (13.553)$$

where  $\mathbf{K} = \text{diag}\{k_1, k_2, k_3\} > 0$ . This results in

$$\dot{V} = -cz_1^2 - \mathbf{z}_2^\top \mathbf{K}\mathbf{z}_2 < 0, \quad \forall z_1 \neq 0, \mathbf{z}_2 \neq \mathbf{0} \quad (13.554)$$

and by standard Lyapunov arguments, this guarantees that  $(z_1, \mathbf{z}_2)$  is bounded and converges to zero.

However, notice from (13.553) that it is only possible to prescribe values for  $\tau_1$  and  $\tau_3$ ; that is

$$\tau_1 = m_{11}\dot{\alpha}_1 + n_{11}u - k_1(u - \alpha_1) \quad (13.555)$$

$$\tau_3 = m_{32}\dot{\alpha}_2 + m_{33}\dot{\alpha}_3 + n_{32}v + n_{33}r - k_3(r - \alpha_3) - z_1 \quad (13.556)$$

Choosing  $\alpha_1 = u_d$  clearly solves the dynamic task since the closed-loop surge dynamics becomes

$$m_{11}(\dot{u} - \dot{u}_d) + k_1(u - u_d) = 0 \quad (13.557)$$

The second equation in (13.553) results in a dynamic equality constraint

$$m_{22}\dot{\alpha}_2 + m_{23}\dot{\alpha}_3 + n_{22}v + n_{23}r - k_2(v - \alpha_2) = \frac{Y_\delta}{N_\delta}\tau_3 \quad (13.558)$$

affected by the control input  $\tau_3$ . Substituting (13.556) into this expression yields

$$\begin{aligned}\left(m_{22} - \frac{Y_\delta}{N_\delta}m_{32}\right)\dot{\alpha}_2 + \left(m_{23} - \frac{Y_\delta}{N_\delta}m_{33}\right)\dot{\alpha}_3 + \left(n_{22} - \frac{Y_\delta}{N_\delta}n_{32}\right)v + \left(n_{23} - \frac{Y_\delta}{N_\delta}n_{33}\right)r \\ - k_2(v - \alpha_2) + \frac{Y_\delta}{N_\delta}(k_3(r - \alpha_3) + z_1) = 0\end{aligned}$$

Application of  $\dot{\alpha}_3 = c^2z_1 - cz_{2,3} + \dot{r}_d$ ,  $\alpha_3 = -cz_1 + r_d$ ,  $v = \alpha_2 + z_{2,2}$  and  $r = \alpha_3 + z_{2,3}$  then gives

$$\left(m_{22} - \frac{Y_\delta}{N_\delta}m_{32}\right)\dot{\alpha}_2 = -\left(n_{22} - \frac{Y_\delta}{N_\delta}n_{32}\right)\alpha_2 + \gamma(z_1, \mathbf{z}_2, r_d, \dot{r}_d) \quad (13.559)$$

where

$$\begin{aligned}\gamma(z_1, \mathbf{z}_2, r_d, \dot{r}_d) &= -\left(m_{23} - \frac{Y_\delta}{N_\delta}m_{33}\right)(c^2z_1 - cz_{2,3} + \dot{r}_d) - \left(n_{22} - \frac{Y_\delta}{N_\delta}n_{32}\right)z_{2,2} \\ &\quad - \left(n_{23} - \frac{Y_\delta}{N_\delta}n_{33}\right)(-cz_1 + r_d + z_{2,3}) + k_2z_{2,2} - \frac{Y_\delta}{N_\delta}(k_3z_{2,3} + z_1)\end{aligned}\quad (13.560)$$

The variable  $\alpha_2$  becomes a dynamic state of the controller according to (13.559). Furthermore,  $m_{22} > (Y_\delta/N_\delta)m_{32}$  and  $n_{22} > (Y_\delta/N_\delta)n_{32}$  imply that (13.559) is a stable differential equation driven

by the converging error signals  $(z_1, z_2)$  and the bounded reference signals  $(r_d, \dot{r}_d)$  within the expression of  $\gamma(\cdot)$ . Since  $z_{2,2}(t) \rightarrow 0$ , it follows that  $|\alpha_2(t) - v(t)| \rightarrow 0$  as  $t \rightarrow \infty$ . The main result is summarized by Theorem 13.2, which is a modification of Fossen *et al.* (2003a).

**Theorem 13.2 (LOS Backstepping Controller for Underactuated Craft)**

The LOS maneuvering problem for the 3 DOF underactuated craft (13.538)–(13.539) is solved using the control laws

$$\tau_1 = m_{11}\dot{u}_d + n_{11}u - k_1(u - u_d)$$

$$\tau_3 = m_{32}\dot{\alpha}_2 + m_{33}\dot{\alpha}_3 + n_{32}v + n_{33}r - k_3(r - \alpha_3) - z_1$$

where  $k_1 > 0$ ,  $k_3 > 0$ ,  $z_1 := \psi - \psi_d$ ,  $z_2 := [u - u_d, v - \alpha_2, r - \alpha_3]^\top$  and

$$\alpha_3 = -cz_1 + r_d, \quad c > 0 \quad (13.561)$$

$$\dot{\alpha}_3 = -c(r - r_d) + \dot{r}_d \quad (13.562)$$

The reference signals  $u_d$ ,  $\dot{u}_d$ ,  $\psi_d$ ,  $r_d$  and  $\dot{r}_d$  are provided by the LOS guidance system, while  $\alpha_2$  is given by

$$\left( m_{22} - \frac{Y_\delta}{N_\delta}m_{32} \right) \dot{\alpha}_2 = - \left( n_{22} - \frac{Y_\delta}{N_\delta}n_{32} \right) \alpha_2 + \gamma(z_1, z_2, r_d, \dot{r}_d)$$

This results in a UGAS equilibrium point  $(z_1, z_2) = (0, \mathbf{0})$  and  $\alpha_2 \in \mathcal{L}_\infty$  satisfies

$$\lim_{t \rightarrow \infty} |\alpha_2(t) - v(t)| = 0 \quad (13.563)$$

**Remark 13.1**

Notice that the smooth reference signal  $\psi_d \in \mathcal{L}_\infty$  must be differentiated twice to produce  $r_d$  and  $\dot{r}_d$  while  $u_d \in \mathcal{L}_\infty$  must be differentiated once to give  $\dot{u}_d$ . This is most easily achieved by using reference models represented by low-pass filters (see Section 10.2.1).

**Proof.** The closed-loop equations become

$$\begin{bmatrix} \dot{z}_1 \\ \dot{z}_2 \end{bmatrix} = \begin{bmatrix} -c & \mathbf{h}^\top \\ -\mathbf{M}^{-1}\mathbf{h} & -\mathbf{M}^{-1}\mathbf{K} \end{bmatrix} \begin{bmatrix} z_1 \\ z_2 \end{bmatrix} \quad (13.564)$$

$$\bar{m}\dot{\alpha}_2 = -\bar{n}\alpha_2 + \gamma(z_1, z_2, r_d, \dot{r}_d) \quad (13.565)$$

where

$$\bar{m} = \left( m_{22} - \frac{Y_\delta}{N_\delta}m_{32} \right), \quad \bar{n} = \left( n_{22} - \frac{Y_\delta}{N_\delta}n_{32} \right) \quad (13.566)$$

From the Lyapunov arguments (13.550) and (13.554), the equilibrium  $(z_1, z_2) = (0, \mathbf{0})$  of the  $z$  subsystem is UGAS. The unforced  $\alpha_2$  subsystem ( $\gamma = 0$ ) is clearly exponentially stable. Since  $(z_1, z_2) \in \mathcal{L}_\infty$  and  $(r_d, \dot{r}_d) \in \mathcal{L}_\infty$ , then  $\gamma \in \mathcal{L}_\infty$ . This implies that the  $\alpha_2$  subsystem is input-to-state stable from  $\gamma$  to  $\alpha_2$ . This is seen by applying, for instance,  $V_2 = \frac{1}{2}\bar{m}\alpha_2^2$  which differentiated along the solutions of  $\alpha_2$  gives  $\dot{V}_2 \leq -\frac{1}{2}\bar{n}\alpha_2^2$  for all  $|\alpha_2| \geq \frac{2}{\bar{n}}|\gamma(z_1, z_2, r_d, \dot{r}_d)|$ . By standard comparison functions, it is then possible to show that for all  $|\alpha_2| \geq \frac{2}{\bar{n}}|\gamma(z_1, z_2, r_d, \dot{r}_d)|$  then

$$|\alpha_2(t)| \leq |\alpha_2(0)| e^{-\frac{\bar{n}}{2}t} \quad (13.567)$$

Hence,  $\alpha_2$  converges to the bounded set  $\{\alpha_2 : |\alpha_2| \leq \frac{2}{\bar{n}}|\gamma(z_1, z_2, r_d, \dot{r}_d)|\}$  since  $z_{2,2}(t) \rightarrow 0$  as  $t \rightarrow \infty$ .

### Case Study: Experiment Performed with the CS2 Model Ship

The proposed controller and guidance system were tested out at the *Marine Cybernetics Laboratory* (MCLab). MCLab is an experimental laboratory for the testing of scale models of ships, rigs, underwater vehicles and propulsion systems. The software is developed by using rapid prototyping techniques and automatic code generation under *Matlab/Simulink*. The target PC onboard the model scale vessels runs the real-time operating system, while experimental results are presented in real time on a host PC.

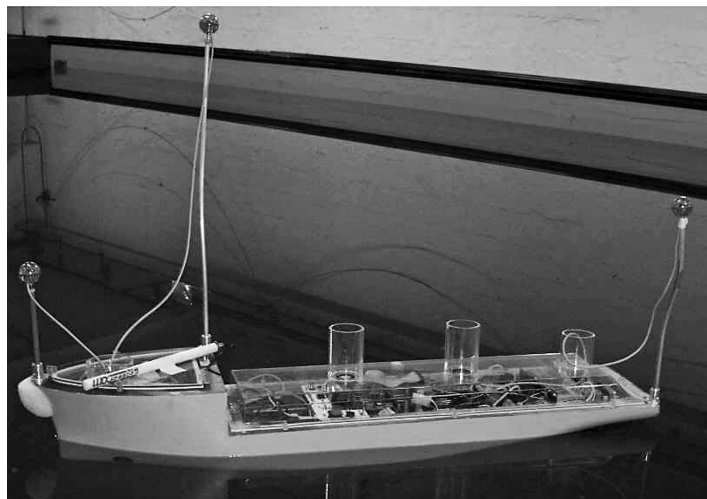
In the experiment, *CyberShip 2* (CS2) was used. It is a 1:70 scale model of an offshore supply vessel with a mass of 15 kg and a length of 1.255 m. The maximum surge force is approximately 2.0 N while the maximum yaw moment is about 1.5 N m. The MCLab tank is  $L \times B \times D = 40 \text{ m} \times 6.5 \text{ m} \times 1.5 \text{ m}$ .

Figure 13.32 shows CS2. Three spheres can be seen mounted on the ship, ensuring that its position and orientation can be identified by infrared cameras. Two infrared cameras mounted on a towing carriage currently supply the position and orientation estimates in 6 DOF, but due to a temporary poor calibration the camera measurements vanished when the ship assumed certain yaw angles and regions of the tank. This affected the results of the experiment and also limited the available space for maneuvering. Nevertheless, good results were obtained.

The desired path consists of a total of eight waypoints:

$$\begin{array}{ll} \text{wpt}_1 = (0.372, -0.181) & \text{wpt}_5 = (6.872, -0.681) \\ \text{wpt}_2 = (-0.628, 1.320) & \text{wpt}_6 = (8.372, -0.181) \\ \text{wpt}_3 = (0.372, 2.820) & \text{wpt}_7 = (9.372, 1.320) \\ \text{wpt}_4 = (1.872, 3.320) & \text{wpt}_8 = (8.372, 2.820) \end{array}$$

representing an S-shape. CS2 was performing the maneuver with a constant surge speed of 0.1 m/s. By assuming equal *Froude numbers*, this corresponds to a surge speed of 0.85 m/s for the full scale supply



**Figure 13.32** CyberShip 2 floating in the MCLab.

ship. A higher speed was not attempted because the consequence of vanishing position measurements at higher speed is quite severe. The controller used

$$\mathbf{M} = \begin{bmatrix} 25.8 & 0 & 0 \\ 0 & 33.8 & 1.0115 \\ 0 & 1.0115 & 2.76 \end{bmatrix}, \quad \mathbf{N}(\nu) = \begin{bmatrix} 2 & 0 & 0 \\ 0 & 7 & 0.1 \\ 0 & 0.1 & 0.5 \end{bmatrix}$$

$$c = 0.75, k_1 = 25, k_2 = 10, k_3 = 2.5$$

In addition, a reference model consisting of three first-order low-pass filters in cascade delivered continuous values of  $\psi_d$ ,  $r_d$  and  $\dot{r}_d$ . The ship's initial states were

$$(x_0, y_0, \psi_0) = (-0.69 \text{ m}, -1.25 \text{ m}, 1.78 \text{ rad})$$

$$(u_0, v_0, r_0) = (0.1 \text{ m/s}, 0 \text{ m/s}, 0 \text{ rad/s})$$

Both the ship enclosing circle and the radius of acceptance for all waypoints was set to one ship length. Figure 13.33 shows an *xy* plot of the CS2's position together with the desired geometrical path consisting of straight-line segments. The ship is seen to follow the path very well. To illustrate the effect of the positioning reference system dropping out from time to time, Figure 13.34 is included. It shows the actual heading angle of CS2 alongside the desired LOS angle. The discontinuities in the actual heading angle are due to the camera measurements dropping out. When the measurements return, the heading angle of the ship is seen to converge nicely to the desired angle.

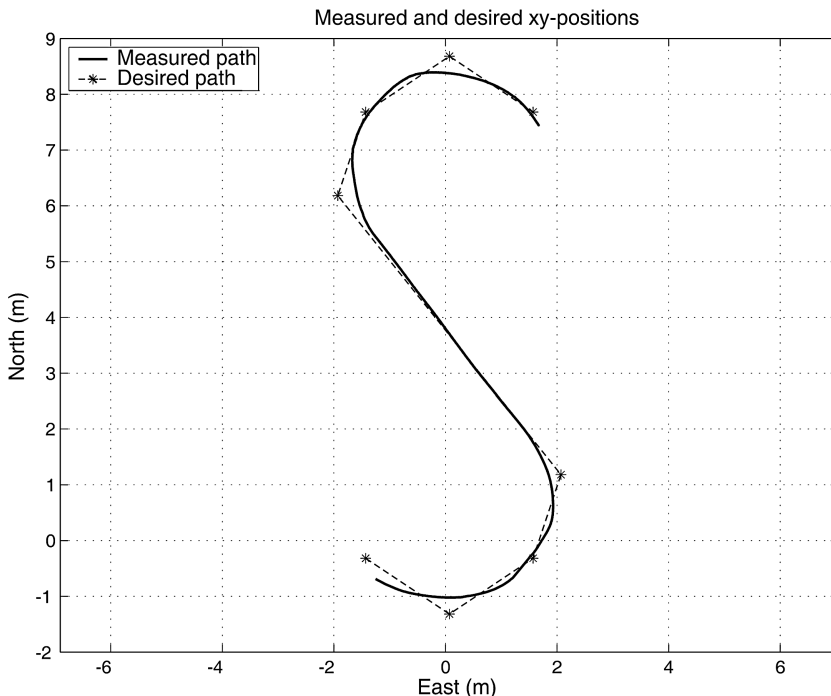


**Figure 13.33** *xy* plot of the measured and desired geometrical path during the experiment.

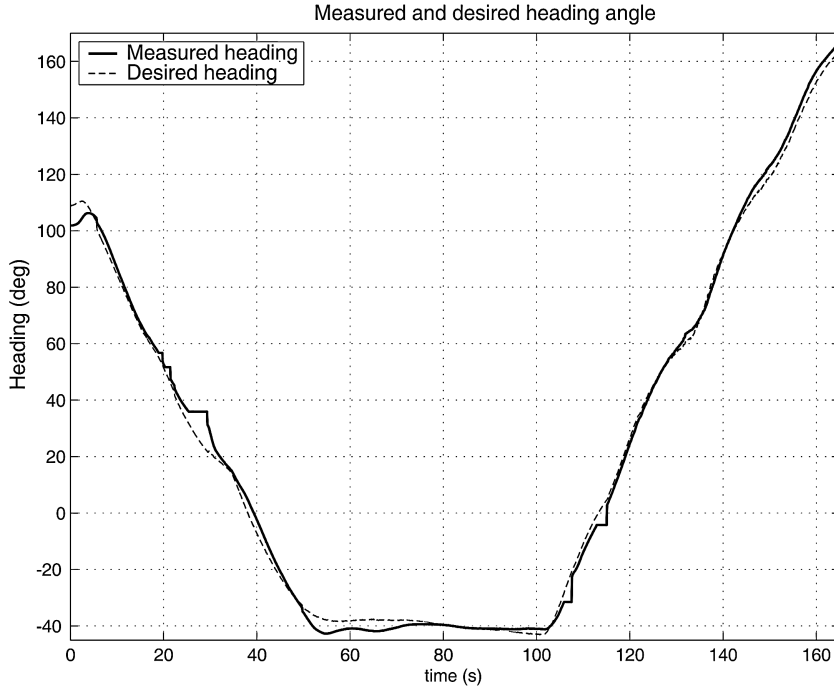


**Figure 13.34** The actual yaw angle of the ship tracks the desired LOS angle well.

## 13.4 Sliding-Mode Control

A robust nonlinear design technique for marine craft is *sliding-mode control* (Utkin, 1977), which incorporates techniques to handle model uncertainty. Sliding-mode techniques are discussed in detail by Utkin (1992) while applications to marine craft are found in Yoerger and Slotine (1985), Slotine and Li (1991), Healey and Lienard (1993) and McGookin *et al.* (2000a, 2000b), for instance.

### 13.4.1 SISO Sliding-Mode Control

Define a scalar measure of tracking:

$$s := \tilde{\psi} + 2\lambda\tilde{\psi} + \lambda^2 \int_0^t \tilde{\psi}(\tau) d\tau \quad (13.568)$$

where  $\tilde{\psi} = \psi - \psi_d$  is the yaw angle tracking error and  $\lambda > 0$  is a design parameter reflecting the bandwidth of the controller. For  $s = 0$  this expression describes a sliding surface (manifold) with exponentially stable dynamics. To see this let us define a second sliding surface:

$$s_0 := \tilde{\psi} + \lambda \int_0^t \tilde{\psi}(\tau) d\tau \quad (13.569)$$

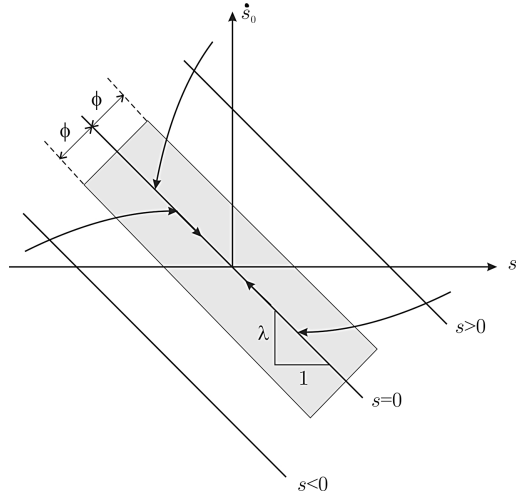


**Figure 13.35** Graphical interpretation of the sliding surface  $s = \dot{s}_0 + \lambda s_0$  and boundary layer  $\phi > 0$ .

such that the manifold  $s = 0$  can be rewritten as

$$s = \dot{s}_0 + \lambda s_0 = 0 \quad (13.570)$$

Hence, both  $s_0$  and  $\tilde{\psi}$  converge exponentially to zero since the linear system

$$\begin{bmatrix} \tilde{\psi} \\ \dot{s}_0 \end{bmatrix} = \begin{bmatrix} -\lambda & 1 \\ 0 & -\lambda \end{bmatrix} \begin{bmatrix} \tilde{\psi} \\ s_0 \end{bmatrix} \quad (13.571)$$

has two real eigenvalues at  $-\lambda$ . This ensures that the tracking error  $\tilde{\psi} \rightarrow 0$  on the manifold  $s = 0$ . Hence, the *control objective* is reduced to finding a nonlinear control law which ensures that

$$\lim_{t \rightarrow \infty} s = 0 \quad (13.572)$$

A graphical interpretation of the *sliding surfaces* is given in Figure 13.35.

It is seen that a trajectory starting at  $s > 0$  will move toward the sliding surface  $s = 0$ . When  $s = 0$  is reached the trajectory will continue moving on the straight line corresponding to  $s = 0$  toward the equilibrium point  $s_0 = 0$ . Similar behavior is observed when starting with a negative value of  $s$ .

### Nonlinear Ship Autopilot

When deriving the control law, a stable ship model with nonlinear damping is considered:

$$T\dot{r} + n_3 r^3 + n_1 r = K\delta + \tau_{\text{wind}} \quad (13.573)$$

where  $\tau_{\text{wind}}$  is the wind moment. Define a new signal  $v$  according to

$$v := r - s \implies s = r - v \quad (13.574)$$

such that

$$\begin{aligned} T\dot{s} &= T\dot{r} - T\dot{v} \\ &= K\delta + \tau_{\text{wind}} - (n_3 r^2 + n_1)r - T\dot{v} \\ &= K\delta + \tau_{\text{wind}} - (n_3 r^2 + n_1)(v + s) - T\dot{v} \end{aligned} \quad (13.575)$$

Consider the CLF:

$$V(s) = \frac{1}{2}Ts^2, \quad T > 0 \quad (13.576)$$

Differentiating  $V$  along the trajectories of  $s$  yields

$$\begin{aligned} \dot{V}(s) &= sT\dot{s} \\ &= s[K\delta + \tau_{\text{wind}} - (n_3 r^2 + n_1)(v + s) - T\dot{v}] \\ &= -[n_3 r^2 + n_1]s^2 + s[K\delta + \tau_{\text{wind}} - (n_3 r^2 + n_1)v - T\dot{v}] \end{aligned} \quad (13.577)$$

Let the control law be chosen as

$$\delta = \frac{\hat{T}}{\hat{K}}\dot{v} + \frac{1}{\hat{K}}[\hat{n}_3 r^2 + n_1]v - \frac{1}{\hat{K}}\tau_{\text{wind}} - K_d s - K_s \text{sgn}(s) \quad (13.578)$$

where  $K_d > 0$  and  $K_s > 0$ , while  $\hat{T}$ ,  $\hat{K}$  and  $\hat{n}_3$  are estimates of  $T$ ,  $K$  and  $n_3$ , respectively. Notice that  $n_1 = 1$  for a stable ship. The signum function is defined as

$$\text{sgn}(s) := \begin{cases} 1 & \text{if } s > 0 \\ 0 & \text{if } s = 0 \\ -1 & \text{otherwise} \end{cases} \quad (13.579)$$

This implies that

$$\begin{aligned} \dot{V}(s) &= -[n_3 r^2 + n_1 + K_d]s^2 - K_s |s| \\ &\quad + \left[ \left( \frac{\hat{T}}{\hat{K}} - \frac{T}{K} \right) \dot{v} + \left( \frac{1}{\hat{K}} - \frac{1}{K} \right) [n_1 v - \tau_{\text{wind}}] \right. \\ &\quad \left. + \left( \frac{\hat{n}_3}{\hat{K}} - \frac{n_3}{K} \right) r^2 v \right] s \end{aligned} \quad (13.580)$$

In order for this expression to become negative,  $K_s$  must be chosen large enough so that the parameter errors are dominated. Consequently,

$$\begin{aligned} K_s &\geq \left| \left( \frac{\hat{T}}{\hat{K}} - \frac{T}{K} \right) \dot{v} \right| + \left| \left( \frac{1}{\hat{K}} - \frac{1}{K} \right) [n_1 v - \tau_{\text{wind}}] \right| \\ &\quad + \left| \left( \frac{\hat{n}_3}{\hat{K}} - \frac{n_3}{K} \right) r^2 v \right| \end{aligned} \quad (13.581)$$

implies that

$$\begin{aligned}\dot{V}(s) &\leq -(n_3 r^2 + n_1 + K_d)s^2 - K_s |s| \\ &< 0, \quad \forall s \neq 0\end{aligned}\quad (13.582)$$

The nonpositive term  $-(n_3 r^2 + n_1 + K_d)s^2$  ensures exponential stability of  $s = 0$ . However, in order to converge to the manifold  $s \rightarrow 0$  in finite time such that  $\tilde{\psi} \rightarrow 0$  in finite time, the gain  $K_s > 0$  must be positive.

One way to find an estimate of  $K_s$  is to assume, for instance, 20 % uncertainty in all elements such that

$$K_s \geq 1.2 \frac{\hat{T}}{\hat{K}} |\dot{v}| + 1.2 \frac{1}{\hat{K}} |n_1 v - \tau_{\text{wind}}| + 1.2 \frac{\hat{n}_3}{\hat{K}} |r^2 v| \quad (13.583)$$

It is well known that the switching term  $K_s \text{sgn}(s)$  can lead to chattering for large values of  $K_s$ . Hence,  $K_s > 0$  should be treated as a design parameter with (13.581) as a guideline. Recall that Lyapunov stability analysis results in conservative requirements for all gains.

Chattering in the controller can, however, be eliminated by replacing the signum function with a saturating function. Slotine and Li (1991) suggest smoothing out the control discontinuity inside a boundary layer according to

$$\text{sat}(s) = \begin{cases} \text{sgn}(s) & \text{if } |s/\phi| > 1 \\ s/\phi & \text{otherwise} \end{cases} \quad (13.584)$$

where  $\phi > 0$  can be interpreted as the boundary layer thickness. This substitution will assign a low-pass filter structure to the dynamics inside the boundary layer (see Figure 13.35). Another possibility is to replace  $K_s \text{sgn}(s)$  with  $K_s \tanh(s/\phi)$ , where  $\phi > 0$  is a design parameter used to shape the slope of  $\tanh(\cdot)$  close to the origin.

### 13.4.2 Sliding-Mode Control using the Eigenvalue Decomposition

Healey and Lienard (1993) have applied the theory of *sliding-mode control* to control the NPS AUV II. A related work discussing the problems of adaptive sliding-mode control in the dive plane is found in Cristi *et al.* (1990). Sliding-mode control for highly maneuverable underwater vehicles is discussed by Lyshevski (2001), who considers the 6 DOF underwater vehicle equations of motion.

The method presented in this section can be applied to the lateral model (7.132), which includes the roll mode, or to the reduced order model (7.33), which is recognized as the linearized maneuvering model (see Section 7.1.4). Consider the state-space model

$$\dot{x} = Ax + bu + f(x, t) \quad (13.585)$$

where  $f(x, t)$  is a nonlinear function describing the deviation from linearity in terms of disturbances and unmodeled dynamics,  $x = [v, r, \psi]^\top$  and  $u = \delta_R$  is the rudder angle. Consequently,

$$A = \begin{bmatrix} a_{11} & a_{12} & 0 \\ a_{21} & a_{22} & 0 \\ 0 & 1 & 0 \end{bmatrix}, \quad b = \begin{bmatrix} b_1 \\ b_2 \\ 0 \end{bmatrix} \quad (13.586)$$

The experiments of Healey and coauthors show that this model can be used to describe a large number of AUV maneuvers. The feedback control law is composed of two parts:

$$u = -\mathbf{k}^\top \mathbf{x} + u_o \quad (13.587)$$

where  $\mathbf{k} \in \mathbb{R}^3$  is the feedback gain vector. Substituting (13.587) into (13.585) yields the closed-loop dynamics

$$\dot{\mathbf{x}} = \underbrace{(\mathbf{A} - \mathbf{b}\mathbf{k}^\top)}_{\mathbf{A}_c} \mathbf{x} + \mathbf{b}u_o + \mathbf{f}(\mathbf{x}, t) \quad (13.588)$$

where  $\mathbf{k}$  is computed by means of pole placement. In order to determine the nonlinear part  $u_o$  of the feedback control law, consider the output mapping

$$s = \mathbf{h}^\top \tilde{\mathbf{x}} \quad (13.589)$$

where  $\mathbf{h} \in \mathbb{R}^3$  is a design vector to be chosen such that  $s \rightarrow 0$ , implying convergence of the state tracking error  $\tilde{\mathbf{x}} = \mathbf{x} - \mathbf{x}_d \rightarrow \mathbf{0}$ . The output mapping  $s$  is also referred to as a *sliding surface*. Premultiplication of (13.588) with  $\mathbf{h}^\top$  and then subtraction of  $\mathbf{h}^\top \dot{\mathbf{x}}_d$  from both sides gives

$$\dot{s} = \mathbf{h}^\top \mathbf{A}_c \mathbf{x} + \mathbf{h}^\top \mathbf{b} u_o + \mathbf{h}^\top \mathbf{f}(\mathbf{x}, t) - \mathbf{h}^\top \dot{\mathbf{x}}_d \quad (13.590)$$

Assume that  $\mathbf{h}^\top \mathbf{b} \neq 0$  and let the nonlinear control law be chosen as (see Figure 13.36)

$$u_o = (\mathbf{h}^\top \mathbf{b})^{-1} [\mathbf{h}^\top \dot{\mathbf{x}}_d - \mathbf{h}^\top \hat{\mathbf{f}}(\mathbf{x}, t) - \eta \text{sgn}(s)], \quad \eta > 0 \quad (13.591)$$

where  $\hat{\mathbf{f}}(\mathbf{x}, t)$  is an estimate of  $\mathbf{f}(\mathbf{x}, t)$ . This gives the  $s$  dynamics

$$\dot{s} = \mathbf{h}^\top \mathbf{A}_c \mathbf{x} - \eta \text{sgn}(s) + \mathbf{h}^\top \Delta \mathbf{f}(\mathbf{x}, t) \quad (13.592)$$

where  $\Delta \mathbf{f}(\mathbf{x}, t) = \mathbf{f}(\mathbf{x}, t) - \hat{\mathbf{f}}(\mathbf{x}, t)$ . The first term in this equation can be rewritten as

$$\mathbf{h}^\top \mathbf{A}_c \mathbf{x} = \mathbf{x}^\top \mathbf{A}_c^\top \mathbf{h} = \lambda \mathbf{x}^\top \mathbf{h} \quad (13.593)$$

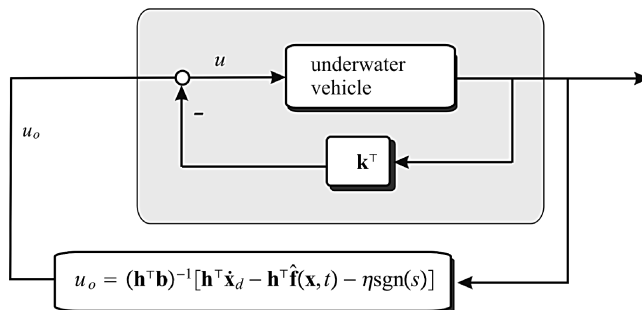


**Figure 13.36** Nonlinear sliding-mode controller.

by requiring that  $\mathbf{h}$  is a *right eigenvector* of  $\mathbf{A}_c^\top$  such that

$$\mathbf{A}_c^\top \mathbf{h} = \lambda \mathbf{h} \quad (13.594)$$

where  $\lambda = \lambda(\mathbf{A}_c^\top)$  is the *eigenvalue* corresponding to  $\mathbf{h}$ . Hence,

$$\dot{s} = \lambda \mathbf{x}^\top \mathbf{h} - \eta \text{sgn}(s) + \mathbf{h}^\top \Delta f(\mathbf{x}, t) \quad (13.595)$$

### Computation of $\mathbf{h}$ and $\mathbf{k}$

The eigenvalue  $\lambda$  in (13.595) can be made zero by noticing that (13.586) has one pure integrator. Let

$$\mathbf{k} = [k_1, k_2, 0]^\top \quad (13.596)$$

such that the linear part of the controller only stabilizes the sway velocity  $v$  and yaw rate  $r$ . The yaw angle  $\psi$  is left uncontrolled in the inner loop since this results in a closed-loop system matrix:

$$\mathbf{A}_c = \begin{bmatrix} a_{11} - b_1 k_1 & a_{12} - b_1 k_2 & 0 \\ a_{21} - b_2 k_1 & a_{22} - b_2 k_2 & 0 \\ 0 & 1 & 0 \end{bmatrix} \quad (13.597)$$

where one of the eigenvalues is zero. Consequently,

$$\lambda \mathbf{x}^\top \mathbf{h} = 0 \text{ if } \mathbf{h} \text{ is a right eigenvector of } \mathbf{A}_c^\top \text{ for } \lambda = 0 \quad (13.598)$$

With this choice of  $\mathbf{h}$ , the  $s$  dynamics (13.595) reduces to

$$\dot{s} = -\eta \text{sgn}(s) + \mathbf{h}^\top \Delta f(\mathbf{x}, t) \quad (13.599)$$

and it follows from

$$V = \frac{1}{2} s^2 \quad (13.600)$$

that

$$\begin{aligned} \dot{V} &= s \dot{s} \\ &= -\eta \text{sgn}(s)s + s \mathbf{h}^\top \Delta f(\mathbf{x}, t) \\ &= -\eta |s| + s \mathbf{h}^\top \Delta f(\mathbf{x}, t) \end{aligned} \quad (13.601)$$

Selecting  $\eta$  as

$$\eta > \| \mathbf{h} \| \cdot \| \Delta f(\mathbf{x}, t) \| \quad (13.602)$$

finally yields

$$\dot{V} \leq 0 \quad (13.603)$$

Hence, by application of Barbălat's lemma,  $s$  converges to zero in finite time if  $\eta$  is chosen to be large enough to overcome the destabilizing effects of the unmodeled dynamics  $\Delta f(\mathbf{x}, t)$ . The magnitude of  $\eta$  will be a trade-off between robustness and performance.

### Implementation Considerations

In practical implementations, chattering should be removed by replacing  $\text{sgn}(s)$  with

$$\text{sat}(s) := \begin{cases} \text{sgn}(s) & \text{if } |s/\phi| > 1 \\ s/\phi & \text{otherwise} \end{cases} \quad (13.604)$$

where the design parameter  $\phi$  is the sliding surface boundary layer thickness. Alternatively, the discontinuous function  $\text{sat}(s/\phi)$  could be replaced by the continuous function  $\tanh(s/\phi)$ . It should be noted that the proposed feedback control with a predescribed  $\eta$  usually yields a conservative estimate of the necessary control action required to stabilize the plant. This suggests that  $\eta$  should be treated as a tunable parameter.

#### 13.4.3 Case Study: Heading Autopilot for Ships and Underwater Vehicles

Consider the autopilot model

$$\begin{bmatrix} \dot{v} \\ \dot{r} \\ \dot{\psi} \end{bmatrix} = \begin{bmatrix} a_{11} & a_{12} & 0 \\ a_{21} & a_{22} & 0 \\ 0 & 1 & 0 \end{bmatrix} \begin{bmatrix} v - v_c \\ r \\ \psi \end{bmatrix} + \begin{bmatrix} b_1 \\ b_2 \\ 0 \end{bmatrix} \delta \quad (13.605)$$

where  $|v_c| < v_c^{\max}$  is the transverse ocean current velocity. The reference trajectory is specified according to

$$\begin{bmatrix} \dot{\psi}_d \\ \dot{r}_d \end{bmatrix} = \begin{bmatrix} 0 & 1 \\ -\omega_n^2 & -2\zeta\omega_n \end{bmatrix} \begin{bmatrix} \psi_d \\ r_d \end{bmatrix} + \begin{bmatrix} 0 \\ \omega_n^2 \end{bmatrix} \psi_{\text{ref}} \quad (13.606)$$

while  $v_d = 0$  during turning. Let  $\mathbf{x} = [v, r, \psi]^T$  and  $\mathbf{h} = [k_1, k_2, k_3]^T$  such that

$$s = \mathbf{h}^T(\mathbf{x} - \mathbf{x}_d) = h_1 v + h_2(r - r_d) + h_3(\psi - \psi_d) \quad (13.607)$$

Feedback from the sway velocity  $v$  and yaw rate  $r$ , that is  $\mathbf{k} = [k_1, k_2, 0]^T$ , implies that

$$\mathbf{A}_c = \mathbf{A} - \mathbf{b}\mathbf{k}^T = \begin{bmatrix} a_{11} - b_1 k_1 & a_{12} - b_1 k_2 & 0 \\ a_{21} - b_2 k_1 & a_{22} - b_2 k_2 & 0 \\ 0 & 1 & 0 \end{bmatrix} \quad (13.608)$$

where the yaw dynamics  $\dot{\psi} = r$  is left unchanged. A pure integrator in yaw corresponding to the eigenvalue  $\lambda = 0$  is necessary in order to satisfy

$$\lambda \mathbf{x}^T \mathbf{h} = 0 \quad (13.609)$$

The eigenvector  $\mathbf{h}$  is computed in Matlab as:

### Matlab

```

p = [-1 -1 0]           % desired poles for Ac
k = place(A,b,p)        % pole placement
Ac = A-b*k'
[V,D]=eig(Ac')         % eigenvalue decomposition
for i = 1:3              % extract the eigenvector h from V
    hi = V(:,i);
    if norm(hi.*Ac') < 1e-10; h = hi; end
end

```

The resulting tracking controller is

$$\delta = -k_1 v - k_2 r + \frac{1}{h_1 b_1 + h_2 b_2} [h_2 \dot{r}_d + h_3 r_d - \eta \text{sat}(s)] \quad (13.610)$$

Since the disturbance  $v_c$  is unknown, the best guess for

$$f(\mathbf{x}, t) = - \begin{bmatrix} a_{11} \\ a_{21} \\ 0 \end{bmatrix} v_c(t) \quad (13.611)$$

is  $f(\hat{\mathbf{x}}, t) = \mathbf{0}$ . Hence,

$$\eta > \| \mathbf{h} \| \cdot \| -[a_{11}, a_{12}, 0]^\top v_c^{\max} \| \quad (13.612)$$

#### 13.4.4 Case Study: Pitch and Depth Autopilot for Underwater Vehicles

Pitch and depth control of underwater vehicles is usually done by using control surfaces, thrusters and ballast systems. For a neutrally buoyant vehicle, stern rudders are effective for diving and depth changing maneuvers, since they require relatively little control energy compared to thrusters. Consider the longitudinal model in Section 7.5.6, which can be written

$$\begin{aligned}
& \begin{bmatrix} m - X_{\dot{u}} & -X_{\dot{w}} & mz_g - X_{\dot{q}} \\ -X_{\dot{w}} & m - Z_{\dot{w}} & -mx_g - Z_{\dot{q}} \\ mz_g - X_{\dot{q}} & -mx_g - Z_{\dot{q}} & I_y - M_q \end{bmatrix} \begin{bmatrix} \dot{u} \\ \dot{w} \\ \dot{q} \end{bmatrix} + \begin{bmatrix} -X_u & -X_w & -X_q \\ -Z_u & -Z_w & -Z_q \\ -M_u & -M_w & -M_q \end{bmatrix} \begin{bmatrix} u \\ w \\ q \end{bmatrix} \\
& + \begin{bmatrix} 0 & 0 & 0 \\ 0 & 0 & -(m - X_{\dot{u}})u \\ 0 & (Z_{\dot{w}} - X_{\dot{u}})u & mx_g u \end{bmatrix} \begin{bmatrix} u \\ w \\ q \end{bmatrix} + \begin{bmatrix} 0 \\ 0 \\ W \overline{B} \overline{G}_z \sin(\theta) \end{bmatrix} = \begin{bmatrix} \tau_1 \\ \tau_3 \\ \tau_5 \end{bmatrix} \quad (13.613)
\end{aligned}$$

The speed dynamics can be removed from this model by assuming that the speed controller stabilizes the forward speed such that

$$u = u_o = \text{constant} \quad (13.614)$$

Hence, (13.613) reduces to a combined pitch and diving model

$$\begin{bmatrix} m - Z_w & -mx_g - Z_{\dot{q}} \\ -mx_g - Z_{\dot{q}} & I_y - M_{\dot{q}} \end{bmatrix} \begin{bmatrix} \dot{w} \\ \dot{q} \end{bmatrix} + \begin{bmatrix} -Z_w & -Z_q \\ -M_w & -M_q \end{bmatrix} \begin{bmatrix} w \\ q \end{bmatrix} + \begin{bmatrix} 0 & -(m - X_{\dot{u}})u_o \\ (Z_w - X_{\dot{u}})u_o & mx_g u_o \end{bmatrix} \begin{bmatrix} w \\ q \end{bmatrix} + \begin{bmatrix} 0 \\ \overline{BG_z} W \sin(\theta) \end{bmatrix} = \begin{bmatrix} \tau_3 \\ \tau_5 \end{bmatrix}$$

A state-space representation of this model is

$$\dot{\mathbf{x}} = \mathbf{A}\mathbf{x} + \mathbf{b}u + \mathbf{f}(\mathbf{x}, t) \quad (13.615)$$



$$\begin{bmatrix} \dot{w} \\ \dot{q} \\ \dot{\theta} \\ \dot{d} \end{bmatrix} = \begin{bmatrix} a_{11} & a_{12} & 0 & 0 \\ a_{21} & a_{22} & a_{23} & 0 \\ 0 & 1 & 0 & 0 \\ 1 & 0 & -u_0 & 0 \end{bmatrix} \begin{bmatrix} w \\ q \\ \theta \\ d \end{bmatrix} + \begin{bmatrix} b_1 \\ b_2 \\ 0 \\ 0 \end{bmatrix} \delta_s + \mathbf{f}(\mathbf{x}, t) \quad (13.616)$$

where  $\mathbf{f}(\mathbf{x}, t)$  is a nonlinear function describing the deviation from linearity in terms of disturbances and unmodeled dynamics,  $\mathbf{x} = [w, q, \theta, d]^\top$  and  $u = \delta_s$  is the stern rudder. The kinematic equations are based on the approximations (see Section 2.2.1)

$$\dot{\theta} = p \cos(\phi) - \sin(\phi) \approx q \quad (13.617)$$

$$\dot{d} = -u_0 \sin(\theta) + v \cos(\theta) \sin(\psi) + w \cos(\theta) \cos(\psi) \approx w - u_0 \theta \quad (13.618)$$

for  $v = p = 0$  and small values of  $\theta$  and  $\phi$ .

The sliding surface for pitch and diving control can be constructed as

$$s = \mathbf{h}^\top \tilde{\mathbf{x}} = h_1(w - w_d) + h_2(q - q_d) + h_3(\theta - \theta_d) + h_4(d - d_d) \quad (13.619)$$

where  $h_i$  for  $i = 1, \dots, 4$  are the components of  $\mathbf{h}$ . Let  $\mathbf{x}_d = [w_d, q_d, \theta_d, d_d]^\top$  be a desired state vector given by a reference model. From (13.587) and (13.591) it is seen that

$$u = -\mathbf{k}^\top \mathbf{x} + u_o \quad (13.620)$$

$$u_o = (\mathbf{h}^\top \mathbf{b})^{-1} [\mathbf{h}^\top \dot{\mathbf{x}}_d - \mathbf{h}^\top \hat{\mathbf{f}}(\mathbf{x}, t) - \eta \operatorname{sgn}(s)], \quad \eta > 0 \quad (13.621)$$

where  $\mathbf{k} = [k_1, k_2, 0, k_4]^\top$ . Notice that  $k_3 = 0$  since there is one pure integration in the pitch channel. Hence,  $\mathbf{h}$  is found by computing the eigenvalues  $\lambda(\mathbf{A}_c) = \lambda(\mathbf{A} - \mathbf{b}\mathbf{k}^\top)$  where  $\mathbf{A}_c^\top \mathbf{h} = \mathbf{0}$  for  $\lambda_3 = 0$ . Consequently,

$$\delta_S = -k_1 w - k_2 q - k_4 d + \frac{1}{h_1 b_1 + h_2 b_2} [h_1 \dot{w}_d + h_2 \dot{q}_d + h_3 \theta_d + h_4 d_d - \eta \operatorname{sgn}(s)] \quad (13.622)$$